NON-CONTIGUOUS SPECTRUM ACCESS AND SMALL CELL NETWORK DESIGN

By

MUHAMMAD NAZMUL ISLAM

A Dissertation submitted to the

Graduate School—New Brunswick

Rutgers, The State University of New Jersey

in partial fulfillment of the requirements

for the degree of

Doctor of Philosophy

Graduate Program in Electrical and Computer Engineering

written under the direction of

Dr. Narayan B. Mandayam

and approved by

_____

_____

_____

_____

New Brunswick, New Jersey

October, 2014

ABSTRACT OF THE DISSERTATION

Non-contiguous Spectrum Access and Small Cell Network Design

By MUHAMMAD NAZMUL ISLAM

Dissertation Director:
Dr. Narayan B. Mandayam

The explosive demand for high data rate wireless services cannot be sustained through improvements in the PHY layer technologies alone. Opportunistic use of additional bandwidth through dynamic spectrum access and densification of wireless networks are necessary to meet this increasing demand, and this dissertation covers both these aspects.

The first part of the thesis focuses on a cooperative spectrum access scenario where nodes exchange non-contiguous spectrum chunks as incentives for cooperative forwarding. An autonomous network is considered where each node receives an initial amount of bandwidth, and uses this bandwidth as a flexible incentive for two hop relaying. This dissertation proposes an incentivized forwarding based resource allocation algorithm which maximizes the global utility of the network while preserving the initial utility of each cooperative node. The second part of thesis studies power optimal non-contiguous spectrum access. Non-Contiguous Orthogonal Frequency Division Multiple Access (NC-OFDMA), a popular technique in software defined radio research, accesses non-contiguous spectrum chunks by nulling intermediate spectrum. However, nulling subcarriers increases the sampling rate (spectrum span) which, in turn, increases the

power consumption of radio front ends. This dissertation characterizes this trade-off from a cross-layer perspective, specifically by showing how the slope of ADC/DAC's power consumption versus sampling rate curve influences scheduling decisions in a multi-hop network.

The final part of the thesis focuses on two aspects of small cell network design: (i) a prototype wireless channel measurement system that allows network operators to measure path loss and multipath fading characteristics between multiple candidate small cell locations and their potential users; and (ii) the placement of aggregator nodes which would aggregate multiple small cells data and transport it to macrocell, specifically joint cost optimal aggregator node placement, power allocation, channel scheduling and routing for the wireless backhaul network.

Acknowledgements

Many people have supported me in various phases of my life. As I come to the finishing stages of my educational career, I want to acknowledge them for their contributions.

First of all, I want to thank Dr. Narayan B. Mandayam, my PhD supervisor, for guiding me throughout my PhD journey. He introduced me to my initial PhD topic. Later, he introduced new topics and helped me come up with new ideas. He appreciated ideas that I brought from my summer internship projects on small cells and helped me develop those ideas further. His guidance, feedback and never-ending encouragement were invaluable in my scholarly pursuits.

Several other members of the WINLAB faculty have also guided me during the last four years. Ivan Seskar's name comes first to my mind. He introduced me to the world of cognitive and software defined radios. He guided my experimental work on ORBIT testbed and introduced me to the concepts of GNUradio. His feedback immensely helped me to model system power consumption in radio front ends.

Dr. Roy Yates also gave me valuable suggestions during my PhD thesis. His door was always open for discussion and sharing new concepts. I also thank Dr. Dipankar Raychaudhuri for his feedback on my PhD proposal and thesis. Dr. Sastry Kompella, a researcher of Naval Research Laboratory, strengthened my knowledge on resource allocation and multi-hop networking. He provided regular feedback on my work and suggested how I could improve my solution methodologies.

I had a really great time with Paul Henry, Byoung-jo "J" Kim, and Eric Rozner, my internship mentors at AT&T Labs, during the summer of 2012. I remember one particular afternoon when I was very tensed about some experiments that were not working as expected. Paul Henry came to my desk and said, "Son, within at most eighty years, all of your worries will be over!" This comment made me realize that we

often focus on minor issues of our lives and miss the bigger perspectives.

I learned a lot from Ashwin Sampath, Atul Maharshi, and Ozge Koymen, my internship mentors at Qualcomm, during the summer of 2013. I worked in a group of nine members where each member had expertise in a different field. This group showed me how to tackle a research problem from different angles.

I fondly remember many other teachers who have inspired me during my graduate life. Dr. Ravi Adve, my Masters thesis supervisor at the University of Toronto, introduced me to the physical layer wireless communications research. Dr. Michael J. Carter, my professor of "Communication Systems" course at the University of New Hampshire, inspired me to consider wireless communications as my major. Dr. L. G. Kraft, my undergraduate thesis supervisor at the University of New Hampshire, was the first person who taught me how to pursue research. Dr. Mung Chiang, my professor of "Optimization of Communication Systems" course at Princeton University, made me realize why algorithm designers should always consider the practical constraints of experimental research.

I have made many friends during my four years at Rutgers University. My busy work hours at WINLAB became enjoyable due to the presence of Shweta Sagari, Yi Hu, Dragoslav Stojadinovic, Akash Baid, Ashwin Ashok, Chenren Xu, Abhishek Chanda, Ben Firner, Shubham Jain, Gorkem Kar, Narayanan Krishnan, Xiruo Liu, Tam Vu, Gautam Bhanage, Feixiong Zhang, Shreyasee Mukherjee, Francesco Bronzino, and many others. I also thank all of my friends from around the globe.

I was born in an upper middle class family of Dhaka, the capital of Bangladesh. Hence, I got the chance to attend the best educational institutions of my country. These institutions were built through the taxes or labor of all citizens of Bangladesh, including the "poorest of the poor" class who would find it very difficult to attain these institutions due to their financial barrier. I thank all these people and hope that I will return their favor one day.

Starting from primary school days, I have been lucky enough to share classroom with many great students. I have paid great attention to their work ethic and method of analytic reasoning. Competition and coordination with these students made me

attain some qualities that I could never have attained otherwise. I thank all of them for their indirect contributions in my life.

I remember my sisters who have always loved me unconditionally and taken care of me. They will be among the happiest people on earth to know about my PhD degree completion.

I thank my spouse, Nafisa Tanjeem, who has endured the ups and downs of my graduate life during the last four years. This beautiful but lonely city of Piscataway, my home residence since last four years, became lively due to her presence.

Lastly but most importantly, I want to thank my parents for being the beacons of my life. They have sacrificed immensely for me. They have always inspired me to achieve my dreams. I can never repay their debts but I will never forget their extraordinary contributions.

Dedication

Dedicated to Sayeda Mustab Shera and Muhammad Saiful Islam, my parents,

who have been the beacons of my life ;

to Maliha Sultana and Rabeya Sultana, my sisters,

who have always taken care of me ;

and to Nafisa Tanjeem, my spouse,

who has accompanied me in my toughest hurdles in the last decade.

Table of Contents

Abstract ii

Acknowledgements iv

Dedication vii

List of Tables xiv

List of Figures xvi

1. Introduction 1

1.1. Bandwidth exchange based cooperative forwarding 1

1.1.1. Related Work and Our Contributions 2

1.2. Power Optimal Non-contiguous Spectrum Access 4

1.2.1. Related Work 7

1.3. Wireless Backhaul Node Placement for Small Cell Networks 9

1.3.1. Related work 10

1.4. Wireless Channel Measurement Platform Design for Small Cell Networks 11

1.4.1. Essential features 12

(i) Multiple transmitter single receiver channel sounding 12

(ii) Small form factor 12

(iii) Low cost 12

(iv) Flexibility 13

1.4.2. Our contributions 13

1.5. Publications 13

2. Bandwidth Exchange based Cooperative Forwarding 16

2.1. Introduction 16

2.2. System Model 16
Rate analysis in the BE scenario: 19
2.3. Design Objective 20
2.4. Optimization Problem Solution 21
2.4.1. Modified Optimization Problem 21
2.4.2. Optimal bandwidth and rate allocation for a fixed sender-forwarder set 23
2.4.3. Optimal sender-forwarder set selection 25
2.4.4. Distributed BE incentivized forwarding protocol 27
2.4.5. Outage probability reduction in BE 27
2.5. Numerical Simulations 28
2.6. Experimental Setup 32
2.6.1. ORBIT Testbed & USRP Nodes 32
2.6.2. Selection of Parameters 33
2.7. Experimental Evaluation 33
2.7.1. Illustration of MWM in Relay Selection 33
2.7.2. Sum Goodput Maximization 35
2.7.3. Proportional Fair Maximization of Goodput 35
2.8. Chapter Summary 36

3. Power Optimal Non-contiguous Spectrum Access 37
3.1. Introduction 37
3.2. System Model 38
3.2.1. System Power Model 38
3.2.2. Multi-hop cross-layer model 41
Power Control and Scheduling Constraints 41
Routing and Link Capacity Constraints 42
3.2.3. System Power Constraints 43
3.2.4. Main Optimization Problem 44

3.3. Relation between Channel Scheduling and System Power 44
3.3.1. Bundle Constraint 48
3.4. Solution Overview 48
3.4.1. Linearization of the Optimization Problem 48
3.4.2. Feasible Solution 50
3.5. Theoretical Insights 50
3.5.1. Influence of System Power on Scheduling 50
Case I: Transmit Power Minimization 51
Case II: Circuit Power Minimization 52
Trade-off between transmit and circuit power minimization . . . 53
3.6. Low Complexity Algorithm for point-to-point link 53
3.7. Polynomial Time Algorithm for a Multihop Networks 54
3.7.1. Central Program 56
3.7.2. Greedy Scheduling Algorithm 57
3.7.3. Interference Checking Algorithm 59
3.7.4. Computational Complexity 59
3.8. Simulation Results 60
3.8.1. System Power Minimization in a Single Point-to-Point Link . . . 60
3.8.2. System power minimization in a multi-hop network 63
Channel Indexing Notations in Optimization Formulation 64
Comparison of “waterfilling” algorithm and our approach 64
3.9. A case for NC-OFDMA in Multi-Channel-Multi-Radio platforms 66
3.9.1. System Model 67
3.9.2. Theoretical Insights 69
Case I: Contiguous Spectrum Access 70
Use of MC-MR over NC-OFDM 70
Use of NC-OFDM over MC-MR 70
3.9.3. Low Complexity Algorithm 71
3.9.4. Computational Complexity 72

3.9.5. Other Algorithms . . . 72
3.9.6. Simulation Results . . . 72
3.10. Chapter Summary . . . 75

4. Wireless Backhaul Node Placement for Small Cell Networks . . . 78
4.1. Introduction . . . 78
4.2. Interference Models . . . 79
4.2.1. Interference limited versus interference free setting between edge and aggregator/gateway nodes . . . 79
4.2.2. Interference free setting between aggregator and gateway nodes . 80
4.3. Network optimization with microwave band in NLOS paths and mm wave band in LOS path . . . 80
4.4. Network optimization with sub-6 GHz in NLOS paths and mm-wave in LOS paths . . . 84
4.5. Solution of the Optimization Problem . . . 86
4.5.1. Linear relaxation of the capacity function . . . 86
4.5.2. Branch-and-bound algorithm . . . 87
4.5.3. Feasible solution . . . 88
4.5.4. Algorithm running time . . . 89
4.6. Greedy Set Covering based Network Optimization with sub-6 GHz in NLOS Path and mm-wave band in LOS path . . . 90
4.6.1. Performance bound . . . 92
4.7. Numerical results . . . 92
4.7.1. Network connectivity with microwave band . . . 93
4.7.2. Network connectivity with sub-6 GHz band . . . 94
Performance of greedy algorithm with sub-6 GHz in NLOS and mm-wave band in LOS path . . . 95
4.7.3. Relationship between Interference Suppression and the number of spatially multiplexed edge nodes . . . 97

4.8. Chapter Summary 98

5. A Wireless Channel Sounding System for Small Cell Networks . . . 100

5.1. Introduction 100

5.2. Measurement System 100

5.3. Sliding Correlator Channel Sounding 102

5.3.1. Methodology 102

Transmission 102

Multipath Channel 103

Reception 103

5.3.2. Multiple transmitter sliding correlator channel sounding algorithm 105

5.3.3. Challenges of multiple transmitter channel sounding in the sliding correlator method 106

Time synchronization 106

Near-far effect 106

5.4. Frequency Domain Channel Sounding 107

5.4.1. Methodology 107

5.4.2. Multiple transmitter frequency domain channel sounding algorithm 107

5.4.3. Challenges of multiple transmitter channel sounding in the frequency domain method 108

5.4.4. Mean wideband path loss 109

5.5. Experimental Results 109

5.5.1. Sliding correlator channel sounding results 109

5.5.2. Frequency domain channel sounding results 110

5.5.3. Chapter Summary 113

6. Conclusion & Future Work 114

6.1. Thesis Summary 114

6.2. Future Works 118

Appendix A. Power Consumption of Different Blocks in the Transmitter and Receiver 120

A.1. Power Consumption of Different Blocks in the Transmitter and the Receiver 120

A.1.1. Power consumption of analog blocks 121

A.1.2. Power consumption of programmable amplifier 121

A.1.3. Power consumption of ADC and DAC 122

Appendix B. Codebook Design and Matching Algorithms in Bandwidth Exchange 124

B.1. Codebook Design in Proposed DF Relaying 124

B.2. Matching and nonbipartite MWM algorithm 125

B.3. Distributed Local Greedy MWM 125

References 127

List of Tables

1.1. (Maximum Sampling Rates and Power Dissipation of Different Commercial ADC and DAC) 6

1.2. Maximum Allowed Power and Operating Frequencies in IEEE 802.22 standard [1] 6

2.1. Summary of used notations 18

3.1. List of Notations 40

3.2. Spectrum Span Calculation of Different Nodes of Fig. 3.2 46

3.3. Greedy Algorithm to Minimize System Power in a point-to-point link . 55

3.4. Polynomial Time Algorithm to Minimize System Power in a Multi-hop Network 57

3.5. Greedy Scheduling Algorithm 58

3.6. Primary and Secondary Interference Checking Algorithm 59

3.7. Available TV channels for fixed devices in Wichita, Kansas. 63

3.8. Comparison between the spectrum span of 'TxPowerMin' and our 'BnB-SysPowerMin' algorithm in the network of Fig. 3.8. 'TxPowerMin' selects the channels with higher gain in most links and spans wider spectrum. Our algorithm spans less spectrum than 'TxPowerMin' in most of the links. 64

3.9. Greedy Algorithm to Minimize System Power in a Multi-front end radio enabled point-to-point link 77

3.10. Available channels for the point-to-point link 77

3.11. Values of different parameters used in Sec. 3.9.6 77

4.1. List of Notations 81

4.2. Greedy Set Covering based Network Optimization with sub-6 GHz in NLOS Paths and mm-wave band in LOS paths 90
4.3. Backhaul features at different bands 92
4.4. Performance comparison between branch-and-bound and greedy algorithm in network optimization with sub-6 GHz in NLOS and mm-wave band in LOS 96
5.1. (Sliding correlator channel sounder system parameters) 103
5.2. (Frequency domain channel sounder system parameters) 104

List of Figures

1.1. Left subfigure shows the number of available TV channels [2] in seven fastest growing cities of USA [3]. Right subfigure shows the number of non-contiguous spectrum chunks among these TV channels in these cities. 4

1.2. Advantages and drawbacks of NC-OFDMA in multi-hop networks . . . 5

1.3. Necessity of wireless backhaul in urban small cell networks. This figure is reproduced from [4] 9

2.1. Direct Transmission and BE enabled Incentivized Forwarding 17

2.2. BE Enabled Forwarding in a 3 Node Network 18

2.3. MWM in BE Enabled Relay Network 25

2.4. Sumrate Maximization in a 3 Node Network, 10 MHz per Node, P = 100 mW, Near node-AP distance = 150m 29

2.5. Minimum Rate Maximization in a 3 Node Network, 10 MHz per Node, P = 100 mW, Near node-AP distance = 150m 29

2.6. Spectrum Efficiency in an N Node Network, 1 MHz per Node, P = 20 dBm 30

2.7. Outage Probability in an N Node Network, 1 MHz per Node, P = 20 dBm 30

2.8. Orbit Testbed 31

2.9. USRP Daughterboards 32

2.10. Illustration of MWM in sender-forwarder pair selection 34

2.11. Sum Goodput Maximization in 3 node (Packet length = 1500 bytes, CRC checking, GMSK modulation) 35

2.12. Proportional Fair Maximization of Goodput (Packet length = 1500 bytes, CRC checking, GMSK modulation) 36

3.1. Radio front end circuit blocks (reproduced from [5]) 38
3.2. Spectrum span, occupied subcarrier and nulled subcarrier in an NC-OFDMA based multi-hop network. 45
3.3. Optimization problem based on spectrum span 47
3.4. A convex hull for $c_{ij}^m = ln(1 + s_{ij}^m)$ 48
3.5. Power allocation across 20 channels in a single transceiver pair. 61
3.6. Comparison of our algorithms with the 'TxPowerMin' approach with the high slope ADC/DAC's of Fig. A.1 and Fig. A.2. 61
3.7. Comparison of our algorithms with the 'TxPowerMin' approach with the low slope ADC/DAC's of ig. A.1 and Fig. A.2. 62
3.8. 12 node 3 session multi-hop network. Node 1, 2 and 3 transmit to node 12, 11 and 10 respectively. Both "TxPowerMin" and our approach select the same routes for both sessions. 63
3.9. Performance comparison of "TxPowerMin" approach and our algorithm ("BnBSysPowerMin") in the network of Fig. 3.8, based on the low slope ADC and DAC models of Fig. A.2 and A.1. Our approach reduces system power by 30% percent. 65
3.10. Multi-Channel Multi-Radio based Non-Contiguous Orthogonal Frequency Division Multiplexing operation 67
3.11. Power allocation among available channels (Demand = 75 Mbps) 73
3.12. Power allocation among available channels (Demand = 10 Mbps) 74
3.13. Comparison of system power consumption among different approaches . 75
4.1. An example wireless backhaul network in downtown Manhattan scenario. Figure taken from [6] 79
4.2. Network optimization formulation when edge and aggregator nodes communicate in an interference free setting 82
4.3. Network optimization formulation when edge and aggregator nodes communicate using a protocol interference model 83

4.4. Linear relaxation of the capacity function. First order Taylor approximation at points p_1,p_i and p_{max} provide an upper bound of the log function. 86
4.5. Branch and bound algorithm of an optimization problem that contains three binary variables (x_4, x_5 and x_6). 87
4.6. A realistic network scenario in downtown Manhattan. Orange and light blue markers denote locations of edge nodes and gateway nodes. Green markers denote candidate locations of aggregator node deployment. . . . 93
4.7. Network connectivity when edge nodes (orange markers) transmit in 28 GHz (red lines) to aggregator nodes (green markers) and gateway nodes (highlighted with light blue rectangle around it). Aggregator nodes transmit in 60 GHz (dashed blue lines) to gateway nodes. Figure taken from [6] 94
4.8. Network connectivity when edge nodes transmit in 5.8 GHz and aggregator nodes transmit in 60 GHz. Figure taken from [6] 95
4.9. CDF of SINR curves 98
5.1. USRP block diagram 101
5.2. Sliding Correlator Channel Sounder System 103
5.3. Frequency Domain Channel Sounder System 104
5.4. Path loss data for indoor transmitter 1 106
5.5. Path loss data for indoor transmitter 2 108
5.6. Path loss data for outdoor transmitter 1 109
5.7. Path loss for outdoor transmitter 2 111
5.8. Path loss data of outdoor transmitter 3 111
5.9. Location of the transmitters and the measurement point 112
5.10. Narrowband path loss (at co-ordinate (200, 130) of Fig. 8) of transmitter 1 and 2 113

A.1. Power consumption of AD 9777 (digital-to-analog-converter of USRP radio) and DAC 3162 (low power DAC for software defined radios). The rectangular [7] and the circular [8] dots are taken from the data sheets; the straight lines are the linear interpolations of the dots. 123

A.2. Power consumption of ADS 62P4 (ADC of USRP radio) and ADS 4249 (low power ADC of TI). The rectangular [9] and the circular [10] dots are taken from the data sheets; the straight lines are the linear interpolations of the dots. 123

Chapter 1

Introduction

The demand for wireless services is becoming much greater than that can be accommodated by the currently available spectrum. Some experts predict a 1000 fold increase in data traffic by 2020 [11]. Improvements at the physical layer alone cannot sustain such high data rates [12]. Extreme densification of wireless networks [13] (e.g. small cells) and the use of additional bandwidth (e.g. TV white space [14], 3.5 GHz [15], microwave and millimeter wave [16]) are necessary to meet this increasing demand. This thesis focuses on both these aspects.

The first two chapters of this thesis design efficient algorithms to utilize these additional spectrum chunks in a cooperative and non-cooperative manner. The last two chapters focus on designing different aspects of small cell networks [15].

1.1 Bandwidth exchange based cooperative forwarding

We start our work by investigating how efficient exchange of bandwidth increases performance in a cooperative network. The benefits of cooperative forwarding have been well documented in wireless communications literature [17, 18]. However, forwarding always incurs additional costs, e.g., power and/or delay. A forwarder node's data rate may drop if it has to relay the sender node's data. Existing cooperative communications literature includes several incentive based mechanisms to encourage forwarder nodes to cooperate. These techniques include pricing [19], reputation [20] and credit [21] based cooperative forwarding. However, these mechanisms require a stable economy or a shared understanding of what things are worth, which might not be realizable in a dynamic wireless network.

In light of this, the authors of [22] developed a bandwidth exchange (BE) enabled incentive mechanism where nodes offer a portion of their allocated bandwidths to other nodes as immediate incentives for relaying. The authors assumed that nodes can exchange non-contiguous spectrum chunks with each other and thereby improve performance through cooperative forwarding. They used a Nash bargaining solution based resource allocation and a heuristic relay selection policy in their work.

We use the BE mechanism as a starting point, and in this part of our work, we focus on the distributed joint relay selection and resource allocation in the α-fair network utility maximization and outage probability reduction of the BE enabled network. We consider an N node autonomous network where each node receives an initial amount (equal, optimal based on direct path transmission or arbitrary) of bandwidth and connects directly to an access point (AP) / base station (BS). We focus on a two-hop incentivized cooperative forwarding scheme where a sender node provides bandwidth as an incentive to a forwarder node for relaying its data to an AP/BS. In this context, we design algorithms for optimal bandwidth exchange and sender-forwarder pair selection in the network. We also implement time exchange algorithms among four software defined radios of ORBIT [23] testbed. In this setup, we implement algorithms for optimal time slot exchange and sender-forwarder pair selection among these four nodes.

1.1.1 Related Work and Our Contributions

Our contributions can be summarized as follows. First, we consider incentivized relaying in a network setting where each node has been allocated an initial amount of bandwidth. Previously, the authors of [24] and [25] considered incentivized forwarding in a cognitive radio network where only the primary users initially receive resources and later transfer some of their resources to the secondary users as incentives for relaying. In contrast, our work focuses on distributed incentivized two-hop relaying in an autonomous network where a centralized algorithm might be infeasible due to the associated long estimation delay and high complexity.

Second, our proposed decode & forward (DF) BE enabled resource allocation maximizes the summation of the utilities while preserving the initial utilities of the individual nodes. Previously, the authors of [26] proposed a similar half duplex DF relaying approach. However, they considered a commercial relay network where the relay does not have its own data [26]. To the best of our knowledge, our proposed BE based resource allocation algorithm has not been investigated before.

Third, our definition of link weight in the use of MWM is different from that of existing literature. Inspired by the seminal work on maximum weighted scheduling [27], most of the work on MWM based scheduling have defined link weights as the differential backlog size of that particular link [28, 29]. Based on this definition and using the network layer capacity perspective, the MWM algorithm of these works finds the set of links that will be activated at each slot [30, 31]. However, we adopt an information theoretic capacity perspective in our work. We define the link weights of the MWM graph as the utility gain that a DF relaying enabled cooperative pair offers to the system. Therefore, the 'matched' nodes of the MWM algorithm communicate with the AP using a DF cooperation strategy whereas, the 'unmatched' nodes transmit to the AP without cooperating with any other node. In this regards, our relay selection approach is closer to the work of [32] where the authors defined link weights of each cooperative pair as the energy savings of cooperation over non-cooperation. However, [32] considered energy minimization from a bit error rate (BER) perspective whereas, we focus on α-fair NUM from capacity perspective.

If two nodes exchange their originally allotted bandwidth slots to implement cooperative forwarding, they have to utilize non-contiguous spectrum chunks to transmit or receive data. This leads us to the following question: *how do nodes access non-contiguous spectrum chunks? What are the advantages and pitfalls of the popular mechanisms that are commonly used in non-contiguous spectrum access?* While finding answers to the two questions mentioned above, we realize that non-contiguous spectrum access is useful not only in a cooperative forwarding setup, but also in most dynamic spectrum access scenarios.

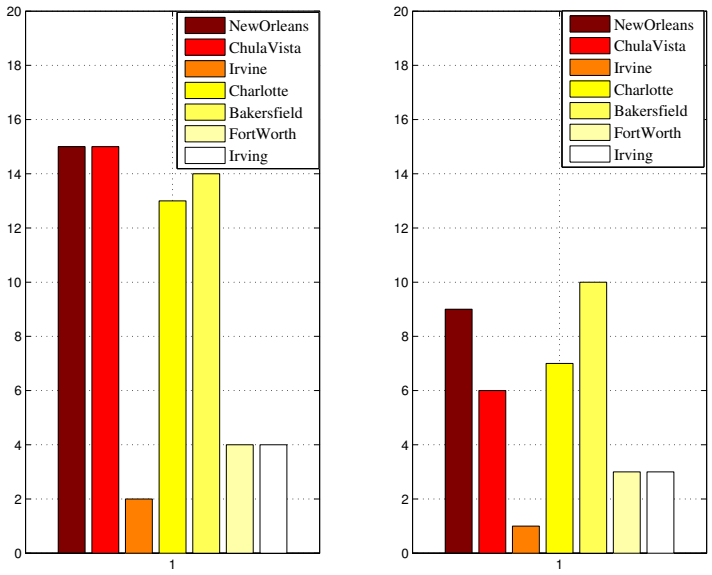

Figure 1.1: Left subfigure shows the number of available TV channels [2] in seven fastest growing cities of USA [3]. Right subfigure shows the number of non-contiguous spectrum chunks among these TV channels in these cities.

1.2 Power Optimal Non-contiguous Spectrum Access

The FCC has opened up 300 MHz in TV bands [14] and plans to open up an additional 500 MHz by 2020 [15] to meet the increasing wireless demand. These channels will be license-by-rule; i.e., any radio can use these channels if it abides by the FCC specifications [15]. If uncoordinated networks (e.g. different broadband wireless service providers) use these channels, they will have to adjust spectrum usage according to their individual traffic demands. As a result, the available spectrum will become partitioned into a set of non-contiguous segments. For some bands, like white space [14], the available spectrum itself is non-contiguous. Fig. 1.1 shows how the number of non-contiguous spectrum chunks varies across seven fastest growing cities of USA [3].

Multi-Channel Multi-Radio (MC-MR) technology allows nodes to simultaneously access multiple fragmented spectrum chunks [33, 34]. However, MC-MR suffers from its traditional hardware based technology. The number of non-contiguous spectrum chunks that a fixed MC-MR radio can access is limited by the number of available radio front ends. In contrast, software defined radio based Non-Contiguous Orthogonal Frequency Division Multiple Access (NC-OFDMA) technology allows nodes to transmit

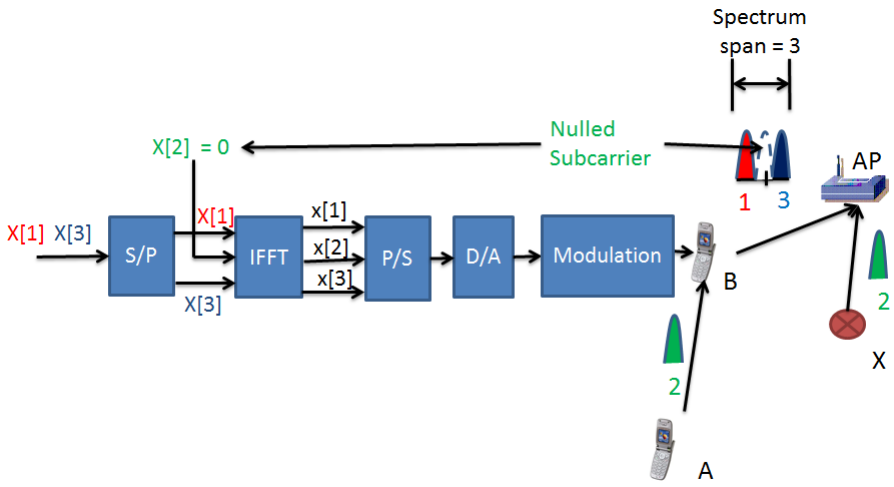

Figure 1.2: Advantages and drawbacks of NC-OFDMA in multi-hop networks

in these non-contiguous spectrum chunks with a single radio front end. Nodes can null interference-limited channels in NC-OFDMA networks. NC-OFDMA also reduces transmission power of the nodes by enabling them to select better channels. Hence, NC-OFDMA has received significant attention in cognitive radio research [35–40]. However, nulling unwanted subcarriers increases the spectrum span and the sampling rate of nodes, since the sampling rate should be at least twice the spectrum span. This, in turn, increases the circuit power consumption of the network.

Fig. 1.2 illustrates the benefits and this inherent challenge of NC-OFDMA in a two-hop network. Node A transmits to the AP via node B. Node B transmits directly to the AP. There are three channels: 1, 2 and 3. Node X, an external interferer, transmits in channel 2. Node B can use NC-OFDMA, transmit in channel 1 and 3 (node A transmits in channel 2) and place null subcarrier in interference limited channel 2. In this scenario, Node B spans 3 channels, instead of 2.

It is well known that the circuit power consumptions of ADC and DAC increase linearly and exponentially with sampling rate and the number of quantization bits respectively [5, 41]. As software defined radios continue to go for higher quantization resolution, the ADC and DAC that are used in the radio circuits will dominate the amount of power consumed. A comparison between Table 1.1 and Table 1.2 shows that power consumption of some commercial ADCs is more than 10 dB higher than

Device Name	Device Type	Max. Sampling Rate (MS/s)	Power Dissipation (mW)
AD 9777 [7]	DAC	150	1056
ADS62P4 [9]	ADC	125	908
ADC 9467B [42]	ADC	250	1333

Table 1.1: (Maximum Sampling Rates and Power Dissipation of Different Commercial ADC and DAC)

Device Type	Allowed Power (mW)	Operating Frequency (MHz)
Fixed	4000	54 - 698
Portable	100	512-698

Table 1.2: Maximum Allowed Power and Operating Frequencies in IEEE 802.22 standard [1]

the maximum allowed transmission power for portable devices in the 802.22 standard. On the one side, NC-OFDMA reduces transmission power by selecting channels with better link gains, while on the other side, this increased spectrum span increases circuit power consumptions of the transceiver. Besides, each ADC/DAC has its maximum sampling rate. A single front end radio might not even be able to occupy two non-contiguous channels that are far apart from each other. We investigate this trade-off between transmission power reduction and circuit power increase and additional hardware constraints in the context of cross-layer optimization of NC-OFDMA based wireless networks.

Specifically, we ask the following question in this work: *How can single front end radio based nodes of a multi-hop network access non-contiguous spectrum chunks?* We investigate this question from a system power perspective and find that *scheduling a small subset of channels may outperform traditional transmit power minimization based approaches since it consumes lesser circuit power.* Our algorithm selects scheduling variables based on the slope of the ADC & DAC's power consumption versus sampling rate curves. We show two special sub-cases of this finding. We find that if the slopes of ADC and DAC's power consumption curves are almost flat, our algorithm converges to transmission power minimization based scheduling algorithms. If the slopes of ADC & DAC's power consumption versus sampling rate curves are very high, our algorithm

selects the channel with the highest link gain. For commercial ADC & DACs whose slopes lie between these two extreme cases, our algorithm selects channels that minimize the summation of transmit and circuit powers of the network.

Our findings regarding the influence of NC-OFDMA on ADC & DAC's circuit power consumption leads us to investigate system power consumption in MC-MR platforms. In the second part of this chapter, we focus on a point-to-point link where both the transmitter and the receiver are equipped with multiple front ends. In this context, we perform joint optimal power allocation and scheduling in each front end of the transmitter and the receiver to minimize the system power of the whole network. *Theoretical analysis and simulation results suggest that, in a practical setting, each front end of an MC-MR enabled node should access "nearby" non-contiguous spectrum chunks using NC-OFDMA.*

1.2.1 Related Work

The authors of [33, 34] characterized the capacity region of an MC-MR based multi-hop network. The authors of [43, 44] focused on software defined radio based multi-hop networks and performed cross layer optimization using a protocol and signal-to-interference-plus-noise-ratio model respectively. Shi and Hou extended the work of [43] and provided a distributed algorithm in [45]. However, none of these works focused on total system power, i.e., summation of transmit and circuit power, and addressed how spectrum fragmentation influences cross-layer decisions.

Consideration of system power has been gaining attention in energy efficient wireless communications literature [46]. Cui et. al. focused on system energy constrained modulation optimization in [5]. Sahai et. al. investigated system power consumption, especially decoder power consumption, in [47]. Isheden and Fettweis assumed circuit power to be a linear function of the data rate [48]. All these works focused on single transceiver pair. Our approach differs from these works in the following way: in NC-OFDMA technology, ADC and DAC consume power not only for the used channels (i.e. transmitted data) but also for the nulled channels. Our work considers the power consumption related with spectrum span and investigates the performance of NC-OFDMA

based multi-hop networks.

The impact of hardware constraints on the performance of NC-OFDMA networks was previously studied in [49, 50]. The authors of [49] performed cross-layer resource allocation when each node's maximum spectrum span is limited by its ADC/DAC. The authors of [50] investigated how guardband, a requirement to reduce cross-band interference, affects the performance of NC-OFDMA based distributed transceiver pairs. Our work incorporates the bundle constraint and uses system power to investigate the performance of NC-OFDMA based multi-hop networks.

Time and frequency mismatch affect NC-OFDMA networks more severely due to their use of a large number of nulled sub-carriers. Therefore, several researchers have implemented different techniques to reduce interference between unsynchronised NC-OFDMA nodes. The authors of [37] have used adaptive multi-bank stop-band filters to reduce interference of unwanted channels. The authors of [36] have used wider guard bands to reduce leakage power into neighbouring channels. We do not focus on synchronization techniques and testbed implementation of NC-OFDMA nodes in our work. What we focus on, instead, is the cross-layer resource allocation of an NC-OFDMA network with a system power perspective. Interested readers are suggested to go through [35–37, 51] to understand the implementation and synchronization details of NC-OFDMA technology.

Up to now, we have focused on the efficient use of additional bandwidth to improve perforamce – both in terms of bandwidth exchange in cooperative networks and non-contiguous spectrum access in non-cooperative networks. Apart from looking for additional spectrum, future network designers will have to focus their efforts on reducing cell sizes to improve the signal-to-noise-ratio between base station and users and to allow more frequency reuse in the system design [12]. This leads us to investigate two different aspects of small cell network design. We introduce these aspects of our work in the following two sections.

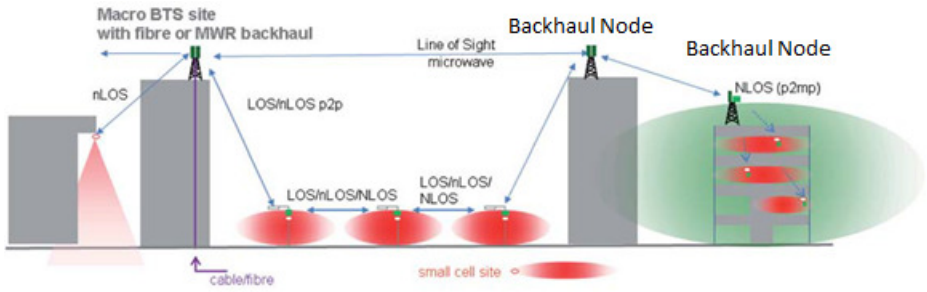

Figure 1.3: Necessity of wireless backhaul in urban small cell networks. This figure is reproduced from [4]

1.3 Wireless Backhaul Node Placement for Small Cell Networks

This part of the thesis focuses on the backhaul design for small cell networks. Small cells come with a significant challenge of providing backhaul to transport data to(from) a gateway node (i.e., a node with existing fiber point, often co-located with a macrocell) in the core network. Fiber based backhaul offers the high data rates needed to meet this requirement, but is costly [52] and time-consuming to deploy, if not already available.

Wireless backhaul can be a valuable option in this regard. One needs to utilize the available bands judiciously to attain the maximum advantage of wireless backhaul. There are multiple candidate bands for wireless backhaul: first, sub-6 GHz band that is useful in non-line-of-sight (NLOS) point-to-multipoint scenarios, microwave band ($6-42$ GHz) that is useful in line-of-sight (LOS) point-to-point scenarios and is currently going through experimental research in NLOS scenarios [53], and millimetre wave band (60, 70 and 80 GHz) that is recently being considered for commercial use in LOS scenarios [16,52]. Small cells that are located at lamp posts, street corners, low rooftops, etc., may not have line-of-sight (LOS) path to the gateway nodes. An effective way to utilize the available bands for wireless backhaul is to place aggregator nodes on top of tall buildings that are located close to small cells. Aggregator nodes can provide high data rate to multiple small cells in NLOS paths, sustain the same data rate to gateway nodes using LOS paths and take advantage of all available bands.

Fig. 1.3 shows the importance of aggregator nodes. The macrocell is located at the second building from the left and it has access to a fiber connection. The red bubbles

denote coverage of the small cells. The small cells located on the left side can directly communicate with the macrocell. The small cells located on the right side do not have good one-hop wireless links with the macrocell and require routing through backhaul nodes to reach the macrocell.

Deployment of aggregator nodes on roof tops of tall buildings consume operational leasing cost. The network operator wants to minimize the operational expenses while ensuring the network connectivity between the small cell and the gateway node. Hence, optimal aggregator node deployment and network connectivity design to minimize the operational expenses is essential for small cell networks. We focus on these two problems in this part of our work. This requires joint cost optimal aggregator node placement, power control, channel scheduling and routing in order to minimize operational expenses of the overall network, which is the focus of this work.

1.3.1 Related work

Relay or aggregator node placement problems have appeared in different scenarios, such as wireless sensor networks (WSN) [54, 55], wireless local area networks (WLAN) [56] and IEEE 802.16j WiMAX networks [57, 58].

In [54], the authors assume a radius coverage based propagation model, and deploy sensor and relay nodes optimally among unconstrained number of candidate locations to solve the connectivity and routing problem. The authors of [55] deploy sensor and relay nodes among a constrained set of candidate locations but assume a radius coverage based propagation model. The authors of [56] solve the relay placement problem in WLAN with uniformly distributed mobile users. In [58], the authors solve relay placement problem in IEEE 802.16j networks while assuming an arbitrary user distribution and distance based propagation. The authors of [57] also focus on IEEE 802.16j networks. They assume nomadic relay nodes and place relays for time varying user demand.

Backhaul node placement in urban small cell networks differs from the mentioned relay placement problems in the following aspects. First, link gain between a candidate

aggregator location and two nearby small cells in a metropolitan setting can vary significantly because of difference in diffraction angles. Coverage radius based backhaul node placement becomes inapplicable. Second, a large subset of relay placement algorithms that assume an unconstrained number of candidate locations cannot be applied here, since only a subset of building rooftops can be leased. Third, both sub-6 GHz and microwave bands are candidate spectrum for future generation small cells. The nature of interference pattern and spatial multiplexing capability varies between the two scenarios and leads to different network optimization problems. Our work encapsulates all these features. We assume an interference free region and time/frequency division multiple access while considering microwave band, and protocol interference model with space division multiple access while considering sub-6 GHz band. Using these assumptions, we optimize the wireless backhaul network in a metropolitan scenario.

Our aggregator node placement module relies heavily on the reliability of the estimated link gains between different nodes of the backhaul network. This leads us to investigate whether existing channel models for dense urban networks can be reliably used in modeling wireless backhaul networks.

1.4 Wireless Channel Measurement Platform Design for Small Cell Networks

There are numerous path loss and delay spread models based on measurements made in a variety of environments, using different transmitter heights and carrier frequencies [59–64]. However, most models have substantial errors when compared to reality [65], due to the complicated nature of wireless propagation through complex environments. Radio propagation measurement, in general, is essential for developing propagation models [66]. A new environment to deploy wireless systems (e.g., small cell systems with base stations that are located at low heights in urban areas) often requires a measurement campaign to determine if existing models can be adapted to it, and if so, what parameters must be changed.

In deployment of small cells in complex, high-value locations (such as dense urban

areas, or unique and complex buildings), propagation modeling or even ray-tracing prediction tools may not account for important and unpredictable realities of target locations. At least spot verification of the modeling outputs and calibrations, by means of a small measurement campaign, may be required. In addition, sophisticated modeling approaches [63,64] may require 3D models of the environment or the associated material properties, which may be difficult and expensive to obtain and yet may not account for hidden metal structures or openings. As a result, a flexible rapid wireless channel measurement approach becomes essential for a small cell network design.

1.4.1 Essential features

We believe that a channel measurement system for designing small cell networks should have the following essential features:

(i) Multiple transmitter single receiver channel sounding

A network designer may have several candidate locations to place small cell base stations. Hence, a multiple transmitter single receiver based channel sounding is desirable since it allows network designers to measure channel propagation characteristics from multiple transmitters during a single run of measurement.

(ii) Small form factor

To further ease the preparation and measurement, the transmitters and the receivers should be reasonably small and light so that they can be quickly and safely placed or mounted on desired locations.

(iii) Low cost

The cost of an individual unit should be low since we will have to use multiple transmitters and receivers.

(iv) Flexibility

The frequency of interests for small cells may vary from one network operator to the other. Hence, the experimental approach should be flexible enough to support channel measurement across a wide frequency region.

1.4.2 Our contributions

To meet the essential features of a channel sounder, we use USRP [67], an inexpensive software defined radio, as our measurement platform. Our approach incorporates the simultaneous measurement of channel propagation characteristics from multiple transmitter locations. Previous works in the related literature [63, 66, 68–71] focused on channel sounding measurements from a single transmitter location. To the best of our knowledge, ours is the only work in the literature that measures channel propagation characteristics simultaneously from multiple transmitter locations.

Traditional channel sounding systems use expensive measurement equipment like vector network analyzers [68,69], vector signal generators [65], spread spectrum channel sounders [63] etc. Due to the open source GNU Radio software [72] and inexpensive USRP radios, our proposed channel sounding system costs only around $1500 per radio and we anticipate reduced costs as SDRs become more popular.

The carrier frequency of the USRP daughterboards can be varied from 1 megahertz (MHz) to 6 gigahertz (GHz). Therefore, our approach can perform channel measurements in this wide frequency range. We expect that the proposed approach, with a few further refinements, can transform the task of propagation measurement for small cell networks as a routine part of day-to-day wireless network engineering.

1.5 Publications

I have published the findings of my PhD thesis in the following conference publications and journal articles:

- *Wireless Backhaul Node Placement for Small Cell Networks*, M. N. Islam, A. Sampath, A. Maharshi, O. Koymen and N. B. Mandayam. Invited paper at

Conference on Information Science & Systems 2014, pp. 1-6, March 2014 [73].

- *A Wireless Channel Sounding System for Rapid Propagation Measurements*, M. N. Islam, B. J. Kim, P. S. Henry and E. Rozner. Proc. International Conference on Communications (ICC) 2013, pp. 5720-5725, June 2013 [74].

- *Implementation of Distributed Time Exchange Based Cooperative Forwarding*, M. N. Islam, S. Balasubramanian, N. B. Mandayam, I. Seskar and S. Kompella, Proc. Military Communications Conference (MILCOM) 2012, pp. 1-6, Oct 2012 [75].

- *Optimal Resource Allocation and Relay Selection in Bandwidth and Time Exchange Based Cooperative Forwarding*, M. N. Islam, N. B. Mandayam and S. Kompella, Proc. 10th International Symposium on Modeling and Optimization in Mobile, Ad Hoc & Wireless Networks (WiOpt), pp. 192-199, May, 2012 [76].

- *Optimal Resource Allocation in a Bandwidth Exchange Enabled Relay Network*, M. N. Islam, N. B. Mandayam and S. Kompella, Proc. MILCOM 2011, pp. 242-247, Nov 2011 [77].

- *Rate Optimal Design of a Wireless Backhaul Network using TV White Space*, R. Kumbhkar, M. N. Islam, N. B. Mandayam and I. Seskar. Submitted to the 7th International Conference on Communication Systems & Networks (COMSNETS 2015). Available online at http://arxiv.org/abs/1409.1661 [78].

- *Power Optimal Non-contiguous Spectrum Access*, M. N. Islam, N. B. Mandayam, S. Kompella and I. Seskar. To be submitted to the IEEE Transactions on Wireless Communications. Available online at http://arxiv.org/abs/1309.0861 [79].

- *Power Optimal Non-contiguous Spectrum Access in Multi Front End Radio Enabled Point-to-point Link*, M. N. Islam, N. B. Mandayam, S. Kompella and I. Seskar. To be submitted to the IEEE Communication Letters. Available online at http://arxiv.org/abs/1409.1606 [80].

- *Wireless Backhaul Network Design for Small Cell Networks*, M. N. Islam, A. Sampath, A. Maharshi, O. Koymen and N. B. Mandayam. Currently under preparation for the IEEE Transactions on Wireless Communications.

Chapter 2

Bandwidth Exchange based Cooperative Forwarding

2.1 Introduction

This part focuses on our work in bandwidth exchange based cooperative forwarding where non-contiguous spectrum chunks are used as incentives for relaying. We consider an N node autonomous network where each node receives an initial amount (equal, optimal based on direct path transmission or arbitrary) of bandwidth and connects directly to the access point (AP) / base station (BS). We consider a frequency division multiple access system where all nodes transmit at the same time with different bandwidth slots. In this context, we focus on a two-hop incentivized cooperative forwarding scheme where a sender node provides bandwidth as an incentive to a forwarder node for relaying its data to the AP/BS. We first prove the concavity of the resource allocation problem and then show that the optimal relay selection problem in α-fair network utility maximization (NUM) reduces to the classical non-bipartite maximum weighted matching (MWM) algorithm [81]. Using the distributed local greedy MWM [82], we propose a simple distributed BE enabled incentivized forwarding protocol. We also show that the outage probability reduction problem reduces to the bipartite maximum matching algorithm in this context. Numerical simulations show that the proposed algorithm provides 20-25% spectrum efficiency gain and 90-98% outage probability reduction in a 20 node network.

2.2 System Model

We consider the uplink of an N node single cell FDMA network. Let $\mathcal{V} = \{1, 2, \cdots, N\}$ denote the set of N nodes that transmit data to the BS (node 0). Each node uses the

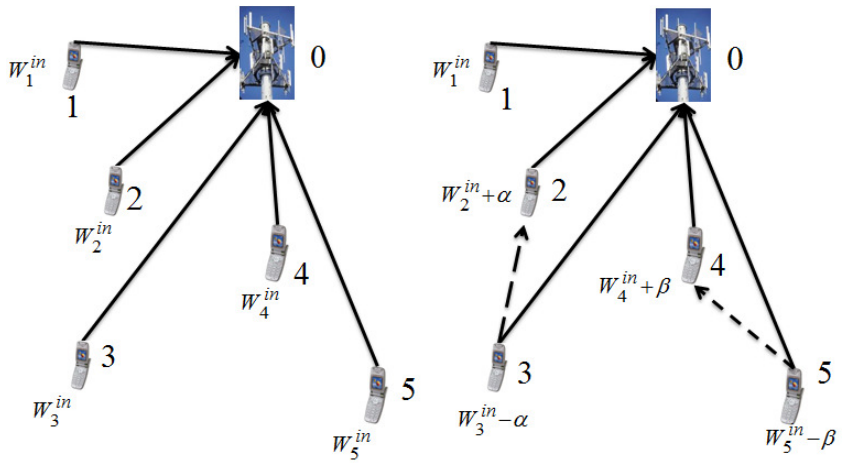

Figure 2.1: Direct Transmission and BE enabled Incentivized Forwarding

total time slot. Node $i \in \mathcal{V}$ is initially allotted a bandwidth of W_i^{in}. Let ρ_{ij} and R_{ij} denote the link gain and achievable rate of the ij path respectively. For a given node $i \in [1, N]$ with W_i^{in} bandwidth and direct link gain ρ_{i0}, the achievable throughput is:

$$R_i^{in} = R_{i0} = W_i^{in} \log_2\big(1 + \frac{\rho_{ij} P_{i,max}}{W_i^{in}}\big) \tag{2.1}$$

Here, $P_{i,max}$ denotes the maximum transmission power of node i and R_i^{in} is expressed in bit per second (bps).

In BE, nodes perform two hop half duplex DF cooperative relaying. The forwarder node hears the sender nodes' data and relays some of that data along with transmitting its own data to the AP. Since each node is a power constrained device, the forwarder nodes' data rate may drop if it continues to transmit with the same bandwidth. Therefore, the sender node delegates some of its bandwidth to the forwarder node as incentives for relaying. We consider one forwarder for one sender and vice versa to reduce the relay searching complexity. Let $\mathcal{SF} = \{\mathcal{SF}_1, \cdots, \mathcal{SF}_K\} = \{(s_1, f_1), (s_2, f_2), \cdots, (s_K, f_K)\}$ denote the sender-forwarder pair set, i.e., f_i relays s_i's data along with transmitting f_i's own data. Let $\mathcal{D} = d_1, d_2, \cdots, d_L$ denote the direct set, i.e., the set of remaining nodes that transmit data without cooperation. Note that, K and L are variables and further, $2 * K + L = N$. We assume pairwise bandwidth constraint in this work.

The left and right sides of Fig. 2.1 show the considered direct transmission model

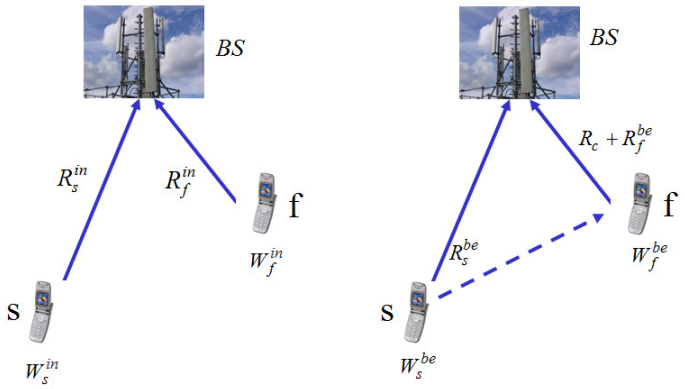

Figure 2.2: BE Enabled Forwarding in a 3 Node Network

Table 2.1: Summary of used notations

Notation	Meaning
N	Total number of users
P	Maximum transmission power
ρ_{ij}	Gain of the ij link
W_i^{in}	Initial bandwidth of node i
W_i^{be}	Node i's bandwidth in BE
R_i^{in}	Initial rate of node i
R_i^{be}	Node i's rate in BE
R_{ij}	Achievable rate in the ij link
$\mathcal{V}$	Set of all nodes
$\mathcal{D}$	Set of nodes that transmit without cooperation
$\mathcal{SF}$	Set of sender-forwarder pairs
SF_i	i^{th} sender-forwarder pair (s_i, f_i)

and the proposed BE model. In BE, node 2 relays data for node 3. Node 3 delegates α amount of bandwidth to node 2 as incentive for relaying. Let W_i^{be} represent the bandwidth of node i in the BE scenario. Now, $W_2^{be} = W_2^{in} + \alpha$ and $W_3^{be} = W_3^{in} - \alpha$. Node 4 and 5 operate in the same manner.

Nodes don't do power allocation among different streams in our framework. Since capacity is a non-decreasing function of transmission power, each node utilizes the maximum transmission power in its allotted bandwidth slot. Without loss of generality, we assume $P_{i,max} = P \, \forall \, i \in \mathcal{V}$ in the subsequent analysis.

Rate analysis in the BE scenario:

Let R_i^{be} represent the achievable rate of node i in the BE scenario. The right side of Fig. 2.2 shows the interaction between a sender node s and a forwarder node f. If node s transmits to node f and the BS *separately* using W_s^{be} bandwidth, the achievable throughput in the respective paths are:

$$R_{sf} = W_s^{be} \log_2\big(1 + \frac{\rho_{sf} P}{W_s^{be}}\big) \tag{2.2}$$

$$R_{s0} = W_s^{be} \log_2\big(1 + \frac{\rho_{s0} P}{W_s^{be}}\big) \tag{2.3}$$

If f transmits to the BS using W_f^{be} bandwidth,

$$R_{f0} = W_f^{be} \log_2\big(1 + \frac{\rho_{f0} P}{W_f^{be}}\big) \tag{2.4}$$

Assuming $\rho_{sf} \geq \rho_{s0}$, it is easily seen that $R_{sf} \geq R_{s0}$. Due to the nature of the wireless environment, when sender s transmits, both f and BS hear it. If node s transmits at rate R_{sf}, node f can decode it properly. The BS also receives the same signal but can't decode it properly since $R_{sf} \geq R_{s0}$. However, node f can forward R_c bits to the BS to resolve the BS's uncertainty about node s's data. Node f also transmits its own data, R_f^{be}, to the BS. The information theoretic generalization of the maximum-flow-minimum-cut-theorem [83] provides the following relationship between these achievable rates,

$$R_s^{be} \leq \min(R_{sf}, R_{s0} + R_c) \tag{2.5}$$

$$R_c + R_f^{be} \leq R_{f0} \tag{2.6}$$

The codebook design procedure to achieve these rates is summarized in Appendix B.1. A detailed description can be found in [83, 84].

Using this rate analysis, we focus on the distributed joint optimal bandwidth allocation and relay selection in maximizing the summation of the α-fair utilities of the network.

α-fair utility: The α-fair utility is defined for any $\alpha \in [0, \infty)$, as [85],

$$U^{\alpha}(R) = \begin{cases} \frac{R^{1-\alpha}}{1-\alpha}, & \text{if} \quad \alpha \neq 1 \\ log(R), & \text{if} \quad \alpha = 1 \end{cases} \tag{2.7}$$

where R represents the rate of the user. Summation of α-fair utility functions takes the form of different well known utility functions, e.g., sum rate maximization ($\alpha = 0$), proportional fairness ($\alpha = 1$) and minimum rate maximization ($\alpha = \infty$).

2.3 Design Objective

We begin with a focus on α-fair NUM of the overall network through optimal bandwidth and rate allocation for all possible sender-forwarder pairing sets.

Problem I

$$\max . \sum_{d \in \mathcal{D}} U^{\alpha}(R_d^{be}) + \sum_{(s,f) \in \mathcal{SF}} \left(U^{\alpha}(R_f^{be}) + U^{\alpha}(R_s^{be}) \right) \tag{2.8a}$$

$$\textbf{s.t.} \ (R_f^{be}, R_s^{be}) \in conv(W_f^{be}, W_s^{be}) \ \forall \, (s,f) \in \mathcal{SF} \tag{2.8b}$$

$$R_f^{be} \geq R_f^{in} \, , \, R_s^{be} \geq R_s^{in} \ \forall \, (s,f) \in \mathcal{SF} \tag{2.8c}$$

$$W_f^{be} + W_s^{be} \leq W_f^{in} + W_s^{in} \ \forall \, (s,f) \in \mathcal{SF} \tag{2.8d}$$

$$W_f^{be}, \, W_s^{be} \geq 0 \ \forall \, (s,f) \in \mathcal{SF} \tag{2.8e}$$

$$\mathcal{D} \subseteq \mathcal{V} \, , \, \mathcal{SF} \in \mathcal{V} \times \mathcal{V} \, , \, \mathcal{SF}_i \cap \mathcal{SF}_j = \emptyset \ \forall i \neq j \tag{2.8f}$$

$$\mathcal{SF}_i \cap \mathcal{D} = \emptyset \, \forall \, i \in [1, K] \tag{2.8g}$$

$$\mathcal{SF}_1 \cup \mathcal{SF}_2 \cdots \cup \mathcal{SF}_K \cup \mathcal{D} = \mathcal{V} \tag{2.8h}$$

$$Variables \ \mathcal{D}, \mathcal{SF}, R_s^{be}, R_f^{be}, W_s^{be}, W_f^{be}$$

Here, $R_d^{be} = R_d^{in} \, \forall \, d \in D$. Therefore, the rates of the direct node set are not optimization variables. Equation (2.8b) denotes that the rate of the sender and forwarder

lie in the convex hull of the allocated bandwidth. The details of this convex hull has already been explained in the system model. It will also be mentioned in the next section. Eq. (2.8c) represents that the sender and the forwarders' rate cannot drop below their initial rates. Equation (2.8d) shows that the total bandwidth used by the cooperative pair is constrained by the summation of the initial bandwidths allocated to the individual nodes. Equation (2.8f)- (2.8h) represent the relay selection constraints. Equation (2.8f) shows that the direct and sender-forwarder sets are all subsets of the overall set. Eq. (2.8g) denotes that the sender-forwarder pairs and direct set cannot have any common nodes. Eq. (2.8h) represents that the union of the pairs and the direct set form the overall set $\mathcal{V}$.

The solution of the above optimization problem depends on the selected sender-forwarder and direct node set and the corresponding bandwidth and rate allocations. Hence, it involves an exponential number of variables and constraints. In the rest of the chapter, we focus on solving this problem.

2.4 Optimization Problem Solution

2.4.1 Modified Optimization Problem

Let $U^{\alpha}(R_{tot}) = \sum_{i \in \mathcal{V}} U^{\alpha}(R_i^{in})$ denote the summation of the initial utilities of the nodes. For a fixed $\mathcal{SF}$, $U^{\alpha}(R_{tot})$ can be expressed in the following form:

$$
\begin{aligned}
& U^{\alpha}(R_{tot}) \\
= & \sum_{i \in \mathcal{V}} U^{\alpha}(R_i^{in}) \\
= & \sum_{d \in \mathcal{D}} U^{\alpha}(R_d^{in}) + \sum_{(s,\, f) \in \mathcal{SF}} \left(U^{\alpha}(R_f^{in}) + U^{\alpha}(R_s^{in}) \right) && (2.9) \\
= & \sum_{d \in \mathcal{D}} U^{\alpha}(R_d^{be}) + \sum_{(s,\, f) \in \mathcal{SF}} \left(U^{\alpha}(R_f^{in}) + U^{\alpha}(R_s^{in}) \right) && (2.10)
\end{aligned}
$$

Equation (2.9) follows from eq. (2.8h). Equation (2.10) uses the fact that $R_d^{be} = R_d^{in} \, \forall \, d \in D$. Subtracting $U^{\alpha}(R_{tot})$ from the objective function of I, we find the following optimization problem:

Problem II

$$\sum_{(s,\,f)\in\mathcal{SF}} \left(U^{\alpha}(R_f^{be}) + U^{\alpha}(R_s^{be}) - U^{\alpha}(R_f^{in}) + U^{\alpha}(R_s^{in})\right) \tag{2.11a}$$

$$\textbf{s.t. } (R_f^{be}, R_s^{be}) \in conv(W_f^{be}, W_s^{be}) \; \forall\, (s,f) \in \mathcal{SF} \tag{2.11b}$$

$$R_f^{be} \geq R_f^{in}\,,\; R_s^{be} \geq R_s^{in} \; \forall\, (s,f) \in \mathcal{SF} \tag{2.11c}$$

$$W_f^{be} + W_s^{be} \leq W_f^{in} + W_s^{in} \; \forall\, (s,f) \in \mathcal{SF} \tag{2.11d}$$

$$W_f^{be},\, W_s^{be} \geq 0 \; \forall\, (s,f) \in \mathcal{SF} \tag{2.11e}$$

$$\mathcal{D} \subseteq \mathcal{V}\,,\; \mathcal{SF} \in \mathcal{V} \times \mathcal{V}\;,\; \mathcal{SF}_i \cap \mathcal{SF}_j = \emptyset \; \forall i \neq j \tag{2.11f}$$

$$\mathcal{SF}_i \cap \mathcal{D} = \emptyset \, \forall\, i \in [1, K] \tag{2.11g}$$

$$\mathcal{SF}_1 \cup \mathcal{SF}_2 \cdots \cup \mathcal{SF}_K \cup \mathcal{D} = \mathcal{V} \tag{2.11h}$$

$$Variables\; \mathcal{D}, \mathcal{SF}, R_s^{be}, R_f^{be}, W_s^{be}, W_f^{be}$$

The inclusion of constant terms in the objective function does not change the optimal variables of an optimization problem [86]. As a result, the same set of sender-forwarder pairs maximize both problem I and II. We will focus on solving problem II in the subsequent analysis. The optimal variables of problem II will directly lead to the optimal solution of problem I.

Problem II depends on both relay selection and resource allocation. The very nature of the design objective allows us to split the optimization formulation into the following two parts:

- For any fixed set of sender-forwarder pairs, perform DF based optimal rate and bandwidth allocation.
- Choose the relay set that maximizes the summation of the α-fair utility of the nodes.

We, at first, focus on resource allocation in a fixed sender-forwarder pair set $\mathcal{SF}$ and

direct node set $\mathcal{D}$. Later, we will show the optimal sender-forwarder pair selection policy.

2.4.2 Optimal bandwidth and rate allocation for a fixed sender-forwarder set

The optimal resource allocation problem for fixed $\mathcal{SF}$ and $\mathcal{D}$ takes the following form:

Problem III

$$\sum_{(s,\,f)\in\mathcal{SF}} \big(U^{\alpha}(R_f^{be}) + U^{\alpha}(R_s^{be}) - U^{\alpha}(R_f^{in}) - U^{\alpha}(R_s^{in})\big) \tag{2.12a}$$

$$\mathbf{s.t.}\,(R_f^{be}, R_s^{be}) \in conv(W_f^{be}, W_s^{be})\ \forall\,(s,f) \in \mathcal{SF} \tag{2.12b}$$

$$R_f^{be} \geq R_f^{in}\ ,\ R_s^{be} \geq R_s^{in}\ \forall\,(s,f) \in \mathcal{SF} \tag{2.12c}$$

$$W_f^{be} + W_s^{be} \leq W_f^{in} + W_s^{in}\ ,\ W_f^{be}, W_s^{be} \geq 0\ \forall\,(s,f) \in \mathcal{SF} \tag{2.12d}$$

$$Variables\ R_s^{be},\, R_f^{be},\, W_s^{be},\, W_f^{be} \tag{2.12e}$$

Now, due to the pairwise bandwidth constraint of (2.12d), the bandwidth allocation in one cooperative pair does not affect other nodes. Therefore, problem III is just the summation of K independent three node (sender, forwarder and BS) resource allocation problems and can be decomposed into the subproblems. Hence, we now focus on an arbitrary sender-forwarder pair (s, f) and describe the resource allocation problem formulation in this pair.

Problem IV

$$\max.\ U^{\alpha}(R_f^{be}) + U^{\alpha}(R_s^{be}) - U^{\alpha}(R_f^{in}) - U^{\alpha}(R_s^{in}) \tag{2.13a}$$

$$\begin{aligned}
\mathbf{s.t.}\ R_{sf} &\leq W_s^{be}\log_2\big(1 + \frac{P * \rho_{sf}}{W_s^{be}}\big)\\
R_{s0} &\leq W_s^{be}\log_2\big(1 + \frac{P * \rho_{s0}}{W_s^{be}}\big)\\
R_c + R_f^{be} &\leq W_f^{be}\log_2\big(1 + \frac{P * \rho_{f0}}{W_f^{be}}\big)
\end{aligned} \tag{2.13b}$$

$$R_s^{be} \leq \min(R_{sf}, R_{s0} + R_c)\,,\; R_f^{be} \geq R_f^{in}\,,\; R_s^{be} \geq R_s^{in} \tag{2.13c}$$

$$W_f^{be} + W_s^{be} \;\leq\; W_f^{in} + W_s^{in}\;,\; W_f^{be}, W_s^{be} \geq 0 \;\forall\, (s,f) \in \mathcal{SF} \tag{2.13d}$$

$$Variables\;\; R_s^{be}, R_f^{be}, W_s^{be}, W_f^{be}, R_c$$

Equation (2.13b) and (2.13c) show the convex hull of the allotted bandwidths and the achievable rates. They have also already been described in the system model.

Lemmma 1: Problem IV is a concave maximization problem.

Proof: $U^{\alpha}(R_f^{in})$ and $U^{\alpha}(R_s^{in})$ are the utilites of the initial data rates and constants, in terms of the optimization variables. The concavity of α-fair utility functions and the capacity expressions can be easily shown [86]. The minimum of linear (concave) functions is concave. Thus, the objective function is concave and the constraints are convex or linear in terms of the optimization variables. This proves the concavity of Problem IV. ■.

Problem IV can be solved using standard convex optimization algorithms, e.g., interior point methods [86].

Lemma 2: $(R_s^{be}, R_f^{be}, W_s^{be}, W_f^{be}, R_c) = (R_s^{in}, R_f^{in}, W_s^{in}, W_f^{in}, 0)$ is a feasible set of variables of Problem IV.

Proof: Let $W_f^{be} = W_f^{in}$, $W_s^{be} = W_s^{in}$, $R_c = 0$. Then,

$$\begin{aligned} R_{sf} &= W_s^{in} \log_2\big(1 + \frac{P * \rho_{sf}}{W_s^{in}}\big) \\ R_{s0} &= W_s^{in} \log_2\big(1 + \frac{P * \rho_{s0}}{W_s^{in}}\big) = R_s^{in} \end{aligned} \tag{2.14}$$

$$\begin{aligned} R_f^{be} &= W_f^{in} \log_2\big(1 + \frac{P * \rho_{f0}}{W_f^{in}}\big) = R_f^{in} \\ R_s^{be} &= \min(R_{sf}, R_{s0} + R_c) = \min(R_{sf}, R_{s0}) = R_s^{in} \end{aligned}$$

This is a feasible solution of problem IV. ■

Thus, if Node s and f use their initial bandwidths and if the forwarder f does not relay any data of the sender s, both sender and forwarder will continue to transmit at

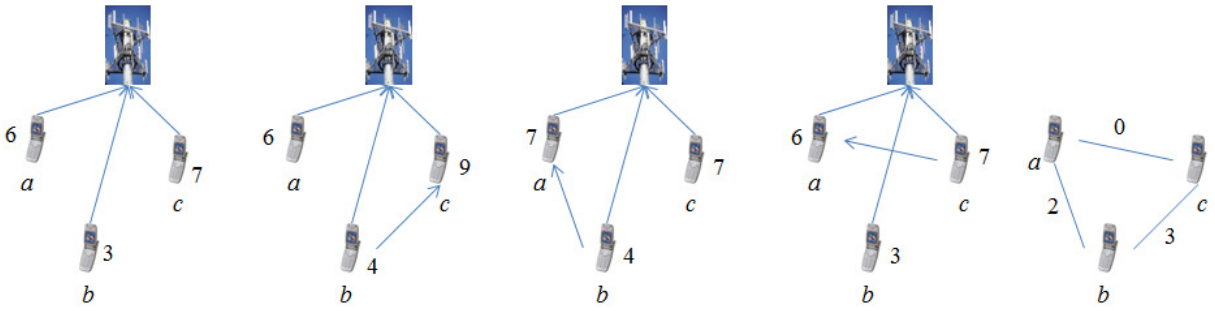

Figure 2.3: MWM in BE Enabled Relay Network

their initial rates. The corresponding feasible solution for these variables can be found as follows,

$$U^{\alpha}(R_f^{be}) + U^{\alpha}(R_s^{be}) - U^{\alpha}(R_f^{in}) - U^{\alpha}(R_s^{in})$$
$$= U^{\alpha}(R_f^{in}) + U^{\alpha}(R_s^{in}) - U^{\alpha}(R_f^{in}) - U^{\alpha}(R_s^{in}) = 0$$

Since, problem IV is a concave maximization probelm, the optimal solution will not drop below 0 [86]. Hence, the proposed BE enabled relaying scheme will perform at least as good as the initial allocation and *seek to maximize the global utility while preserving the initial rates of the individual nodes.*

Lemma 3: Problem III is a concave maximization problem.

Proof: Problem III is the combination of K disjoint concave maximization problems and hence it's concave. ■

2.4.3 Optimal sender-forwarder set selection

Let g_{sf}^* denote the solution of problem IV, i.e., the optimal gain obtained through cooperation of (s, f). Let, $U_{\mathcal{D},\mathcal{SF}}^*$ represent the optimal solution of problem III, i.e., the optimal cooperation gain for the selected sender-forwarder pair set $\mathcal{SF}$. Then, $U_{\mathcal{D},\mathcal{SF}}^* = \sum_{(s,f)\in\mathcal{SF}} g_{sf}^*$. Therefore, the sender-forwarder pairing set selection part of problem II is equivalent to finding the set of pairs that maximize the gain in utility through cooperation, over noncooperation. It can be written in the following form:

Problem V

$$\arg\max_{\mathcal{SF}} \sum_{(s,\,f)\in\mathcal{SF}} g^*_{sf} \tag{2.15a}$$

$$\mathcal{SF} \in \mathcal{V}\times\mathcal{V}\ ,\ \mathcal{SF}_i \cap \mathcal{SF}_j = \emptyset\ \forall i \neq j\,, \tag{2.15b}$$

Now, consider a graph $\mathcal{G} = (\mathcal{V}, \mathcal{E})$ where the vertices $\mathcal{V}$ represent the set of N nodes under consideration and $\mathcal{E}$ denote the edges between these nodes. Define the edge weight of any (i, j) pair by $U^\alpha(R_i^{be}) + U^\alpha(R_j^{be}) - U^\alpha(R_i^{in}) - U^\alpha(R_j^{in})$, i.e., the difference, in terms of utility, between the cooperation and non-cooperation scenario. The optimal sender-forwarder pairing set selection of problem V is equivalent to finding the set of pairs that maximize the difference between cooperation and noncooperation utility. Hence, the optimal sender-forwarder pair selection problem can be reduced to the problem of finding the set of pairs that maximizes the link weights mentioned above. Thus, the optimal relay selection converges to the classical nonbipartite MWM problem. The nonbipartite MWM algorithm has been summarized in Appendix B.2. A detailed description can be found in [81].

Fig. 2.3 illustrates the application of MWM in the sender-forwarder pairing selection. The left figure of Fig. 2.3 denote the initial scenario where node a, b and c transmit through the direct path and transmit 6, 3 and 7 bits respectively. The three figures in the middle show the obtained rates for different sender-forwarder pair selection. The second figure from the left shows that b and c transmit 4 and 9 bits respectively through BE enabled DF cooperation. Thus, the utility gain of cooperation, over noncooperation, is 3 bits. The middle figure and the 2nd figure from the right represent the cooperation scenarios of (a, b) and (a, c) respectively. The rightmost figure represents the edge weights of each cooperative pair in terms of the utility gain of cooperation, over noncooperation. The MWM algorithm will select node (b, c) as the cooperative pair and node a will transmit without cooperation.

Centralized nonbipartite MWM can be solved optimally in $O(N^3)$ time [81]. Our proposed distributed incentivized forwarding is based on the distributed local greedy MWM [82] ($O(N^2)$) and is described below. The distributed MWM algorithm [82] is summarized in Appendix B.3.

2.4.4 Distributed BE incentivized forwarding protocol

- Focus on an arbitrary node, node v. Node v sends training symbols to the AP and obtains its own direct channel, ρ_{v0}, through feedback. Node v is initially allocated W_v^{in} bandwidth and transmits at R_v^{in} rate.
- Let node u be a neighbouring node of v. Due to the nature of wireless channels, node u receives node v's channel estimation training symbols and finds the inter-node channel gain, ρ_{uv}.
- v sends an omnidirectional signal containing ρ_{v0}, W_v^{in} and R_v^{in} to the neighbouring nodes.
- Node u may relay node v's data if $min(\rho_{uv}, \rho_{u0}) \geq \rho_{v0}$. Thus, v knows its potential forwarders or senders.
- v solves problem IV for the suitable neighbours. Thus, each node knows its adjacent link weights.
- v solves the distributed local greedy MWM algorithm of [82].
- The 'matched pairs' allocate resources among themselves. The 'unmatched' nodes transmit without cooperation.

2.4.5 Outage probability reduction in BE

We define outage probability as the ratio of the number of nodes that do not get minimum data rate to the total number of nodes. We assume that each node in the network starts with an initial amount of resource. Depending on the resource and link gains, nodes fall in the following two groups:

- Outage group: Node that cannot meet the minimum required rate with initially allocated resources.
- Non-Outage group: Node that can meet the minimum rate with initially allocated resources.

The outage probability reduction problem can be defined as providing minimum data rate to the most number of users in the outage group, while maintaining the minimum data rate of the nodes, in the non-outage group. MWM based matching and pairwise resource allocation based incentivized two-hop forwarding can help in this case. We propose the following scheme in this regard:

- Each node in the outage group solves the pairwise sumrate maximization, with minimum rate constraints, for each of its neighbouring node. Nodes can solve sumrate maximization by plugging $\alpha = 0$ in the α-fair utility function.
- If the node in outage can maintain minimum data rate by pairing with the forwarder, i.e., the non-outage node, we assume that an edge exists between these nodes.
- The relay selection problem in outage probability reduction becomes maximizing the number of edges in the network. This reduces to the maximum matching (MM) algorithm in a bipartite graph [87].

Our focus here is to maximize the number of users that receive minimum data rate, not to maximize any utility function. That's why, we use MM, instead of MWM, in this part of the work. Besides, cooperation between two nodes in the non-outage group do not change the outage probability of the network. Therefore, we consider a bipartite graph by dividing the graph into outage and non-outage group.

2.5 Numerical Simulations

We assume equal initial bandwidth allocation in all of our simulations, i.e., nodes start with equal bandwidth. However, our work is readily applicable to the scenario where nodes start with optimal bandwidth allocation (based on direct path transmission) and then use bandwidth as incentives for two hop relaying.

Fig. 2.4 and Fig. 2.5 compare the performance of BE relaying with that of direct path transmission in the sumrate maximization and minimum rate maximization of a 3 node network (sender, forwarder and BS). Both sender and forwarder initially receive

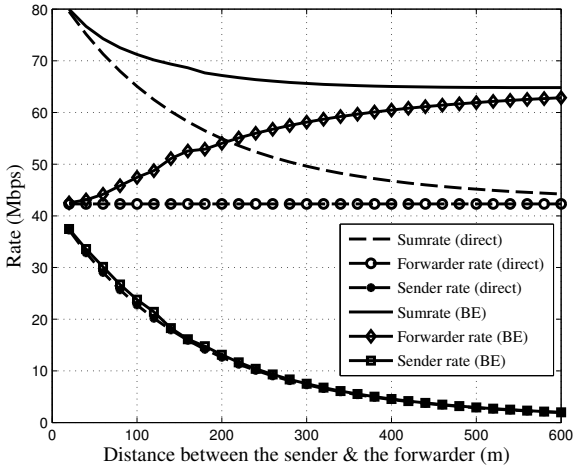

Figure 2.4: Sumrate Maximization in a 3 Node Network, 10 MHz per Node, $P = 100$ mW, Near node-AP distance = 150m

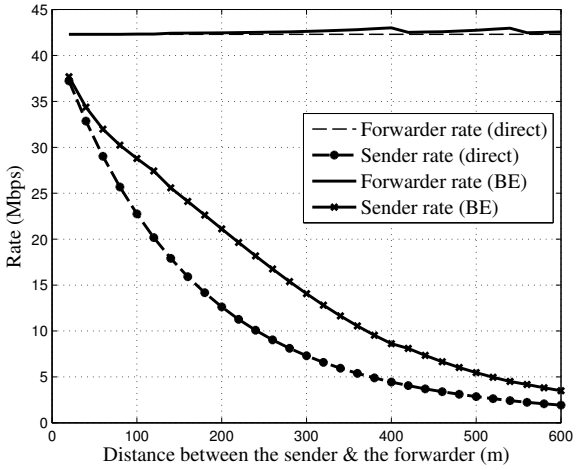

Figure 2.5: Minimum Rate Maximization in a 3 Node Network, 10 MHz per Node, $P = 100$ mW, Near node-AP distance = 150m

10 MHz bandwidth and transmit uplink data to the BS. The forwarder node is placed in the straight line that connects the BS and the sender node. The distance between the forwarder node and the BS is kept fixed at 150m, whereas, the distance between the BS & the sender node is varied. In these two simulations, we assumed the link gains to take the form, $\rho_{ij} = kd_{ij}^{-3}$ where d_{ij} is the distance between the i^{th} and j^{th} node. k is the proportionality constant that also captures the noise spectral density and is set to $k = 6 \times 10^6 MHz * m^3/mW$ [22].

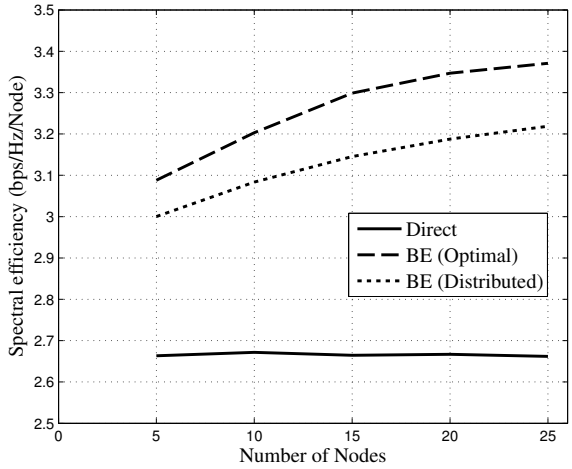

Figure 2.6: Spectrum Efficiency in an N Node Network, 1 MHz per Node, $P = 20$ dBm

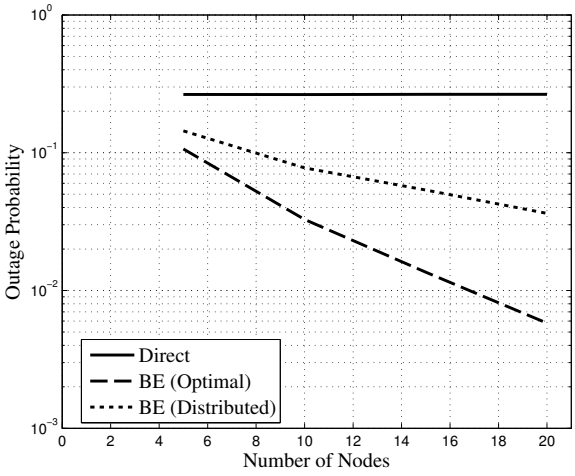

Figure 2.7: Outage Probability in an N Node Network, 1 MHz per Node, $P = 20$ dBm

The sumrate maximization objective based plot of Fig. 2.4 shows that BE relaying improves the rate of the forwarder (near user) while ensuring that the sender's (far user) rate does not drop below its initial value. This increase in the forwarders' rate gets reflected in the sumrate gain of the network. On the other hand, the minimum rate maximization objective based plot of Fig. 2.5 shows that BE relaying improves the senders' (far user) rate while ensuring that the forwarders' (near user) rate does not drop. This diverse contribution of BE relaying comes from the problem objectives of the respective simulations; sumrate maximization ($\alpha = 0$) is the most efficient allocation whereas minimum rate maximization ($\alpha = \infty$) is the most fair one. Therefore, the use of any $\alpha \in (0, \infty)$ would have increased both users' rates in this simulation scenario.

Figure 2.8: Orbit Testbed

Fig. 2.6 and Fig. 2.7 show the performance of BE relaying in an N node network. In these simulations, we assumed that links are under independent Rayleigh fading and the link gain in each slot is an independent realization of Rayleigh random variable. This means that the link gain, ρ_{ij}, is exponentially distributed, $p(\rho_{ij}) = \frac{1}{\bar{\rho}_{ij}} exp\big(-\frac{\rho_{ij}}{\bar{\rho}_{ij}}\big)$ where $\bar{\rho}_{ij} = kd_{ij}^{-3}$ and $k = 6 \times 10^6 MHz * m^3/mW$. We consider a circular cell of $800m$ radius. The AP is located at the center, whereas, the nodes are placed randomly in the cell. We considered transmission scheme much like the one used in mobile Wimax. Each node is preassigned 20 dBm transmit power and 1 MHz bandwidth. We used the matching code of [88] to implement the MWM algorithm in Matlab.

We showed the performance of both centralized and distributed algorithms in Fig. 2.6 and Fig. 2.7. In the simulation of the distributed algorithm, we assumed that each node can only talk to its neighbours that are located within 500m from the sender node. Fig. 2.6 shows that the centralized and decentralized algorithm improves the spectral efficiency by 25% and 20% respectively. The performance of the distributed algorithm will improve if we allow each node to talk to neighbours with greater distances.

Fig. 2.7 shows that BE enabled relaying provides cooperative diversity and significantly reduces the outage probability (90-98%). Thus, BE can be used to extend the coverage in an autonomous network.

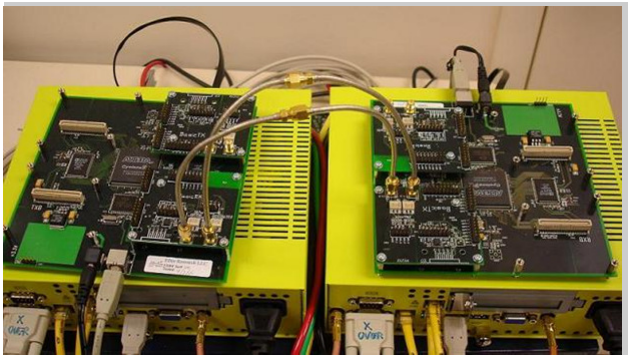

Figure 2.9: USRP Daughterboards

2.6 Experimental Setup

Inspired by the simulation results of bandwidth exchange, we investigate the influence of resource exchange in an experimental setup. Due to experimental constraints, we implement time exchange to observe the advantages of incentive based cooperative forwarding. In time exchange protocol, sender node offers a portion of its own allotted time slot to the forwarder node as an incentive of relaying.

2.6.1 ORBIT Testbed & USRP Nodes

We implement the proposed TE based incentivized algorithm among the USRP nodes of ORBIT, an indoor wireless testbed of Wireless Information Network Laboratory (WINLAB), Rutgers University. ORBIT has 400 nodes, overall, in a $20m \times 20m$ square grid. Fig. 2.8 shows a snapshot of the ORBIT testbed.

ORBIT has 28 USRP nodes that can be used in software defined radio based experiments. Fig. 2.9 shows the snapshots of two USRP daughter boards. We use the GNU radio software toolkil [72] to run experiments in these USRP nodes. Specifically, we use the benchmark-tx.py and benchmark-rx.py codes to transmit and receive packets between two USRP nodes [72]. The flexibility of GNUradio allows us to change the transmission power level and packet sizes through software. This variable power capability of GNUradio, along with the spatial separation among the nodes, allow us to create links with different strengths between different node pairs.

As shown in the top left subfigure of Fig. 2.10, we use four USRP nodes of the

ORBIT testbed to conduct the TE based cooperative forwarding experiments. Node 1, 2 and 3 constitute the user set $\mathcal{V}$ and node 0 serves as the BS. The ORBIT grid is used as a global control plane to exchange the control information between the nodes.

2.6.2 Selection of Parameters

The benchmark-tx.py and benchmark-rx.py codes of GNUradio allow the following four modulation schemes: a) GMSK, b) differential binary phase shift keying (DBPSK), c) differential quadrature phase shift keying (DQPSK) and d) differential 8 phase shift keying (D8PSK). DBPSK, DQPSK and D8PSK are found to be very sensitive to peak power clippings due to their variable envelope waveform. Therefore, we use a fixed modulation scheme, GMSK, in our experiments.

Each node transmits at 1 Mbps and each packet contains 1500 bytes. As a result, it takes $(1500 * 8)/(1 * 10^6)$, i.e., 0.012 second to transmit one packet. We assume each time slot to be 0.012 second long, i.e., one packet is transmitted in each slot.

The total transmission time is assumed to be 3 second. Each node is initially allotted 1 second transmission time, i.e., 1/0.012 or 83 time slots. We approximate the number of time slots since fractional packet transmission is not considered.

We also add 32 bit CRC sequence in each packet and make it similar to the Ethernet packet structure [89]. Note that, we do not use error control coding in these experiments. Therefore, the presence of a single bit error leads to the 'loss' of the whole packet due to CRC.

2.7 Experimental Evaluation

2.7.1 Illustration of MWM in Relay Selection

Fig. 2.10 shows the use of MWM in the optimal sender-forwarder pair selection among 3 testbed nodes. The left figure of the top row shows the packet loss probability between the inter-node pairs. These packet error probabilities were based on 1500 byte packet length, GMSK modulation, some fixed power level and CRC checking. The middle figure of the top row focuses on the direct transmission scenario and shows the goodput

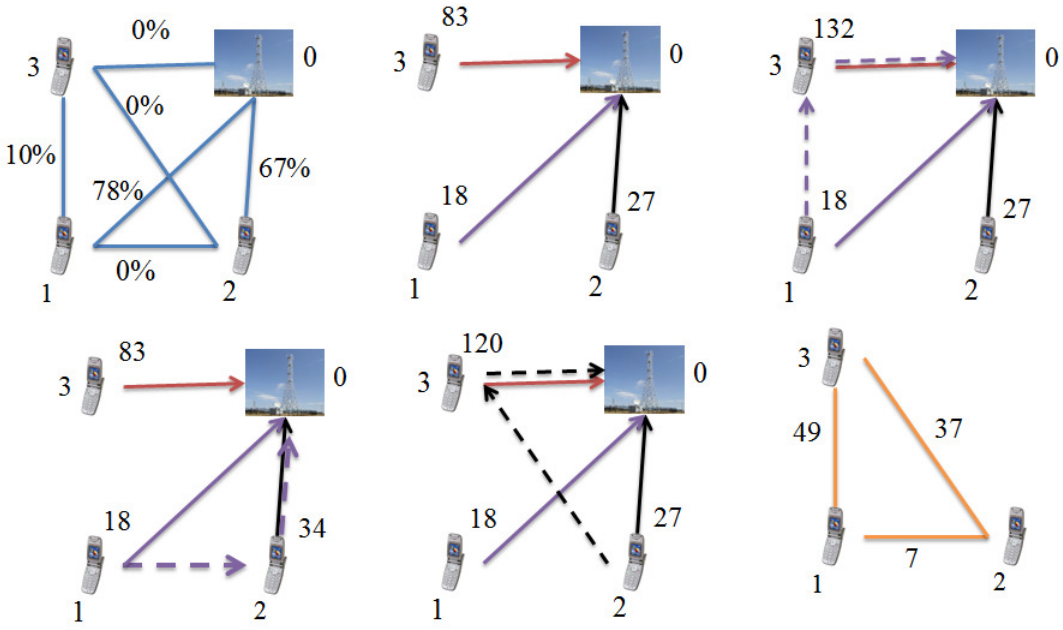

Figure 2.10: Illustration of MWM in sender-forwarder pair selection

(in packet/3 second) of each node. Each node initially receives 83 time slots and transmits one packet at each slot through the direct path. The packet error probability in link 30 is 0%. Therefore, all transmitted packets of node 3 reach the BS. Node 1 and 2's goodputs are considerably lower due to the high packet error probability in link 10 and 20 respectively.

The top right, the bottom left and the bottom middle figure show the goodput (in packet/3 second) of different sender-forwarder cooperation scenarios. The top right figure focuses on the TE based cooperation between node 1 and 3. Here, node 1 and 3 solve the two node time slot allocation optimization of problem III. The cooperation allows node 3 to achieve a goodput of 132 packets and ensures that node 1's goodput does not drop below 18 packets, its initial value. Therefore, the overall goodput gain obtained through the cooperation of node 1 and 3 is 49 packets. As a result, the 13 link of the MWM graph, shown in the bottom right figure, is assigned a weight of 49.

The bottom left and bottom middle figures demonstrate the cooperation scenario in node 1–2 and 2–3 respectively. The bottom right figure shows the link weight of the corresponding cooperation pairs. The distributed local greedy MWM selects link

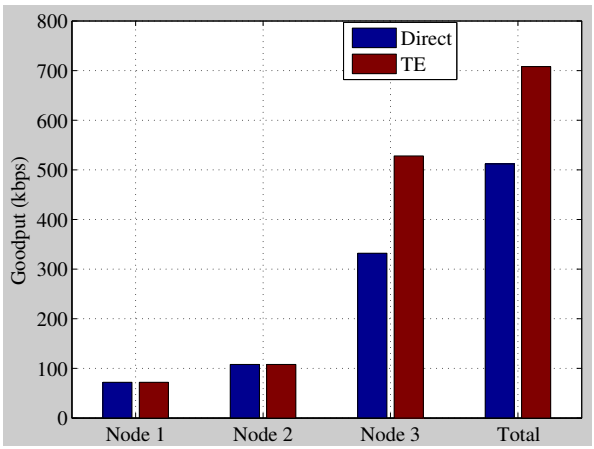

Figure 2.11: Sum Goodput Maximization in 3 node (Packet length = 1500 bytes, CRC checking, GMSK modulation)

13. Therefore, node 1 and 3 cooperate using TE, whereas, node 2 transmits without cooperation.

2.7.2 Sum Goodput Maximization

Fig. 2.11 compares the sum goodput (in kilo bit per second (kbps)) of TE and direct path transmission. Fig. 2.10 shows that node 1 and 3 get selected as the cooperative pair due to the MWM algorithm. Therefore, node 1 and 3 solve problem III to find the optimal time slot transfers. Due to the sum goodput maximization objective, the benefits of cooperation go to node 3, i.e., the node with the better channel. Node 3's goodput increases by 70%. Our optimization formulation ensures that node 1 gets its initial goodput, at least. On the other hand, node 2 transmits without cooperation and its goodput does not change from the initial value.

2.7.3 Proportional Fair Maximization of Goodput

Fig. 2.12 compares the proportional fair maximization performance of direct transmission and TE. Here, the selected cooperative nodes, s and f, solve a modified version of problem III. In this modified problem, s and f maximize $(R_s^{te} - R_s^{in}) * (R_f^{te} - R_f^{in})$ instead of maximizing $(R_s^{te} + R_f^{te})$. Hence, the goodput of both nodes increase due to cooperation. Fig. 2.12 shows that the goodputs of node 1 and 3 increase by 70% and 30% respectively.

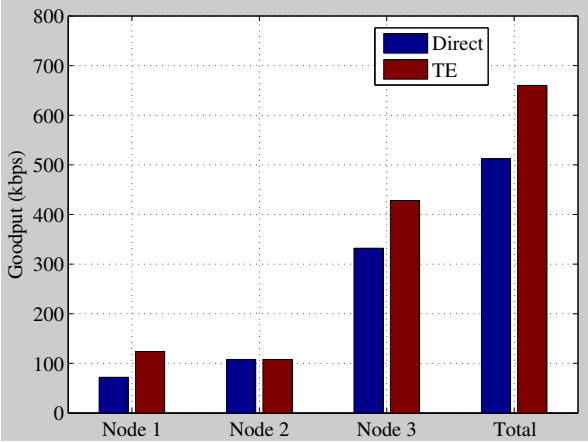

Figure 2.12: Proportional Fair Maximization of Goodput (Packet length = 1500 bytes, CRC checking, GMSK modulation)

2.8 Chapter Summary

This part of our work considered joint optimal relay selection and resource allocation in the α-fair network utility maximization and outage probability reduction of a BE network. Our proposed resource allocation formulation maximized the global utility of the cooperative pair while preserving the initial utilities of each individual node. We showed that the relay selection part of the α-fair NUM problem reduced to the non-bipartite matching algorithm. Numerical simulations suggested that the proposed BE enabled relaying provided 20-25% spectrum efficiency gain and 90-98% outage probability reduction in a 20 node network.

We also designed and implemented time exchange based cooperative forwarding among four USRP nodes of ORBIT indoor wireless testbed. We solved the joint time slot allocation and sender-forwarder pair selection problem in this setup. Our proposed algorithm maximized the global goodput of the network while ensuring that no node's goodput drops below its initial value. The ORBIT grid was used as a global control plane to exchange the control information between USRP nodes. Experimental results suggested that resource delegation based cooperative forwarding could significantly improve the sum goodput and proportional fair goodput performance of the network.

Chapter 3

Power Optimal Non-contiguous Spectrum Access

3.1 Introduction

This chapter focuses on system power minimization in non-contiguous spectrum access. We investigate two different systems in this chapter. The first (and the major) part focuses on a multi-hop network where each node is equipped with a single front end and access non-contiguous spectrum chunks using NC-OFDMA. In this context, we perform joint optimal power control, scheduling, spectrum span selection and routing in the network to minimize the system power consumption of the overall network. We develop a mixed integer non-linear program to attain our objective and provide a branch and bound algorithm based solution. We also provide a low complexity greedy algorithm that runs in $(O(E^2M^2))$ time where E and M denote the number of edges and channels in the network.

The second part of this chapter focuses on a point-to-point link where both nodes are equipped with multiple front end radios and access non-contiguous spectrum chunks using NC-OFDMA. In this setting, we perform joint optimal power control and channel scheduling across each front end of the radio to minimize the system power of the point-to-point link. We develop a mixed integer non-linear program and provide a low complexity algorithm ($O(M^2I)$ where M and I denote the number of available channels and front ends respectively.

This chapter is organized as follows: Section 3.2-3.8 focus on our first system model, i.e., a multi-hop network where nodes have single radio front ends. Section 3.2 presents system power and multi-hop network model. Section 3.3 relates spectrum span and sampling rate with channel scheduling decisions. Section 3.4 provides a feasible solution

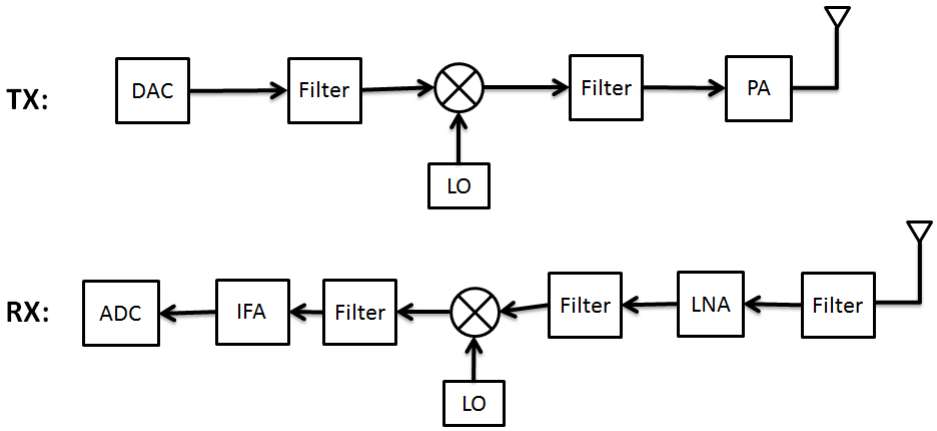

Figure 3.1: Radio front end circuit blocks (reproduced from [5])

of the optimization problem. We present a low complexity greedy algorithm to minimize system power in Section 3.7. We present numerical results for this setting in section 3.8. Sec. 3.9- 3.9.6 focuses on our second system model, i.e., a point-to-point link where nodes have multiple radio front ends, and presents system model, theoretical insights, low complexity algorithm and simulation results.

3.2 System Model

3.2.1 System Power Model

We assume that baseband signal processing techniques like multi-user detection and iterative decoding are not employed in the circuit. In this context, power consumption in the baseband is negligible compared with that in the radio frequency (RF) circuitry [90]. Each radio node has two front ends: one for transmission and the other for reception. Nodes are half-duplex, i.e., they can simultaneously transmit and receive using these two front ends but not in the same channel.

Fig. 3.1 shows signal level blocks in the transmit and receiver. At the transmitter, the baseband digital signal goes through DAC, filters, mixer (where it gets multiplied by the local oscillator (LO)) and programmable amplifier (PA) and reaches transmitter antenna. The received signal at the antenna goes through low noise amplifiers (LNA), filters, mixer, intermediate frequency amplifier (IFA) and ADC to reach the baseband

circuit [5].

Typically, transceiver circuits work on a multi-mode basis. When there is a signal to transmit, all RF circuits work in active mode; when there is no signal to transmit, all RF circuits remain in sleep mode; circuits switch from sleep to active mode through transient mode [5].

In this work, we focus on system power minimization of all RF circuits in the active mode. Let p_t, p_r and p denote active mode power consumption of the transmitter and receiver, and transmitter's emitted power at radio frequency respectively. Now

$$p_t = \frac{PAPR}{\eta} p + p_{tc} \tag{3.1}$$

$$p_r = p_{rc}\,, \tag{3.2}$$

where $PAPR$ and η denote the peak-to-average-power-ratio and drain efficiency of the programmable amplifier. $\frac{PAPR}{\eta}p$ denotes the total power consumption at the programmable amplifier [5]. Also, p_{tc} and p_{rc} are the circuit (analog and digital) power consumption of the transmitter (excluding programmable amplifier's power consumption) and the receiver, respectively.

The power consumption of almost all the blocks of the radio front end, except ADC and DAC, does not depend on the sampling rate [5, 91]. The power consumption of ADC and DAC are affine functions of the sampling rate [5, 41]. Denoting $k_{pa} = \frac{PAPR}{\eta}$, system power consumption in the transmitter and receiver front end (in the active mode) can be denoted as:

$$p_t = \alpha_1 + \alpha_2 f_{st} + k_{pa} p \tag{3.3}$$

$$p_r = \beta_1 + \beta_2 f_{sr} \tag{3.4}$$

In the above, f_{st} and f_{sr} are sampling rates of the transmitter and receiver path. α_1, α_2, β_1 and β_2 are constants that depend on the power consumption of different blocks. We use appendix A.1 to describe power consumption of each block in details.

Notation	Description
$\mathcal{N}$	Set of nodes
N	Total number of nodes
$(s(l), d(l))$	Source and destination of session l
$r(l)$	Rate requirements of session l
W	Bandwidth of each channel
N_0	Noise spectral density
$f_{ij}^m(l)$	Flow on link ij in channel m for session l
c_{ij}^m	Capacity on link ij in channel m
s_{ij}^m	Signal-to-noise ratio on link ij in channel m
$\mathcal{M}$	Set of all available channels across all nodes
$\mathcal{M}_i$	Set of available channels in node i
P_I	Interference threshold
$\mathcal{M}_{ij}$	Set of available channels between node i and j
M	Total number of available channels
g_{ij}^m	Link gain of ij in channel m
$p_{ij,m}$	Allocated power between i and j in channel m
x_{ij}^m	If link ij uses channel m
$x_i^{t,m}$	If node i uses channel m for transmission
$x_i^{r,m}$	If node i uses channel m for reception
$q_{t,i}$	Spectrum span of the transmitter path of node i
$q_{r,i}$	Spectrum span of the receiver path of node i
$f_{st,i}$	Sampling rate of node i's transmitter path
$f_{sr,i}$	Sampling rate of node i's receiver path
$f_{s,max}$	Maximum allowed sampling rate of the nodes
$P_{s,max}$	Maximum allowed system power consumption
A	An arbitrary large number

Table 3.1: List of Notations

3.2.2 Multi-hop cross-layer model

We consider a multi-hop network with a set of $\mathcal{N}$ cognitive radio nodes, $|\mathcal{N}| = N$. Let $\mathcal{M}$ denote the set of all available channels. Bandwidth of each channel is W.

Power Control and Scheduling Constraints

We focus on frequency scheduling. Denote the binary scheduling decision x_{ij}^m as follows:

$$x_{ij}^m = \begin{cases} 1, & \text{if node } i \text{ transmits to node } j \text{ using channel } m. \\ 0, & \text{otherwise.} \end{cases} \tag{3.5}$$

Due to self-interference, node i can use channel m only for receiving from node k or transmitting to node j. In other words:

$$\sum_{j \in \mathcal{N}, j \neq i} x_{ij}^m + \sum_{k \in \mathcal{N}, k \neq i} x_{ki}^m \leq 1 \;\; \forall\, i \in \mathcal{N}\,, \forall\, m \in \mathcal{M} \tag{3.6}$$

A node can allocate power in a link only if it is scheduled, i.e.

$$p_{ij}^m \leq A x_{ij}^m \;\; (i\,, j \;\in \mathcal{N})\,,\; m \in \mathcal{M} \tag{3.7}$$

Here, A is a big number that couples power control and scheduling variables. We select A in such a way so that it remains higher than the possible maximum transmission power of any node.

We use the protocol interference model. Assume that node i transmits to node j in channel m, i.e., $x_{ij}^m = 1$. Let p_{ij}^m and g_{ij}^m denote the transmission power and channel gain in channel m of link ij. Let P_I denote the interference threshold. P_I should be chosen in such a way so that it is negligible compared to the noise power $N_0 W$ where N_0 is the noise spectral density. Another node k can transmit to node h in channel m if p_{kh}^m causes negligible interference in node j. Now,

$$x_{ij}^m = 1 \implies p_{kh}^m \leq \frac{P_I}{g_{kj}^m} \, \forall (k,h) \in \mathcal{N},\, k \neq i,\, h \neq j \tag{3.8}$$

If $x_{ij}^m = 0$, then node k's transmission power is bounded by A. In other words,

$$x_{ij}^m = 0 \implies p_{kh}^m \leq A \, \forall (k,h) \in \mathcal{N},\, k \neq i,\, h \neq j \tag{3.9}$$

Equation (3.8) and (3.9) can be combined to the following:

$$p_{kh}^m + (A - \frac{P_I}{g_{kj}^m}) x_{ij}^m \leq A \, \forall \, k \in \mathcal{N},\, h \in \mathcal{N},\, k \neq h \tag{3.10}$$

Note that, our algorithm can be easily extended to signal-to-interference-plus-noise-ratio model [44], too.

Routing and Link Capacity Constraints

Assume that $\mathcal{L}$ is the set of active sessions and $|\mathcal{L}| = L$. Let $s(l)$, $d(l)$ and $r(l)$ denote the source node, destination node, and minimum rate requirements of session l. Let $f_{ij}^m(l)$ denote the flow from node i to node j in channel m for session l. If i is the source (destination) node of session l, the total outgoing (incoming) flow from (to) node i should exceed the minimum rate requirements of session l, i.e.,

$$\sum_{j \in \mathcal{N}} \sum_{m \in \mathcal{M}} f_{ij}^m(l) \geq r(l) \quad (l \in \mathcal{L}\,,\, i = s(l)) \tag{3.11}$$

$$\sum_{k \in \mathcal{N}} \sum_{m \in \mathcal{M}} f_{ki}^m(l) \geq r(l) \quad (l \in \mathcal{L}\,,\, i = d(l)) \tag{3.12}$$

If i is an intermediate node of session l, the incoming flow of session l should match with the outgoing flow:

$$\sum_{j \in \mathcal{N}}^{j \neq s(l)} \sum_{m \in \mathcal{M}} f_{ij}^m(l) = \sum_{k \in \mathcal{N}}^{k \neq d(l)} \sum_{m \in \mathcal{M}} f_{ki}^m(l) \;\; \forall \, (l \in \mathcal{L},\, i \in \mathcal{N},\, i \neq s(l), d(l)) \tag{3.13}$$

Additionally, the aggregated flows of all sessions in a particular link should not exceed the capacity of the link. Therefore,

$$\sum_{l \in \mathcal{L}} f_{ij}^m(l) \leq c_{ij}^m \;\; (i\,, j \;\in \mathcal{N}\,,\, i \neq j\,,\, \mathcal{M} \neq \emptyset) \tag{3.14}$$

where

$$c_{ij}^m \leq W \log(1 + s_{ij}^m) \ (i\,, j \in \mathcal{N}\,,\, i \neq j) \tag{3.15}$$

$$s_{ij}^m = \frac{g_{ij}^m p_{ij}^m}{N_0 W},\ (i\,, j \in \mathcal{N}\,,\, i \neq j). \tag{3.16}$$

In the above, c_{ij}^m and s_{ij}^m denote the capacity and signal-to-noise-ratio in link ij of channel m. The denominator of s_{ij}^m only contains $N_0 W$ because (3.8) ensures that the interference from other nodes is negligible compared to the noise power.

The constraints described above resemble previous works that focus on *transmission power* based cross-layer optimization (i.e., power control, scheduling and routing). The novelty of the work here is in relating the hardware constraints imposed by the radio front-end to the above cross-layer optimization as we describe next.

3.2.3 System Power Constraints

Let $p_{t,i}$ and $p_{r,i}$ denote the system power consumption in the transmitter and receiver path of node i. The total system power consumption, P_{tot}, is:

$$P_{tot} = \sum_{i \in \mathcal{N}} \big(p_{t,i} + p_{r,i}\big) \tag{3.17}$$

We also assume that a radio node consumes analog power if it transmits or receives in a channel. Denoting α_{1_i} and β_{1_i} as the analog power consumption of node i's transmit and receive path respectively, we find,

$$\alpha_{1_i} \geq \alpha_1 x_{ij}^m \ \ \forall m \in \mathcal{M},\, j \in \mathcal{N},\, i \in \mathcal{N} \tag{3.18}$$

$$\beta_{1_i} \geq \beta_1 x_{ki}^m \ \ \forall m \in \mathcal{M},\, k \in \mathcal{N}\,,\, i \in \mathcal{N}. \tag{3.19}$$

Using (3.3), (3.4), (3.17), (3.18) and (3.19),

$$\sum_{i \in \mathcal{N}} (\alpha_1 + \alpha_2 f_{st,i} + \sum_{j \in \mathcal{N}} \sum_{m \in \mathcal{M}} k_{pa} p_{ij}^m + \beta_1 + \beta_2 f_{sr,i}) = P_{tot} \tag{3.20}$$

where $f_{st,i}$ and $f_{sr,i}$ denote the sampling rates in the transmitter and receiver of node

i.

3.2.4 Main Optimization Problem

In this work, we minimize the total system power subject to minimum rate requirements and solve the following problem:

Problem I

$$\min P_{tot} \tag{3.21a}$$

$$\sum_{i\in\mathcal{N}}(\alpha_1+\alpha_2 f_{st,i}+\sum_{j\in\mathcal{N}}\sum_{m\in\mathcal{M}} k_{pa}p_{ij}^m+\beta_1+\beta_2 f_{sr,i})\leq P_{tot} \tag{3.21b}$$

s.t. constraints in (3.28j), (4.4), (3.28b) - (3.16), (3.18) - (3.19)

$$x_{ij}^m\in\{0,1\}\,,\; s_{ij}^m\geq 0\,(i,j\in\mathcal{N}, i\neq j, m\in\mathcal{M}) \tag{3.21c}$$

$$P_{tot}\;, f_{ij}^m(l)\geq 0\,(l\in\mathcal{L},\, m\in\mathcal{M},\; i,j\in\mathcal{N},\, i\neq j) \tag{3.21d}$$

3.3 Relation between Channel Scheduling and System Power

The sampling rate at a transceiver depends on the spectrum span, which in turn is determined by the choice of channels (subcarriers) selected for its intended transmission. We now formally relate channel scheduling decisions with the spectrum span and the sampling rate of the nodes.

Let $x_i^{t,m}$ and $x_i^{r,m}$ denote the following:

$$x_i^{t,m}=\begin{cases}1, & \text{if } i \text{ transmits to any node } j\in\mathcal{N} \text{ in channel } m.\\ 0, & \text{otherwise.}\end{cases}$$

$$x_i^{r,m}=\begin{cases}1, & \text{if } i \text{ receives from any node } j\in\mathcal{N} \text{ in channel } m.\\ 0, & \text{otherwise.}\end{cases}$$

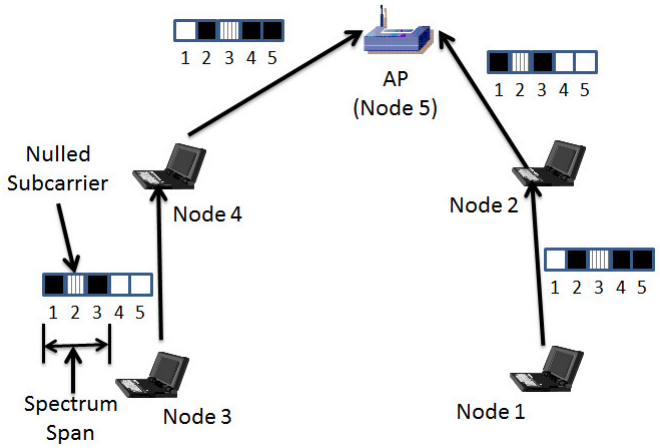

Figure 3.2: Spectrum span, occupied subcarrier and nulled subcarrier in an NC-OFDMA based multi-hop network.

In other words,

$$\begin{aligned} x_i^{t,m} &\geq x_{ij}^{m} \; \forall \, j \in \mathcal{N}, \\ x_i^{r,m} &\geq x_{ki}^{m} \; \forall \, k \in \mathcal{N}, \end{aligned} \tag{3.22}$$

Using this notation, analog power equations of (3.18) and (3.19) are redefined as,

$$\alpha_{1_i} \geq \alpha_1 x_i^{t,m}, \quad \beta_{1_i} \geq \beta_1 x_i^{r,m}, \; \forall m \in \mathcal{M}, \; \forall i \in \mathcal{N} \tag{3.23}$$

We define spectrum span as the gap between the furthest edge of the used channels. Node i's uppermost used channel index in the transmitter path is:

$$\max_{m \in \mathcal{M}} m \cdot x_i^{t,m}. \tag{3.24}$$

Node i's lowermost used channel index in the transmitter path is:

$$\min_{m \in \mathcal{M}} (m \cdot x_i^{t,m} + |M| \cdot (1 - x_i^{t,m})). \tag{3.25}$$

The second term of (3.25) ensures that we do not consider the index i's for which $x_i^{t,m} = 0$. Let $q_{t,i}$ and $q_{r,i}$ denote the spectrum spans of the transmitter and receiver path of node i.

Node	Mode of Operation	Used Channel	Spectrum Span
1	Transmitter	$2, 4, 5$	$(5-2+1)\cdot W = 4W$
	Receiver	$\{\emptyset\}$	0
2	Transmitter	$1, 3$	$(3-1+1)\cdot W = 3W$
	Receiver	$2, 4, 5$	$(5-2+1)\cdot W = 4W$
3	Transmitter	$1, 3$	$(3-1+1)\cdot W = 3W$
	Receiver	$\{\emptyset\}$	0
4	Transmitter	$2, 4, 5$	$(5-2+1)\cdot W = 4W$
	Receiver	$1, 3$	$(3-1+1)\cdot W = 3W$
5	Transmitter	$\{\emptyset\}$	0
	Receiver	$1, 2, 3, 4, 5$	$(5-1+1)\cdot W = 5W$

Table 3.2: Spectrum Span Calculation of Different Nodes of Fig. 3.2

$$q_{t,i} = W \cdot \max\big(\big(\max_{m\in\mathcal{M}}\big(m \cdot x_i^{t,m}\big) - \min_{m\in\mathcal{M}}\big(m \cdot x_i^{t,m} + |M| \cdot (1 - x_i^{t,m})\big) + 1\big), 0\big) \quad (3.26)$$

$$q_{r,i} = W \cdot \max\big(\big(\max_{m\in\mathcal{M}}\big(m \cdot x_i^{r,m}\big) - \min_{m\in\mathcal{M}}\big(m \cdot x_i^{r,m} + |M| \cdot (1 - x_i^{r,m})\big) + 1\big), 0\big) \quad (3.27)$$

Using above equations, we modify (3.21b) to the following:

$$q_{t,i} \geq W \cdot \max\big(\big(\max_{m\in\mathcal{M}}\big(m \cdot x_i^{t,m}\big) - \min_{m\in\mathcal{M}}\big(m \cdot x_i^{t,m} + |M| \cdot (1 - x_i^{t,m})\big) + 1\big), 0\big) \quad (3.29)$$

$$q_{r,i} \geq W \cdot \max\big(\big(\max_{m\in\mathcal{M}}\big(m \cdot x_i^{r,m}\big) - \min_{m\in\mathcal{M}}\big(m \cdot x_i^{r,m} + |M| \cdot (1 - x_i^{r,m})\big) + 1\big), 0\big) \quad (3.30)$$

$$\sum_{i\in\mathcal{N}}(\alpha_{1_i} + 2\alpha_2 q_{t,i} + \sum_{j\in\mathcal{N}}\sum_{m\in\mathcal{M}} p_{ij}^m + \beta_{1_i} + 2\beta_2 q_{r,i}) \leq P_{tot} \quad (3.31)$$

We replace (3.21b) with the above set of equations.

Fig. 3.2 shows spectrum span in a multi-hop network. Here, black solid, lined ash and white boxes denote occupied, nulled and un-spanned subcarriers respectively. Spectrum span is the summation of occupied and nulled subcarriers. Table. 3.2 shows transmit and receive spectrum spans of Fig. 3.2.

$$\min \;\; P_{tot} \tag{3.28a}$$

$$\sum_{j\in\mathcal{N}}\sum_{m\in\mathcal{M}} f_{ij}^{m}(l) \geq r(l) \quad (l\in\mathcal{L}\,,\, i=s(l))\;,\; \sum_{k\in\mathcal{N}}\sum_{m\in\mathcal{M}} f_{ki}^{m}(l) \geq r(l) \quad (l\in\mathcal{L}\,,\, i=d(l)) \tag{3.28b}$$

$$\sum_{j\in\mathcal{N}}^{j\neq s(l)}\sum_{m\in\mathcal{M}} f_{ij}^{m}(l) = \sum_{k\in\mathcal{N}}^{k\neq d(l)}\sum_{m\in\mathcal{M}} f_{ki}^{m}(l)\;\; (l\in\mathcal{L},\, i\in\mathcal{N},\, i\neq s(l),d(l)) \tag{3.28c}$$

$$\sum_{l\in\mathcal{L}} f_{ij}^{m}(l) \leq c_{ij}^{m}\;\; (i\,,j\;\in\mathcal{N}\,,\, i\neq j\,,\, \mathcal{M}\neq\emptyset) \tag{3.28d}$$

$$c_{ij}^{m} \leq W\log(1+s_{ij}^{m})\;\; (i\,,j\;\in\mathcal{N}\,,\, i\neq j)\;,\;\; s_{ij}^{m}=\frac{p_{ij}^{m}}{N_0 W},\;\; (i\,,j\;\in\mathcal{N}\,,\, i\neq j) \tag{3.28e}$$

$$p_{kh}^{m}+(A-\frac{P_I}{g_{kj}})x_{ij}^{m} \leq A\,\forall\, k\in\mathcal{N},\, h\in\mathcal{N},\, k\neq h\;,\; p_{ij}^{m}\leq Ax_{ij}^{m}\;\; (i\,,j\;\in\mathcal{N})\,,\, m\in\mathcal{M} \tag{3.28f}$$

$$q_{t,i} \geq W\cdot\big(\max_{m\in\mathcal{M}}\big(m\cdot x_i^{t,m}\big)-\min_{m\in\mathcal{M}}\big(m\cdot x_i^{t,m}+|M|\cdot(1-x_i^{t,m})\big)+1\big) \tag{3.28g}$$

$$q_{r,i} \geq W\cdot\big(\max_{m\in\mathcal{M}}\big(m\cdot x_i^{r,m}\big)-\min_{m\in\mathcal{M}}\big(m\cdot x_i^{r,m}+|M|\cdot(1-x_i^{r,m})\big)+1\big) \tag{3.28h}$$

$$\alpha_{1_i}\geq\alpha_1 x_i^{t,m}\,,\;\; \beta_{1_i}\geq\beta_1 x_i^{r,m}\;\forall m\in\mathcal{M}\,\forall i\in\mathcal{N}\;,\; q_{t,i}\leq q_{max}\,,\; q_{r,i}\leq q_{max}\;\; \forall i\in\mathcal{N} \tag{3.28i}$$

$$\sum_{j\in\mathcal{N},j\neq i} x_{ij}^{m}+\sum_{k\in\mathcal{N},k\neq i} x_{ki}^{m}\leq 1\;\; \forall\, i\in\mathcal{N}\,,\,\forall\, m\in\mathcal{M} \tag{3.28j}$$

$$\sum_{i\in\mathcal{N}}\big(\alpha_{1_i}+2\alpha_2 q_{t,i}+\sum_{j\in\mathcal{N}}\sum_{m\in\mathcal{M}} p_{ij}^{m}+\beta_{1_i}+2\beta_2 q_{r,i}\big)\leq P_{tot} \tag{3.28k}$$

$$x_{ij}^{m}\in\{0,1\}\,,\, s_{ij}^{m}\geq 0\;\; (i,j\in\mathcal{N},\, i\neq j,\, m\in\mathcal{M})\,,\;\; q_{t,i}\geq 0,\, q_{r,i}\geq 0\;\forall i\in\mathcal{N} \tag{3.28l}$$

$$P_{tot}\,, f_{ij}^{m}(l)\geq 0\,\big(l\in\mathcal{L}, m\in\mathcal{M},\, i,j\in\mathcal{N},\, i\neq j,\, i\neq d(l),\, j\neq s(l),\, \mathcal{M}\neq\emptyset\big) \tag{3.28m}$$

Figure 3.3: Optimization problem based on spectrum span

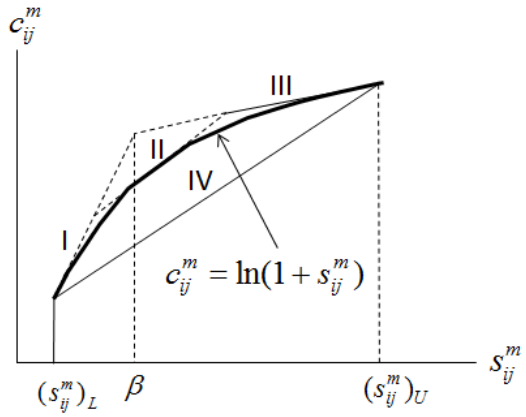

Figure 3.4: A convex hull for $c_{ij}^m = ln(1 + s_{ij}^m)$

3.3.1 Bundle Constraint

A comparison between table 1.1 and table 1.2 suggests that commercially available ADC and DAC's cannot capture all available channels in TV white space. Hence, the transmit and receive spectrum span of each node is limited by the maximum span of the ADC and DAC. Without loss of generality, we assume that the maximum spectrum span of all nodes's ADC and DAC is equal and denoted by q_{max}.

$$q_{t,i} \leq q_{max}\ ,\ \ q_{r,i} \leq q_{max}\ \ \forall i \in \mathcal{N} \tag{3.32}$$

We show our modified optimization problem in Fig 3.3.

3.4 Solution Overview

3.4.1 Linearization of the Optimization Problem

The optimization problem of Fig. 3.3 is a mixed integer non-linear programming (MINLP) problem. We modify logarithm and max-min functions to transform the MINLP into a mixed integer linear programming (MILP) problem.

We use reformulation-linearization techniques [92] and provide a linear relaxation of the non-linear term $ln(1 + s_{ij}^m)$. Assume that the signal-to-noise-ratio is bounded by $(s_{ij}^m)_L \leq s_{ij}^m \leq (s_{ij}^m)_U$. We assume $(s_{ij}^m)_L$ and $(s_{ij}^m)_U$ to be zero and a very high number

respectively. Assume, $c_{ij}^m = ln(1 + s_{ij}^m)$. Now, c_{ij}^m can be bounded by four segments. Fig. 3.4 shows these segments: I, II, III and IV. Segment I, II and III are tangential supports at $\big((s_{ij}^m)_L, ln\big(1+(s_{ij}^m)_L\big)\big)$, $\big(\beta, ln\big(1+\beta\big)\big)$ and $\big((s_{ij}^m)_U, ln\big(1+(s_{ij}^m)_U\big)\big)$, where

$$\beta = \frac{[1+(s_{ij}^m)_L][1+(s_{ij}^m)_U][ln(1+(s_{ij}^m)_U) - ln(1+(s_{ij}^m)_L)}{(s_{ij}^m)_U - (s_{ij}^m)_L} - 1 \tag{3.33}$$

is the intersection of segment I and II. Segment IV joins $\big((s_{ij}^m)_L, ln\big(1+(s_{ij}^m)_L\big)\big)$ and $\big((s_{ij}^m)_U, ln\big(1+(s_{ij}^m)_U\big)\big)$. Using these segments, the convex region of c_{ij}^m can be defined by:

$$(1+(s_{ij}^m)_L)\cdot c_{ij}^m - s_{ij}^m \le (1+(s_{ij}^m)_L)(ln(1+(s_{ij}^m)_L) - 1) + 1 \tag{3.34}$$

$$[1+\beta]\cdot c_{ij}^m - s_{ij}^m \le [1+\beta][ln(1+\beta) - 1] + 1 \tag{3.35}$$

$$[1+(s_{ij}^m)_U]\cdot c_{ij}^m - s_{ij}^m \le [1+(s_{ij}^m)_U][ln(1+(s_{ij}^m)_U) - 1] + 1 \tag{3.36}$$

$$[(s_{ij}^m)_U - (s_{ij}^m)_L]\cdot c_{ij}^m + [ln(1+(s_{ij}^m)_U) - ln(1+(s_{ij}^m)_L)]\cdot s_i^m \ge (s_{ij}^m)_U ln(1+(s_{ij}^m)_U) - (s_{ij}^m)_L ln(1+(s_{ij}^m)_L) \tag{3.37}$$

The linear equations of (3.34)-(3.37) can replace the non-linear equation of $c_{ij}^m \le W\log(1+s_{ij}^m)$ in Fig. 3.3. The spectrum span equations of (3.29) and (3.30) are linearized in the following way:

$$q_{t,i} + W\big(m_2\cdot x_i^{t,m_2} + |M|\cdot(1 - x_i^{t,m_2})\big) \ge W\big(m_1\cdot x_i^{t,m_1} + 1\big)\ \forall (m_1,m_2)\in\mathcal{M}\,,\ \forall i\in\mathcal{N} \tag{3.38}$$

$$q_{r,i} + W\big(m_2\cdot x_i^{r,m_2} + |M|\cdot(1 - x_i^{r,m_2})\big) \ge W\big(m_1\cdot x_i^{r,m_1} + 1\big)\ \ \forall (m_1,m_2)\in\mathcal{M}\,,\ \forall i\in\mathcal{N} \tag{3.39}$$

$$q_{t,i}\ge 0\,,\ q_{r,i}\ge 0\ \ \forall i\in\mathcal{N} \tag{3.40}$$

The optimization problem of Fig. 3.3 with these reformulated linear equations can be directly solved in CVX [93] (with MOSEK [94]) software. This problem is an MILP. CVX uses branch-and-bound algorithm [92] to solve this problem.

3.4.2 Feasible Solution

CVX outputs flow variables $f_{ij}^m(l)$, scheduling decisions x_{ij}^m and power variables p_{ij}^m $\big(l \in \mathcal{L}, m \in \mathcal{M}, i, j \in \mathcal{N}, i \neq j, \big)$. Since we relaxed flow capacity equations to get this output, the resultant flow rates may exceed the capacity of the links. We keep flow variables and scheduling decisions unperturbed and increase power variables to get feasible solutions. We use the following set of equations for flows and powers:

$$\begin{aligned} \sum_{i \in \mathcal{L}} f_{ij}^m(l) &= W log(1 + \frac{p_{ij}^m g_{ij}^m}{N_0 W}) \\ p_{ij}^m &= \frac{N_0 W}{g_{ij}^m}\big[exp\{\frac{\sum_{l \in \mathcal{L}} f_{ij}^m(l)}{W}\} - 1\big] \;\; \forall m \in \mathcal{M},\, i, j \in \mathcal{N},\, i \neq j. \end{aligned} \quad (3.41)$$

These power variables along with flow and scheduling decisions of the CVX output form a feasible solution. We refer to this solution as "BnBSysPowerMin".

3.5 Theoretical Insights

This section focuses on a point-to-point link and shows how the system power constraints imposed due to hardware characteristics influence the cross-layer decisions.

3.5.1 Influence of System Power on Scheduling

Let us focus on power allocation and scheduling in a point-to-point link. The optimization problem of Fig. 3.3 takes the following form:

$$\min \quad \big(P_{tx}(p^1, \cdots, p^{|M|}) + P_{ckt}(q, x^1, \cdots, x^{|M|})\big) \quad (3.42a)$$

$$s.t. \;\; q \geq W\big(\max_{m \in \mathcal{M}}(m \cdot x^m) - \min_{m \in \mathcal{M}}(m \cdot x^m + |M|(1 - x^m)) + 1\big) \;,\; x^m \in \{0, 1\}\,, \forall m \in \mathcal{M}\,,\, q \geq 0 \quad (3.42b)$$

$$\sum_{m \in \mathcal{M}} W \log_2\big(1 + \frac{p^m g^m}{N_0 W}\big) \geq r \;,\; p^m \geq 0, \;\forall m \in \mathcal{M} \quad (3.42c)$$

$$p^m \leq Ax^m \ \forall m \in \mathcal{M} \tag{3.42d}$$

In the above, p^m and g^m denote the allotted power and link gain in channel m, respectively. Rate requirement and spectrum span are denoted by r and q, respectively. Also, $P_{tx}(p^1, \cdots, p^{|M|}) = \sum_{m\mathcal{M}} p^m$ denotes the transmit power and $P_{ckt}(q, x^1, \cdots, x^{|M|}) = \alpha_1 + 2\alpha_2 q + \beta + 2\beta_2 q$ denotes the circuit power consumption.

The above optimization is in essence the combination of two separate optimization problems. The objective is to minimize the summation of transmit and circuit power. Eq. 3.42c denotes the constraints associated with transmit power minimization problem and it only involves power variables. Eq. 3.42b denotes the constraints associated with circuit power minimization problem and it only involves spectrum span and scheduling variables. Eq. 3.42d relates the power and scheduling variables and couples these two optimization problems.

The above optimization problem suggests two sub-cases of our overall problem. These sub-cases depend on the values of α_2 and β_2, i.e., the slope of ADC & DAC's power consumption versus sampling rate curves (Appendix shows power consumption versus sampling rate curves of some commercial ADC's and DAC's).

Case I: Transmit Power Minimization

When α_2 and β_2 are very small, i.e., the slope of ADC and DAC's power consumption versus sampling rate curves are very flat, the impact of spectrum span on system power becomes negligible. In this case, scheduling decisions do not influence system power that much and we can concentrate on minimizing transmit power. Then the optimization problem gets reduced to the following form:

$$\min \sum_{m\in\mathcal{M}} p^m \tag{3.43a}$$

$$\sum_{m\in\mathcal{M}} W\log_2\big(1+\frac{p^m g^m}{N_0 W}\big) \geq r \ , p^m \leq Ax^m \ , p^m \geq 0, \ x^m \in \{0,1\} \ \forall m \in \mathcal{M} \quad (3.43b)$$

Since x^m's are not present in the objective function, we can just solve the problem with p^m variables and then enforce $x^m = 1$ for every positive p^m.

The above problem is similar to the classical waterfilling [84] problem, which maximizes rate subject to a total power constraint. In the remainder of the chapter, we refer to the above problem as the transmit power minimization problem. The solution to this problem selects the "good" channels in the network and spreads power across the whole spectrum [84]. We denote this solution using the term 'TxPowerMin' in the remainder of the chapter.

Case II: Circuit Power Minimization

When α_2 and β_2 are very large, i.e., the slope of ADC and DAC's power consumption are very steep, circuit power consumption dominates system power. Transmit power variables do not influence system power that much and we can just concentrate on minimizing system power. The optimization problem in this case reduces to,

$$\min \quad \alpha_1 + 2\alpha_2 q + \beta + 2\beta_2 q \quad (3.44a)$$

$$s.t. \ \ q \geq W\big(\max_{m\in\mathcal{M}}(m\cdot x^m) - \min_{m\in\mathcal{M}}(m\cdot x^m + |M|(1-x^m)) + 1\big) \ , \ x^m \in \{0,1\} \ , \forall m \in \mathcal{M} \ , \ q \geq 0 \quad (3.44b)$$

$$\sum_{m\in\mathcal{M}} W\log_2\big(1+\frac{p^m g^m}{N_0 W}\big) \geq r \ , \ p^m \geq 0, \ \forall m \in \mathcal{M} \ , \ p^m \leq Ax^m \ \forall m \in \mathcal{M} \quad (3.44c)$$

The objective of the optimization problem increases with spectrum span q. Hence, the minimum circuit power occurs if we schedule only one channel in the network and

allocate enough power in that channel so that it can carry the required data rate.

Scheduling any channel leads to same circuit power in the above optimization problem. Since the original system power minimization problem contains both transmit and circuit powers, it is prudent to select the channel with the best link gain. This greedy channel assignment will require less transmit power to meet rate requirement.

Trade-off between transmit and circuit power minimization

If the slope of ADC and DAC power consumption versus sampling rate curves are very flat, our algorithm converges to transmit power minimization based approaches and selects all good channels in the network. If the slope of ADC and DAC's power consumption vs. sampling rate curves are very steep, our algorithm selects the channel with the best link gain in a greedy manner.

Power consumption vs. sampling rate curves of commercial ADC and DAC's fall between these two extreme cases. Hence, in practical settings, our algorithm selects a subset of channels where the spectrum span is determined by the trade-off between transmit power and circuit power. Simulation results illustrate these scenarios.

3.6 Low Complexity Algorithm for point-to-point link

We have focused on a multi-hop network thus far in this chapter and developed a branch-and-bound algorithm based mixed integer linear programming solution to minimize the system power of the overall network in Sec. 3.4. Although the branch-and-bound algorithm can converge to a solution with any predefined optimality gap, it suffers from exponential computational complexity in the worst case scenario. Using the insights of sec. 3.5, we develop a low complexity greedy algorithms to minimize system power in a simplified network scenario of a single point-to-point link.

Our greedy algorithm can be explained simply as follows: *Pick the channel with the highest link gain at the first iteration. In each subsequent iteration, pick exactly one channel, where the assignment is determined as the feasible assignment that minimizes total system power.* Table 3.9 is the pseudo-code of our algorithm.

The input to the algorithm is the available channel set $\mathcal{M}$, demand r, channel bandwidth W, noise power spectral density N_0 and link gain g^m across all channels ($\forall\, m \in \mathcal{M}$). The output of the algorithm is total system power P_{tot}, scheduled channel indices set $\mathcal{Y}$ (selected iteratively in each iteration), overall scheduling variables x^m, and power variables p^m across all channels ($\forall\, m \in \mathcal{M}$).

At first, we select the channel with the best link gain, store this channel in $\mathcal{Y}$ and find the associated total power with this assignment (line $2-3$). Then at each iteration (line 5), we look at all channels (line 6) and find the spectrum span if the current channel and the previously selected channel set are scheduled together (line $7-8$). Circuit power consumption is fixed if the spectrum span is fixed. Based upon this fixed circuit power, we optimize the minimum transmit power (line $11-12$) and find the associated system power (line 13). We select the channel that minimizes the system power in the current iteration and include it in $\mathcal{Y}$ (line 16). We run this iteration successively unless the obtained power of the current loop increases from the previous loop (line $17-20$). Based on the selected channel indices, we find the overall scheduling channel variables in line $21-25$ and power variables in $26-28$.

In an M channel network, the outer loop of line 5 will run at most M times since each iteration will either select a better channel or the loop will break. The inner loop runs M times, too. Hence, in the worst case scenario, the greedy algorithm consists of $O(M^2)$ number of convex optimization programs. Each convex optimization program has $O(M)$ constraints and can be solved in $O(M \log M)$ time using barrier methods [86]. Once "good" channels are selected, power allocation across the channels can be solved through a one-shot convex optimization procedure like line $26-28$.

3.7 Polynomial Time Algorithm for a Multihop Networks

Using the insights from the point-to-point link case, we develop a low complexity greedy algorithm here. Our greedy algorithm can be explained simply as follows:

- Find the initial route between each sender and receiver using shortest path algorithm [95].

Input:	$\mathcal{M}$, r, W, N_0, $g_m \, \forall m \in \mathcal{M}$
Output:	$x_m, p_m \forall m \in \mathcal{M}$, P_{tot} , $\mathcal{Y}$
Line	Operation
1	$ind = \arg\max_m(g^m)$, $val = \max_m(g^m)$.
2	$x_{ind} = 1$, $\mathcal{Y} = \{ind\}$.
3	$P_{tot} = k_{pa}\big(e^{\frac{r}{W}} - 1\big)\frac{N_0}{val} + \alpha_1 + 2\alpha_2 W + \beta_1 + 2\beta_2 W$
4	$count = 1$
5	while $count == 1$
6	$\forall m \in \mathcal{M}$
7	if $m \in \mathcal{Y}$
8	$MaxInd = max\{\mathcal{Y}, m\}$, $MinInd = min\{\mathcal{Y}, m\}$
9	$q = MaxInd - MinInd + 1$
10	solve
11	$\min \sum_{n\in\{m,\mathcal{Y}\}} Pnew^n$
12	s.t. $\sum_{n\in\{m,\mathcal{Y}\}} Wlog\big(1 + \frac{Pnew^n g^n}{N_0 W}\big) \geq r$, $Pnew^n \geq 0 \, \forall n \in \{m, \mathcal{Y}\}$
13	$IterP_m = k_{pa} \sum_{n\in\{m,\mathcal{Y}\}} Pnew^n + \alpha_1 + 2\alpha_2 q + \beta_1 + 2\beta_2 q$
14	else
15	$IterP_m = \infty$
16	$MinP = \min_m(IterP_m)$, $ind = \arg\min_m(IterP_m)$
17	if $MinP < P_{tot}$
18	$\mathcal{Y} = \{\mathcal{Y}, ind\}$, $P_{tot} = MinP$
19	else
20	$count = 0$.
21	$\forall m \in \mathcal{M}$
22	if $m \in \mathcal{Y}$
23	$x^m = 1$.
24	else
25	$x^m = 0$.
26	solve
27	$\min \sum_{m\in\mathcal{M}} p^m$
28	s.t. $\sum_{m\in\mathcal{M}} Wlog(1 + \frac{p^m g^m}{N_0 W}) \geq r$, $p^m \geq 0 \, \forall m \in \mathcal{Y}$, $p^m == 0 \, \forall m \notin \mathcal{Y}$

Table 3.3: Greedy Algorithm to Minimize System Power in a point-to-point link

- Assign the best channel to each link unless the current assignment interferes with previously assigned channels.
- For each active link, check if any other channel assignment reduces system power.
- Once channels are scheduled, determine power allocation and routing through a convex optimization program.

Our greedy system power minimization algorithm consists of the central program of Table 3.4 and the sub-routines of Table 3.5 and Table 3.6. Next three sub-sections describe the central program and sub-routines. We analyze the complexity of our algorithm in Sec. 3.7.4.

3.7.1 Central Program

Table 3.4 shows the pseudocode of our greedy polynomial time algorithm. Line 1 finds large scale gains of all links by averaging small scale fading in time or frequency domain. Line 2 assigns weight to each link. Line 3 finds the shortest path between each sender and forwarder based on the assigned weights of link 2. Line 5 finds the active links. Line 6 calculates the flow requirement among these links. Line 7 initiates total power (P_{tot}), power allocation (p_{ij}^m) and scheduling (x_{ij}^m) variables to zero for the greedy channel scheduling algorithm. We initiate an outer loop in line 8. Line 9 sorts the active links in each outer loop. Line 10-12 calls the subroutine of Table 3.5 and checks if any link should be assigned a channel. The outer loop breaks at line 12 if none of the active links becomes suitable to be assigned a channel. This outer loop determines the channel scheduling (x_{ij}^m) variables.

We obtain power allocation (p_{ij}^m) and routing path ($f_{ij}(l)$ variables from the optimization problem of Fig. 3.3 where scheduling variables (x_{ij}^m) are constants. Since we fix the integer variables of Fig. 3.3, the total power minimization problem becomes a convex minimization program and can be solved in polynomial time [86].

We assume one path (shortest path), i.e., no flow splitting, per session during the initial routing topology design of line 1-3. This allows us to easily calculate the flow requirement of each link which we later use in the greedy scheduling algorithm. However,

Input:	$\mathcal{M}$, r, W, N_0, $g_m \, \forall m \in \mathcal{M}$
Output:	$x_m, p_m \forall m \in \mathcal{M}$, P_{tot} , $\mathcal{Y}$
Line	Operation
1	Denote g_{ij} as the average gain (e.g. path loss plus shadowing) of link ij.
2	Assign weight w_{ij} to each link, $w_{ij} = \frac{1}{g_{ij}}$.
3	Find shortest path between between source ($s(l)$) and destination ($d(l)$) of every session $l \in \mathcal{L}$ based on the link weights of line 2.
4	$b_{ij}(l) = 1$ if link ij falls in the routing path of any session $l \in \mathcal{L}$.
5	A link is active if it falls in the routing path of any session, i.e., $x_{ij} = 1$ if $\exists l \in \mathcal{L}$ s.t. $b_{ij}(l) = 1$. Define $\mathcal{A}$ to be set of active links.
6	Flow in each link, $f_{ij} = \sum_{l \in \mathcal{L}} b_{ij}(l) r(l)$.
7	$P_{tot} = \infty$, $x_{ij}^m = p_{ij}^m = 0 \, \forall \, (i,j) \in \mathcal{E}$, $\forall m \in \mathcal{M}$
8	while (true)
9	$flag = 0$; $\mathcal{A} = randsort(\mathcal{A})$.
10	$\forall (a,b) \in \mathcal{A}$
11	$\big(flag, x_{ij}^m, p_{ij}^m \, \forall \, m \in \mathcal{M} \, (i,j) \in \mathcal{E}\big) =$ GreedyAlgo$\big(\mathcal{M}, (a,b), f_{ab}, r, W, N_0, flag, P_{tot}, x_{ij}^m, p_{ij}^m, g_{ij}^m \, \forall \, m \in \mathcal{M} \, (i,j) \in \mathcal{E}\big)$
12	if $flag = \lvert A \rvert$, break.
13	Solve the optimization problem of Fig. 3.3 where scheduling variables ($x_{ij}^m \, \forall \, m \in \mathcal{M} \, \forall \, (i,j) \in \mathcal{E}$) are constants, not variables (obtained from the loop of line 8-12). Find power allocation, scheduling and routing variables and total power, P_{tot}

Table 3.4: Polynomial Time Algorithm to Minimize System Power in a Multi-hop Network

we consider optimal flow splitting in the final optimization of line 13 of Table 3.4.

3.7.2 Greedy Scheduling Algorithm

The greedy scheduling algorithm of Table 3.5 is a sub-routine that's called from line 11 of the central program of Table 3.4. The sub-routine receives previously assigned scheduling and power allocation variables from the central program. The central controller also asks the sub-routine to focus on a particular link (a, b). The sub-routine iterates through all available channels and finds the best available channel for (a, b).

Line 1 of Table 3.5 starts the iteration for all channels. Line 2 stores the global scheduling (x_{ij}^m) and power allocation (p_{ij}^m) variables in local dummy variables $x_{new,ij}^m$ and $p_{new,ij}^m$ respectively. Line 3 assigns the current channel to the focus link (a, b). Line 4-7 calculates the transmit schedule ($x_i^{t,m}$), receiver schedule ($x_i^{r,m}$), transmit span ($q_{t,i}$) and receiver span ($q_{r,i}$) for all nodes $i \in \mathcal{N}$. Line 8 assumes equal flow allocation

Input:	$\mathcal{M}$, Link (a,b), f_{ab}, r, W, N_0, $flag$, x_{ij}^m , p_{ij}^m , $g_{ij}^m \, \forall \, (i,j) \in \mathcal{E}$, $\forall m \in \mathcal{M}$
Output:	$flag$, x_{ij}^m , $\forall \, (i,j) \in \mathcal{E}$, $\forall m \in \mathcal{M}$
Line	Operation
1	$\forall m \in \mathcal{M}$ where $x_{ab}^m \neq 1$
2	$x_{new,ij}^m = x_{ij}^m$, $p_{new,ij}^m = p_{ij}^m$, $\forall \, (i,j) \in \mathcal{E}$, $\forall m \in \mathcal{M}$
3	$x_{new,ab}^m = 1$
4	$\forall \, i \in \mathcal{N}$, $x_i^{t,m} = 1$ if $\exists \, j$ s.t. $x_{new,ij}^m = 1$. $\forall \, j \in \mathcal{N}$, $x_j^{r,m} = 1$ if $\exists \, i$ s.t. $x_{new,ij}^m = 1$
5	$\forall \, i \in \mathcal{N}$, $\alpha_{1_i} = \alpha_1$ if $\exists \, m \in \mathcal{M}$ s.t. $x_i^{t,m} = 1$ and $\beta_{1_i} = \beta_1$ if $\exists \, m \in \mathcal{M}$ s.t. $x_i^{r,m} = 1$
6	$q_{t,i} = W \cdot \big(\max_{m \in \mathcal{M}} \big(m \cdot x_i^{t,m}\big) - \min_{m \in \mathcal{M}} \big(m \cdot x_i^{t,m} + \lvert M \rvert \cdot (1 - x_i^{t,m})\big) + 1\big) \, \forall \, i \in \mathcal{N}$
7	$q_{r,i} = W \cdot \big(\max_{m \in \mathcal{M}} \big(m \cdot x_i^{r,m}\big) - \min_{m \in \mathcal{M}} \big(m \cdot x_i^{r,m} + \lvert M \rvert \cdot (1 - x_i^{r,m})\big) + 1\big) \, \forall \, i \in \mathcal{N}$
8	$f_{new,ab}^m = \frac{f_{ab}}{\sum_{m \in \mathcal{M}} x_{new,ab}^m} \cdot x_{new,ab}^m$, $p_{new,ab}^m = \frac{N_0 W}{g_{ab}^m} \cdot \big(2^{\frac{f}{W}} - 1\big) x_{new,ab}^m \, \forall \, m \in \mathcal{M}$.
9	$IntFlag = \text{IntCheck}\big(x_{new,ab}^m, p_{new,ab}^m, \mathcal{M}, \mathcal{A}, W, N_0, x_{ij}^m, p_{ij}^m \, \forall \, (i,j) \in \mathcal{E}\big)$
10	if IntCheck$(\cdot) = 1$, $P_{new,tot}^m = \infty$
11	else, $P_{new,tot}^m = \sum_{i \in \mathcal{N}} \big(\alpha_{1_i} + 2\alpha_2 q_{t,i} + \sum_{j \in \mathcal{N}} \sum_{m \in \mathcal{M}} p_{new,ij}^m + \beta_{1_i} + 2\beta_2 q_{r,i}\big)$
12	$P_{tot,new} = \min_{m \in \mathcal{M}} P_{tot,new}^m$. $ind = \arg\min_{m \in \mathcal{M}} P_{tot,new}^m$
13	if $P_{tot,new} < P_{tot}$,
14	$x_{ab}^{ind} = 1$.
15	$f_{ab}^m = \frac{f_{ab}}{\sum_{m \in \mathcal{M}} x_{ab}^m} \cdot x_{ab}^m$, $p_{ab}^m = \frac{N_0 W}{g_{ab}^m} \cdot \big(2^{\frac{f}{W}} - 1\big) x_{ab}^m \, \forall \, m \in \mathcal{M}$
16	else, $flag = flag + 1$
17	Return.

Table 3.5: Greedy Scheduling Algorithm

among the selected channels and finds the power allocation in link (a,b) to meet rate requirement. Line 9 calls the sub-routine of Table 3.6 and checks if current channel assignment causes interference to other links. Line 11 calculates total system power of the current iteration. Line 12 comes out of the loop and finds the minimum system power ($P_{tot,new}$) among all channels. Line 13 compares ($P_{tot,new}$) with global system power (P_{tot}) and updates scheduling and power variables accordingly.

We assume equal flow per channel in each link in line 9 of Table 3.5. This simplifies the calculation of transmission power per channel and avoids the computation of a convex optimization program in each loop. However, we consider optimal flow and power allocation in our final optimization problem of line 13 of Table 3.4.

Input:	$x^m_{new,ab}$, $p^m_{new,ab}$, $\mathcal{M}$, $\mathcal{A}$, W, N_0, x^m_{ij}, p^m_{ij} $\forall(i,j) \in \mathcal{A}$
Output:	$Intflag$
Line	Operation
1	$count = 0$. $Intflag = 0$
2	$\forall(i,j) \in \mathcal{A}$, $i \neq a$, $j \neq b$
3	if $\big((p^m_{new,ab} g^m_{aj} \geq 0.1 N_0 W x^m_{ij}) \| (p^m_{ij} g^m_{ib} \geq 0.1 N_0 W x^m_{new,ab})\big)$
4	$count = count + 1$
5	if $\big(x^m_{ia} + x^m_{ab} + x^m_{bj} > 0\big)$, $count = count + 1$.
6	if $count \geq 0$, $Intflag = 1$.
7	Return

Table 3.6: Primary and Secondary Interference Checking Algorithm

3.7.3 Interference Checking Algorithm

The sub-routine of Table 3.6 gets called from line 9 of the greedy scheduling algorithm of Table 3.5. This sub-routine checks if the scheduling and power allocation of link ab in channel m, calculated in Table 3.5, interferes with other links. Line 3 of Table 3.6 checks if transmitted power in link ab causes interference to any non-adjacent link that uses channel m. Line 5 checks if link ab maintains half duplex relationships with its adjacent links. Line 6 updates $IntFlag$ and returns this value to the greedy scheduling sub-routine of Table 3.5.

3.7.4 Computational Complexity

Global system power minimization algorithm of Table 3.4 contains three major parts: 1) Initial routing path selection (line 1-3 of Table 3.4), 2) channel scheduling (line 8-12 of Table 3.4 along with Table 3.5 and Table 3.6) , and 3) optimal power control and routing path design (line 13 of Table 3.4).

Initial routing path selection involves computing link weights ($O(E)$) and shortest path ($O(E + N \log N)$) for L sessions. Therefore, the overall complexity for this part is: $O\big(L(E + N \log N)\big)$.

The greedy scheduling algorithm starts with a while loop. The while loop iterates through all active links ($O(E)$). Each link calls the sub-routine of Table 3.5, iterates through M channels. Inside each channel, the code calls the sub-routine of Table 3.6.

Table 3.6 checks if the current channel assignment interferes with other links ($O(E)$). The global while loop of Table 3.4 can iterate at most $O(M)$ times since each iteration will either select a channel for a link or the loop will break. Therefore, the greedy scheduling algorithm runs in $O(E^2M^2)$ time.

The optimal power allocation and routing path selection problem of line 13 of Table 3.4 is a convex optimization program. Barrier method [86] can solve this in $O(R\log(R))$ steps where R is the number of inequality constraints. From Fig. 3.3, we find the complexity to be $O(EM\log(EM)$.

The greedy scheduling part dominates the overall complexity ($O(E^2M^2)$) of Table 3.4. We term this algorithm "GreedySysPowerMin". We compare the performance of both "GreedySysPowerMin" and "BnBSysPowerMin" with that of "TxPowerMin" in Sec. 3.8.

3.8 Simulation Results

3.8.1 System Power Minimization in a Single Point-to-Point Link

We focus on an NC-OFDMA based single transceiver pair. Here, $\mathcal{N} = \{1, 2\}$. There is only one session in the network. $s(1) = 1$, $d(1) = 2$. There are 20 channels available for transmission. Each channel is 3 MHz wide. Minimum data rate requirement is 18 Mbps. The left sub-plot of Fig. 3.5 shows the link gains across these channels. We designed the link gains so that every other channel has better link gain – by approximately 10 dB – than its adjacent neighbours.

The second subplot (from the left) of Fig. 3.5 shows the power allocation and scheduling variables of TxPowerMin approach. This approach minimizes transmit power subject to the rate constraint. Similar to the concept of "waterfilling" algorithm [84], this approach spreads power across all ten "good" channels of the network.

The third and fourth subplot (from the left) of Fig. 3.5 shows the scheduling and power variables of our greedy algorithm (GreedySysMin). We use two different types of ADC and DAC models to investigate the influence of ADC/DAC slopes on our algorithm. We use the high slope ADC and DAC models – ADC 9777 and ADS 62P4

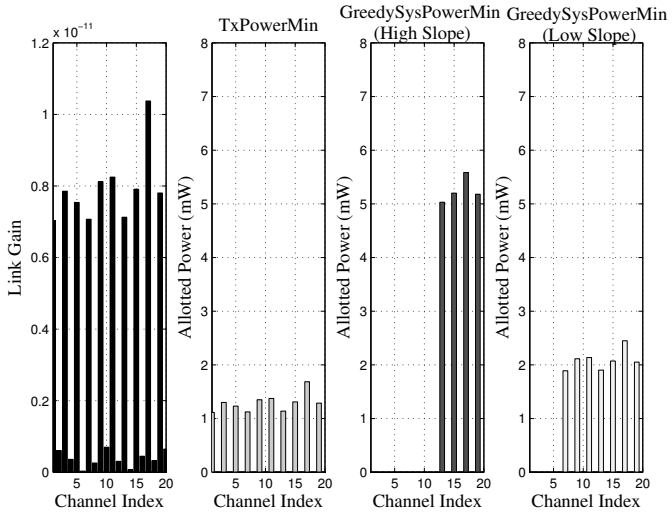

Figure 3.5: Power allocation across 20 channels in a single transceiver pair.

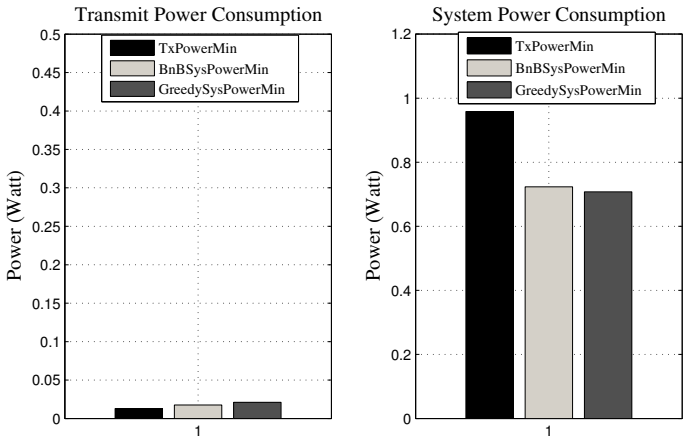

Figure 3.6: Comparison of our algorithms with the 'TxPowerMin' approach with the high slope ADC/DAC's of Fig. A.1 and Fig. A.2.

(see Fig. A.1 and Fig. A.2) – in the third subplot of Fig. 3.5 and the low slope ADC and DAC model – DAC 3162 and ADS 4249 (see Fig. A.1 and Fig. A.2) – in the fourth subplot (the rightmost one) of Fig. 3.5. Compared to the low slope ADC and DAC, the circuit power consumption increases more rapidly with high slope ADC and DAC's. With high slope ADC & DAC's of Fig. A.1 and Fig. A.2, our algorithm focuses more on minimizing circuit power and selects only four channels. With low slope ADC & DAC's of Fig. A.1 and Fig. A.2, our approach finds a trade-off between transmit & circuit power and selects seven channels.

Fig. 3.6 compares the system power consumptions of our algorithms with that of

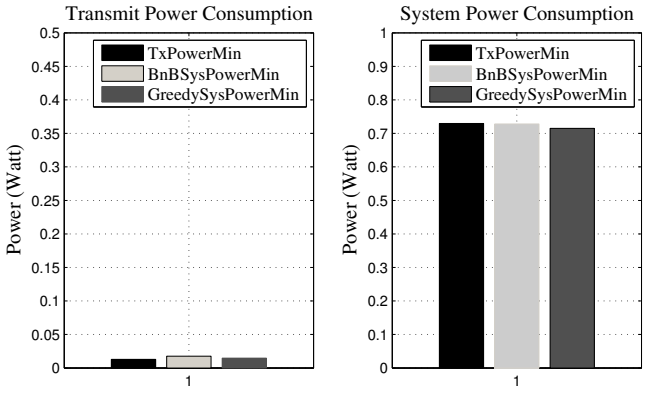

Figure 3.7: Comparison of our algorithms with the 'TxPowerMin' approach with the low slope ADC/DAC's of ig. A.1 and Fig. A.2.

TxPowerMin approach. We use the high slope ADC and DAC models of Fig. A.1 and Fig. A.2 to generate this figure.

Fig. 3.6 compares the performance of our algorithm with that of TxPowerMin approach in a high ADC/DAC slope setting. "TxPowerMin" approach minimizes transmit power by spreading data across all "good" channels of the network. Both of our algorithms consume more transmit power than the "TxPowerMin" approach since selecting a subset of available good channels is a sub-optimal policy in terms of transmit power. Our algorithms consume less circuit power due to the reduced spectrum span. Our algorithms reduce system power – summation of transmit and circuit power – consumption by almost $30 - 40\%$ in the high slope ADC/DAC scenario. Note that, the lower bound of the system power consumption (obtained from the mixed integer linear programming relaxation), was 0.63 watts in this scenario. Hence, both of our algorithms gave feasible results with roughly 15% optimality gap.

Fig. 3.7 compares the performance of our algorithm with that of TxPowerMin approach in a low ADC/DAC slope setting. We use the same link gain, bandwidth and traffic demands of Fig. 3.6 but we use the low power consumption ADC and DAC's – DAC 3162 and ADS 4249 ((see Fig. A.1 and Fig. A.2)) – to generate these new figures. As predicted in Sec. 3.5, our algorithm performs almost similar to the 'TxPowerMin'approach in this scenario because the power consumption of ADC & DAC is negligible compared to the transmit power requirement in this scenario.

Fig. 3.6 and fig. 3.7 suggest that our algorithms can adapt the power allocation and

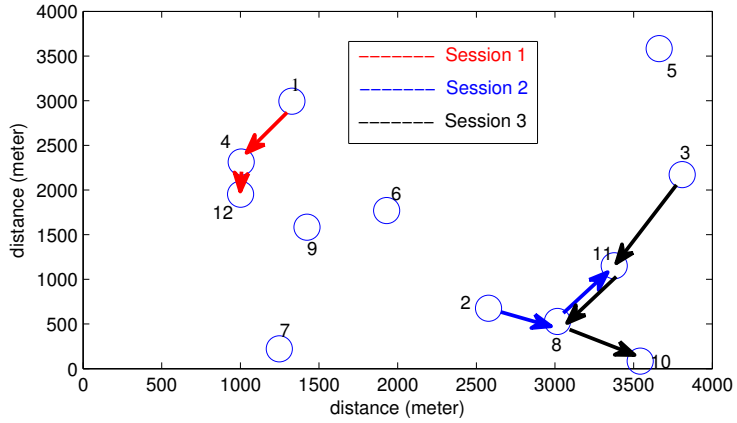

Figure 3.8: 12 node 3 session multi-hop network. Node 1, 2 and 3 transmit to node 12, 11 and 10 respectively. Both "TxPowerMin" and our approach select the same routes for both sessions.

Channel Index	2	5	6	17	23	24	47
Center Freq. (MHz)	57	79	85	491	527	533	671

Table 3.7: Available TV channels for fixed devices in Wichita, Kansas.

scheduling variables according to ADC/DAC slope, link gain and traffic demand.

3.8.2 System power minimization in a multi-hop network

To illustrate the influence of system power minimization in a practical setting of non-contiguous spectrum access, we consider an exemplary scenario of multi-hop networking among fixed devices in the TV white space channels of Wichita, Kansas, USA. We use standard spectrum databases [2] to find the available TV channels in Wichita, Kansas. Fig. 3.8 shows the network topology. Each session requires 10 Mbps data rate. Table 3.10 shows the available channel indexes. Each channel is 6 MHz wide. We consider both large scale fading (with path loss exponent 3) and small scale fading (with 12 dB random fluctuation) in each channel. Maximum transmission power per node is 4 watts for fixed devices that access TV white space [**?**]. We impose this constraint in both traditional transmit power minimization algorithm and our system power minimization algorithms to obtains the results of this simulation.

Node	Mode	TxPowerMin		BnBSysPowerMin	
		Channel Index	Spectrum Span (MHz)	Channel Index	Spectrum Span (MHz)
1	Tx	$\{23, 47\}$	150	$\{17, 23\}$	42
	Rx	$\{\emptyset\}$	0	$\{\emptyset\}$	0
2	Tx	$\{17\}$	6	$\{23\}$	6
	Rx	$\{\emptyset\}$	0	$\{\emptyset\}$	0
3	Tx	$\{6, 47\}$	592	$\{5, 6\}$	12
	Rx	$\{\emptyset\}$	0	$\{\emptyset\}$	0
4	Tx	$\{17\}$	6	$\{6\}$	6
	Rx	$\{23, 47\}$	150	$\{17, 23\}$	42
8	Tx	$\{2, 23\}$	476	$\{2, 47\}$	620
	Rx	$\{5, 24\}$	460	$\{17, 23, 24\}$	48
10	Tx	$\{\emptyset\}$	0	$\{\emptyset\}$	0
	Rx	$\{23\}$	6	$\{47\}$	6
11	Tx	$\{5, 24\}$	460	$\{17, 24\}$	48
	Rx	$\{2, 6, 47\}$	620	$\{2, 5, 6\}$	34
12	Tx	$\{\emptyset\}$	0	$\{\emptyset\}$	0
	Rx	$\{17\}$	6	$\{6\}$	6

Table 3.8: Comparison between the spectrum span of 'TxPowerMin' and our 'BnBSysPowerMin' algorithm in the network of Fig. 3.8. 'TxPowerMin' selects the channels with higher gain in most links and spans wider spectrum. Our algorithm spans less spectrum than 'TxPowerMin' in most of the links.

Channel Indexing Notations in Optimization Formulation

The difference between channel's carrier frequencies in TV bands are not always proportional to the index differences. Channel 17's center frequency is $((23 - 17) * 6)$ 36 MHz far from that of channel 23 but not $((17 - 6) * 6)$ 66 MHz far from that of channel 6. The spectrum span calculation of our optimization formulations depends heavily on the coherence of channel indexing differences. Therefore, we use an index set of $\{9, 13, 14, 81, 87, 88, 111\}$ to denote the channel list of $\{2, 5, 6, 17, 23, 24, 47\}$ in the optimization formulations. We use the original channel list to show the numerical results.

Comparison of "waterfilling" algorithm and our approach

In these simulations, we use the low slope ADC and DAC models of Fig. A.2 and Fig. A.1 to model system power consumption. We use Hou and Shi's algorithm [43]

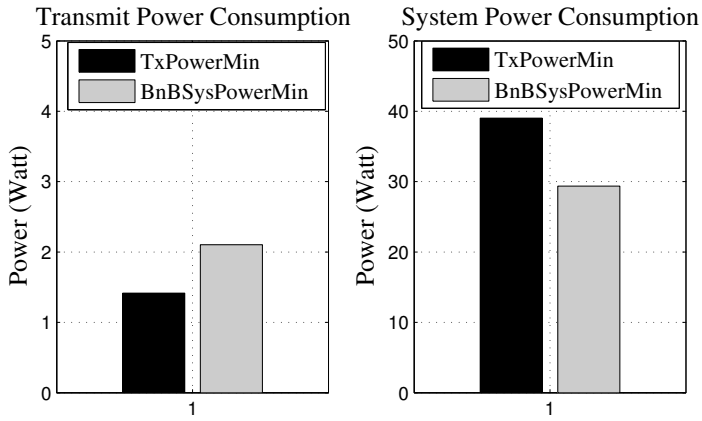

Figure 3.9: Performance comparison of "TxPowerMin" approach and our algorithm ("BnB-SysPowerMin") in the network of Fig. 3.8, based on the low slope ADC and DAC models of Fig. A.2 and A.1. Our approach reduces system power by 30% percent.

to illustrate the scheduling and power control decisions of 'TxPowerMin' approach. In this approach, nodes consume following amount of power:

Channel $m = 2$: $p^2_{8,11} = 0.2411$

Channel $m = 5$: $p^5_{11,8} = 0.1054$

Channel $m = 6$: $p^6_{3,11} = 0.4066$

Channel $m = 17$: $p^{17}_{2,8} = 0.0743$, $p^{17}_{4,12} = 0.038$.

Channel $m = 23$: $p^{23}_{1,4} = 0.1543$, $p^{23}_{8,10} = 0.2316$

Channel $m = 24$: $p^{24}_{11,8} = 0.0958$.

Channel $m = 47$: $p^{47}_{1,4} = 0.1233$, $p^{47}_{3,11} = 0.3683$

Our algorithm selects the following power consumption variables:

Channel $m = 2$: $p^2_{8,11} = 0.2411$

Channel $m = 5$: $p^5_{3,11} = 0.5466$

Channel $m = 6$: $p^6_{3,11} = 0.4066$, $p^6_{4,12} = 0.0476$

Channel $m = 17$: $p^{17}_{1,4} = 0.166$, $p^{17}_{11,8} = 0.0892$.

Channel $m = 23$: $p^{23}_{1,4} = 0.1543$, $p^{23}_{2,8} = 0.1346$.

Channel $m = 24$: $p^{24}_{11,8} = 0.0958$

Channel $m = 47$: $p^{47}_{8,10} = 0.2215$.

Table. 3.8 compares the channel scheduling decisions and spectrum spans of "Tx-PowerMin" approach and our algorithm. Although "TxPowerMin" minimizes transmit

power by selecting channels with better quality, it increases radio front end power by selecting channels that are too far apart. Our approach spans narrow spectrum and reduces circuit power consumption. Fig. 3.9 shows that our algorithm reduces system power by 30% in this scenario.

The lower bound of system power consumption is 24 watts in this scenario. Our algorithm provides a feasible solution (29 watts) with 20% optimality gap.

3.9 A case for NC-OFDMA in Multi-Channel-Multi-Radio platforms

This chapter has shown that both MC-MR and NC-OFDMA bring benefits and pitfalls in non-contiguous spectrum access. MC-MR accesses multiple non-contiguous spectrum chunks by activating multiple radio front ends where each front end captures a contiguous portion of available spectrum and, hence, activates the circuit power consumption of each front end. NC-OFDM accesses non-contiguous spectrum chunks with a single front end radio by nulling intermediate spectrum and, hence, increases spectrum span [79] which, in turn, increases the power consumption of ADC and DAC.

Fig. 3.10 shows the advantages and pitfalls of MC-MR and NC-OFDM. Here, channel 1, 3, 7 and 9 are available channels. One radio front end (shown at the top) accesses channel 1 & 3 and nulls channel 2 using NC-OFDM. Other radio front end (shown at the bottom) accesses channel 7 & 9 and nulls channel 8 using NC-OFDM. Due to the use of two front ends, the circuit power consumption of different components inside modulation block - e.g. filters, mixers, etc. – increases by a factor of 2. Due to the nulling of intermediate spectrum, each front end spans three channels (instead of two) and the circuit power consumption of ADC and DAC increase by a factor of 1.5.

This part of the chapter performs optimal power control and scheduling to minimize the system power – summation of transmit and circuit power – of a point-to-point link where both nodes are equipped with MC-MR and NC-OFDM technology. Given an available list of non-contiguous spectrum chunks, we find the optimal spectrum fragmentation in each radio front end using a greedy algorithm ($O(M^2I)$) where M and I denote the number of channels and radio front ends respectively.

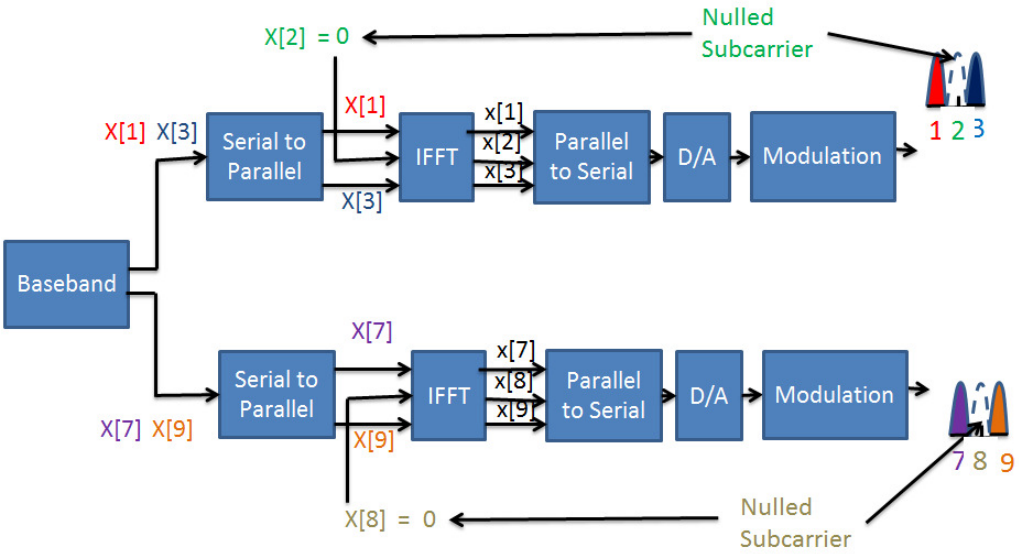

Figure 3.10: Multi-Channel Multi-Radio based Non-Contiguous Orthogonal Frequency Division Multiplexing operation

3.9.1 System Model

We focus on a point-to-point link where both transmitter and receiver are equipped with a set of front ends $\mathcal{I}$. Nodes access a set of available channels $\mathcal{M}$ to meet demand r. Let, $M = |\mathcal{M}|$ and $I = |\mathcal{I}|$. Let g^m denote the link gain at channel $m \in \mathcal{M}$. Let p_i^m and x_i^m represent the power control and scheduling decision variables in channel $m \in \mathcal{M}$ at front end $i \in \mathcal{I}$.

We assume that baseband signal processing techniques like multiuser detection and iterative decoding are not employed. Baseband power consumption is negligible in this scenario [5]. We focus on system power minimization during active mode (when the link is transmitting data) [5]. The authors of [5] show the following system power consumption model of transmitter (p_t) and receiver (p_r):

$$p_t = \alpha_1 + \alpha_2 f_s + k_{pa} p\,,\ p_r = \beta_1 + \beta_2 f_s \tag{3.45}$$

Here, p is the emitted power at radio frequency, $k_{pa} = \frac{PAPR}{\eta}$, $k_{pa}p$ is the power consumption of programmable amplifier, $PAPR$ is the peak-to-average-power-ratio of the modulation scheme, η is the efficiency of the programmable amplifier and f_s is sampling

rate. α_2 and β_2 are the slopes of DAC and ADC's power consumption versus sampling rate curves. α_1 (β_1) is the power consumption of all blocks of transmitter (receiver) - e.g. filter, mixer, etc. - excluding DAC (ADC) and programmable amplifier [5].

The total power consumption of a transmitter and receiver equipped with $\mathcal{I}$ front ends and $\mathcal{M}$ available channels can be written as:

$$\sum_{i\in\mathcal{I}}\big(k_{pa}\sum_{m\in\mathcal{M}}p_i^m+\alpha_{1,i}+\alpha_2 f_{s,i}+\beta_{1,i}+\beta_2 f_{s,i}\big) \tag{3.46}$$

where $\alpha_{1,i}$ ($\beta_{1,i}$) is the power consumption of all blocks of transmitter's (receiver's) i-th front end excluding DAC (ADC) and programmable amplifier. The sampling rate $f_{s,i}$ of i-th front end depends on its spectrum span, which in turn is determined by the choice of channels (subcarriers) selected for its intended transmission. *Spectrum span is defined as the gap between the furthest edges of the used channels.* Let q_i denote the spectrum span of the transmitter's and receiver's i-th front end. Using the analysis of [79],

$$q_i = W\cdot\max\big(\big(\max_{m\in\mathcal{M}}\big(m\cdot x_i^m\big)-\min_{m\in\mathcal{M}}\big(m\cdot x_i^m+|M|\cdot(1-x_i^m)\big)+1\big),0\big) \tag{3.47}$$

Sampling rate should be at least twice the amount of spectrum span. We assume, $f_{s,i}=2q_i$. Our overall optimization problem is shown below:

Problem I

$$\min\sum_{i\in\mathcal{I}}\big(k_{pa}\sum_{m\in\mathcal{M}}p_i^m+\alpha_{1,i}+2\alpha_2 q_i+\beta_{1,i}+2\beta_2 q_i\big) \tag{3.48a}$$

s.t.

$$q_i \geq W\cdot\max\big(\big(\max_{m\in\mathcal{M}}\big(m\cdot x_i^m\big)-\min_{m\in\mathcal{M}}\big(m\cdot x_i^m+|M|\cdot(1-x_i^m)\big)+1\big),0\big) \tag{3.48b}$$

$$\alpha_{1,i}\geq\alpha_{1,i}x_i^m\,,\ \beta_{1,i}\geq\beta_{1,i}x_i^m\ \forall m\in\mathcal{M}\,\forall i\in\mathcal{I} \tag{3.48c}$$

$$\sum_{m\in\mathcal{M}}\sum_{i\in\mathcal{I}} W\log_2\big(1+\frac{p_i^m g^m}{N_0 W}\big)\geq r \tag{3.48d}$$

$$p_i^m \leq A x_i^m \,\forall m\in\mathcal{M}\,,\,\forall i\in\mathcal{I} \tag{3.48e}$$

$$\sum_{i\in\mathcal{I}} x_i^m \leq 1\,\forall m\in\mathcal{M} \tag{3.48f}$$

$$x_{ij}^m\in\{0,1\}\,,\,p_i^m\geq 0\,,q_i\geq 0\,,\,\alpha_{1,i}\geq 0\,,\,\beta_{1,i}\geq 0\,\forall i\in\mathcal{I},\,\forall m\in\mathcal{M}\,, \tag{3.48g}$$

Here, Eq. (3.48c) denote that blocks like filter, mixer, etc. of i-th front end consume power only if the node activates i-th front end. Eq. (3.48d) denotes that summation of capacities across different channels and front ends must exceed demand r where N_0 is noise spectral density. Eq. (3.48e) couples power control and scheduling variables using a pre-defined big number A. Eq. (3.48f) represents that each channel can only be used by one of the front ends.

3.9.2 Theoretical Insights

The objective of problem I is linear. The constraints are convex. MI scheduling decision variables are binary. Problem I is a mixed integer convex program and can be solved optimally by solving 2^{MI} convex optimization programs. This section designs a low complexity algorithm by analyzing the characteristics of problem I.

Problem I is in essence the combination of two separate optimization problems. The objective is to minimize the summation of transmit and circuit power. Eq. 3.48d shows the constraints associated with transmit power. Eq. (3.48b) and (3.48f) denote the constraints circuit power. Eq. 3.48e couples power and scheduling variables. Hence, depending on the values of α_1, α_2, β_1 and β_2, problem I can have three sub-cases.

Case I: Contiguous Spectrum Access

When α_1, α_2, β_1 and β_2 are very large, circuit power completely dominates system power. Ignoring the contribution of transmit power $k_p a \sum_{m \in \mathcal{M}} p_m$ from Eq. (3.48a), problem I gets reduced to the following:

$$\min \sum_{i \in \mathcal{I}} \big(\alpha_{1,i} + 2\alpha_2 q_i + \beta_{1,i} + 2\beta_2 q_i\big) \tag{3.49}$$

$$\text{s.t. Eq. (3.48b),(3.48d), (3.48c), (3.48f), (3.48e) and (3.48g)}$$

The objective of the optimization problem is an affine function of q_i, α_i and β_i for all $i \in \mathcal{I}$. Minimum circuit power occurs if we use only one radio front end and one channel. Since link gain of a channel does not vary across radio front ends, we can arbitrarily select a front end. Since original system power minimization problem contains both transmit and circuit power, it is prudent to select the channel with the best link gain.

Use of MC-MR over NC-OFDM

If $\alpha_2 >> \alpha_1$ and $\beta_2 >> \beta_1$, power consumption of ADC & DAC dominate that of filters, mixers, etc.. Here, problem I gets reduced to the following:

$$\min \sum_{i \in \mathcal{I}} \big(k_{pa} \sum_{m \in \mathcal{M}} p_i^m + 2\alpha_2 q_i + 2\beta_2 q_i\big) \tag{3.50}$$

$$\text{s.t. Eq. (3.48b),(3.48d), (3.48f), (3.48e) and (3.48g)}$$

If number of radio front ends matches the number of non-contiguous spectrum chunks, the optimal solution of above problem activates multiple front ends but accesses contiguous spectrum chunks in each front end.

Use of NC-OFDM over MC-MR

If $\alpha_2 << \alpha_1$ and $\beta_2 << \beta_1$, power consumption of filters, mixers, etc.. dominate that of ADC & DAC. In this context, problem I gets reduced to the following:

$$\min \sum_{i \in \mathcal{I}} \big(k_{pa} \sum_{m \in \mathcal{M}} p_i^m + \alpha_{1,i} + \beta_{1,i} \big) \tag{3.51}$$

(3.48d), (3.48c), (3.48f), (3.48e) and (3.48g)

The optimal solution to this problem selects only one radio front end and accesses non-contiguous spectrum chunks through NC-OFDM to meet rate requirement. In a practical setting, the values of α_1, α_2, β_1 and β_2 fall between the extreme cases mentioned above. In those cases, our algorithm selects a subset of channels and assign them to different front ends to minimize system power.

3.9.3 Low Complexity Algorithm

Using the insights of Sec, 3.9.2, we develop a greedy algorithm here. Our algorithm can be explained simply as follows: *Pick the channel with the highest link gain at the first iteration. In each subsequent iteration, select exactly one channel and assign it to one front end, where both selection and assignment operations are the feasible operations that minimize total system power during the current iteration.* Table 3.9 is the pseudo-code of our algorithm. Here, $\mathcal{Y}_i \, \forall \, i \in \mathcal{I}$, is the set of channel indexes used by i-th front end.

At first, we select the channel with the best link gain (line 1). Without loss of generality, we assign this channel to first front end (line 2) and find associated total power (line 3). Thereafter, an infinite while loop starts (line 5) where each loop looks at all possible combinations of channel and front end assignment (line 6-7) and selects the channel-front end combination that minimizes system power during current iteration. For each channel-front end combination, we calculate spectrum span (line 9-10), flow allocation (line 12), power allocation (line 13) and total power (line 14). Line 15 compares total power values among all channel-front end combinations and finds the channel and front end combination that leads to minimum at the current iteration. If the current value of minimum total power is less than our previously stored value (line 16), we update total power, scheduling and spectrum span to accommodate current assignment (line 17-20). Otherwise, infinite loop breaks (line 21-22). The infinite while

loop of line 4-22 provides scheduling variables, spectrum span and circuit power for all channels and front ends. Line 23-25 allocates optimal power across these scheduled channels and front ends. We assume equal flow per channel (line 12) during the inside iterations of while loop to reduce complexity but our final solution contains optimal flow and power allocation across channels and front ends (line 23-25).

3.9.4 Computational Complexity

Overall complexity comes from the while loop of line 5-22 and the convex minimization program of line 23-25. The loops of line 6 and 7 run M and I times respectively. The outer while loop of line 5 runs at most M times since each iteration will either select a better channel or the loop will break. Hence, the while loop of line 5-22 runs at most $(O(M^2I))$ times. The convex optimization program of line 23-25 contains MI number of constraints and can be solved in $(O(MI\log(MI)))$ time [86]. If number of available channels is much higher than the number of available front ends, then $M \geq \log(MI)$. Based on this assumption, overall complexity is $(O(M^2I))$.

3.9.5 Other Algorithms

We compare our algorithm with two other algorithms. First algorithm only focuses on MC-MR platforms and accesses contiguous spectrum chunks in each of its radio front end [33]. This algorithm puts enough power in contiguous spectrum chunks of each front end to meet rate requirement. We term this approach 'MC-MR'. Second algorithm only focuses on NC-OFDM technology, spreads power across all "good" channels and accesses multiple non-contiguous spectrum chunks with one front end [79]. We term this approach 'NC-OFDM'. Both these approaches try to minimize the transmitted power at radio frequency. We compare the performance of both these algorithms with our algorithm in next section.

3.9.6 Simulation Results

Table 3.10 shows the indexes and center frequencies of available channels. Here, $\mathcal{M} = \{23, 24, 26, 28, 33, 48, 50\}$, $M = 7$. We assume the remaining channels (not shown in

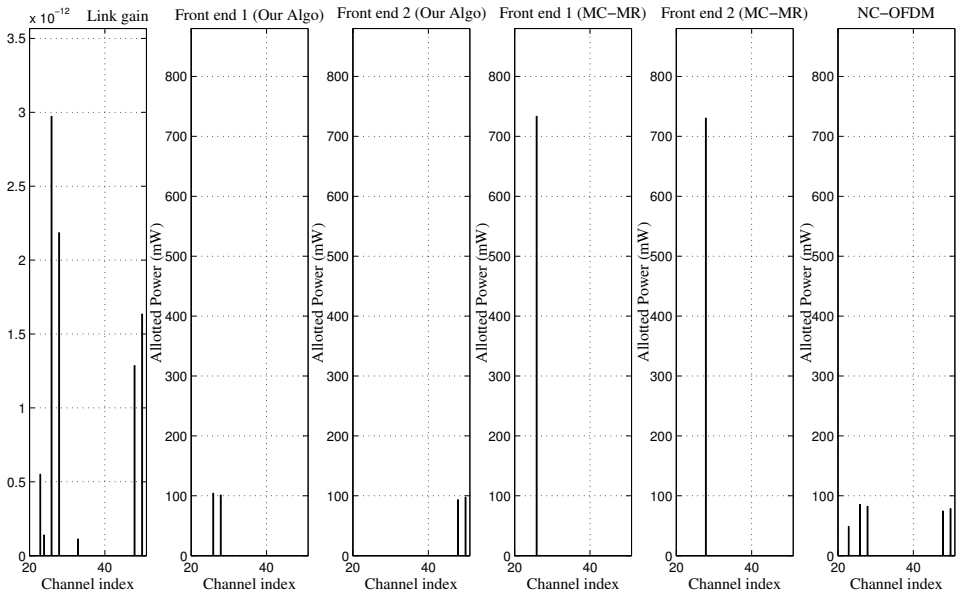

Figure 3.11: Power allocation among available channels (Demand = 75 Mbps)

Table 3.10) in set $20 - 50$ to belong to incumbent users, i.e., those channels cannot be accessed by both transmitter and receiver. We assume that both transmitter and receiver are equipped with two front ends, i.e., $\mathcal{I} = \{1, 2\}$ and $I = 2$. Table 3.11 shows the values of different parameters that we used in this section. A detailed explanation of these values can be found in [79].

The left subfigure of Fig. 3.11 shows the link gain across these channels. We assumed 500m distance between two nodes, path loss with exponent 3 and 15 dB random variation to generate link gain across these channels. We assume 75 Mbps demand (r) for this simulation scenario. The 2nd and 3rd subfigures (from left) of Fig. 3.11 show power allocation variables of our algorithm across both front ends. Our algorithm selects "better" channels - in terms of link gain - among the whole list, accesses "nearby" non-contiguous spectrum chunks in each front end and allocates transmit power to meet demand requirement.

'MC-MR' algorithm can only access contiguous spectrum chunks in each of its front end. Since channel 23 & 24 - the only contiguous chunk with two channels - have poor link gain, this algorithm selects channel 26 and 28 in each of its radio front end. Since demand is much higher than used bandwidth, the 4th and 5th subfigures (from left) of

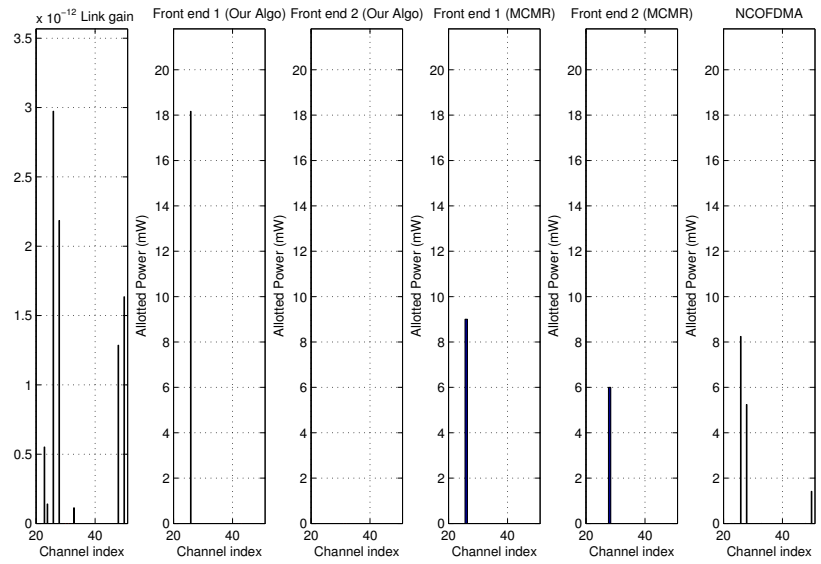

Figure 3.12: Power allocation among available channels (Demand = 10 Mbps)

Fig. 3.11 shows that MC-MR algorithm allocates very high amount of power in each channel and meets rate requirement. The rightmost sub-figure of Fig. 3.11 shows that 'NC-OFDM' algorithm spreads power across all 'good' channels, accesses multiple non-contiguous spectrum chunks *with one front end* and spans a wide amount of spectrum. As a result, 'NC-OFDM' algorithm consumes high power in ADC/DAC circuits [79]. Fig. 3.13 shows that our algorithm consumes less system power than 'MC-MR' by accessing multiple non-contiguous channels in each front end and than 'NC-OFDMA' by spanning lesser spectrum in this scenario.

Fig. 3.12 uses same link gain across the channels but assumes 10 Mbps demand between the transmitter and the receiver. 'NC-OFDM' algorithm selects all 'good' channels in the network to meet rate requirement. As a results, 'NC-OFDM' spans a wide amount of spectrum, accesses multiple non-contiguous spectrum chunks and consumes high power in ADC/DAC circuits. 'MC-MR' algorithm selects one channel in each front end and consumes circuit power at the mixers, filters, etc. in each radio front end. Our algorithm trades off between transmit power and circuit power consumption and selects the channel with the highest gain in one radio front end. Fig. 3.13 shows that our algorithm consumes less system power than 'MC-MR' by deactivating one radio front end and 'NC-OFDMA' by spanning lesser spectrum in this scenario.

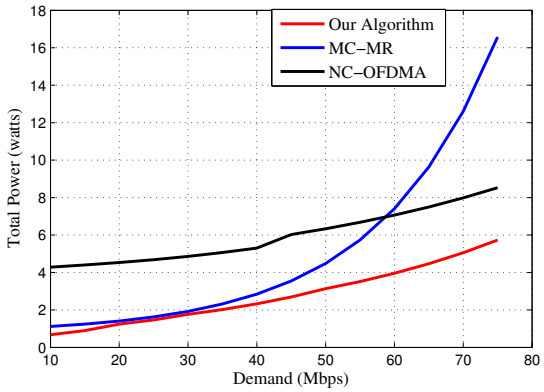

Figure 3.13: Comparison of system power consumption among different approaches

Fig. 3.13 compares the total power consumption of our algorithm with that of 'MC-MR' and 'NC-OFDM' algorithm for different demand values. As evident from Fig. 3.11, 'MC-MR' algorithm consumes a high amount of transmit power for high demand. When demand is low (e.g. 20-30 Mbps), both our algorithm and 'MC-MR' approach access two channels using two front ends and consume equal system power. 'NC-OFDM' approach spans wider amount of spectrum and, hence, consumes excessive circuit power in ADC and DAC. Our algorithm reaps the inherent benefits of 'MC-MR' and 'NC-OFDM' approach and combines them to minimize system power across all scenarios.

3.10 Chapter Summary

MC-MR and NC-OFDMA are the two commercially viable choices to access these non-contiguous spectrum chunks. Fixed MC-MR's do not scale with increasing number of non-contiguous spectrum chunks due to their fixed set of supporting ends. MC-MR also increases circuit power by activating multiple front ends. NC-OFDMA, on the other hand, accesses non-contiguous spectrum chunks with a single front end by nulling the channels where incumbent users are present. NC-OFDMA reduces transmit power consumption by selecting channels with higher link gain but increases circuit power consumption by spanning wider spectrum.

We characterized this trade-off from two perspectives. First, we focused on a multi-hop network where each node is equipped with single front end radio and can employ

NC-OFDMA to access non-contiguous spectrum chunks. We performed joint power control, channel scheduling, spectrum span selection and routing to minimize system power consumption of this multi-hop network. Our algorithm showed *how the slopes of ADC and DAC's power consumption versus sampling rate curve influenced the scheduling decisions of a multi-hop network*. We developed a mixed integer non-linear program to attain our objective and provided a low complexity greedy algorithm. Numerical results suggested that our algorithm could save 40% system power over classical transmission power based cross-layer algorithms.

Secondly, we focused on a point-to-point link where both nodes are equipped with multiple front ends and can employ NC-OFDMA to access non-contiguous spectrum chunks. We performed optimal power control and channel scheduling across both front ends to minimize the system power of this point-to-point link. We designed a mixed integer non-linear program and provided a low complexity greedy algorithm ($O(M^2I)$) where M and I denote the number of channels and radio front ends respectively. Our algorithm showed that, in a practical setting, *each front end of a radio should capture "near-by" non-contiguous spectrum chunks.*

Input:	$\mathcal{M}$, r, W, N_0, $g^m \, \forall m \in \mathcal{M}$
Output:	$x_i^m, p_i^m, \alpha_{1,i}, \beta_{1,i}, q_i, \mathcal{Y}_i \forall m \in \mathcal{M}, \forall i \in \mathcal{Y}$
Line	Operation
1	$ind = \arg\max_m(g^m)$, $val = \max_m(g^m)$.
2	$x_1^{ind} = 1$, $\mathcal{Y}_1 = \{ind\}$, $q_1 = W$, $\alpha_{1,1} = \alpha_1$, $\beta_{1,1} = \beta_1$
3	$P_{tot} = k_{pa}\big(2^{\frac{r}{W}} - 1\big)\frac{N_0}{val} + \alpha_1 + 2\alpha_2 W + \beta_1 + 2\beta_2 W$
4	while $(true)$
5	$\forall m \in \mathcal{M}$
6	$\forall i \in \mathcal{I}$
7	$\widetilde{\alpha}_{1,i} = \alpha_1$, $\widetilde{\beta}_{1,i} = \beta_i$, $\tilde{q}_i = q_i$, $\tilde{x}_i^m = x_i^m$
8	if $m \notin \mathcal{Y}_i \, \forall \, i \in \mathcal{I}$
9	$MaxInd = max\{\mathcal{Y}_i, m\}$, $MinInd = min\{\mathcal{Y}_i, m\}$
10	$\tilde{q}_i = W(MaxInd - MinInd + 1)$, $\tilde{x}_i^m = 1$
11	$\widetilde{\alpha}_{1,i} = \alpha_1$, $\widetilde{\beta}_{1,i} = \beta_1$.
12	$\tilde{f}_j^n = \frac{r}{\sum_{j\in\mathcal{I}}\sum_{n\in\mathcal{M}}\tilde{x}_j^n}\tilde{x}_j^n \;\forall j \in \mathcal{I}, \forall n \in \mathcal{M}$
13	$\tilde{p}_j^n = (2^{\frac{\tilde{f}_j^n}{W}} - 1)\frac{N_0 W}{g^n} \;\forall j \in \mathcal{I}$, $\forall n \in \mathcal{M}$
14	$\tilde{P}_i^m = \sum_{j\in\mathcal{I}}\big(\alpha_{1,j} + \alpha_2 q_j + \beta_{1,j} + \beta_2 q_j +$ $k_{pa}\sum_{n\in\mathcal{M}}\tilde{x}_j^n\big)$
15	$[minP, minC, minI] = \min_m \min_i(\tilde{P}_i^m)$
16	if $minP \leq P_{tot}$,
17	$P_{tot} = minP$, $x_{minI}^{minC} = 1$, $\alpha_{1,minI} = \alpha_1$, $\beta_{1,minI} = \beta_1$.
18	$\mathcal{Y}_{minI} = \{\mathcal{Y}_{minI}, minC\}$.
19	$MaxInd = max\{\mathcal{Y}_{minI}\}$. $MinInd = min\{\mathcal{Y}_{minI}\}$.
20	$q_i = W(MaxInd - MinInd + 1)$.
21	else
22	*break*
23	$\min \sum_{i\in\mathcal{I}}\sum_{m\in\mathcal{M}} p_i^m$
24	s.t. $\sum_{i\in\mathcal{I}}\sum_{m\in\mathcal{M}} W log(1 + \frac{p_i^m g^m}{N_0 W}) \geq r$,
25	$p_i^m \leq A x_i^m$, $p_i^m \geq 0 \, \forall \, m \in \mathcal{M}$, $\forall i \in \mathcal{I}$.

Table 3.9: Greedy Algorithm to Minimize System Power in a Multi-front end radio enabled point-to-point link

Channel Index	23	24	26	28	33	48	50
Center Freq. (MHz)	527	533	545	557	587	677	689

Table 3.10: Available channels for the point-to-point link

Parameters	α_1	α_2	β_1	β_2	k_{pa}	W
Values	45.4 mW	7.2 mW/MSPS	282.3 mW	5.5 mW/MSPS	10.67	6 MHz

Table 3.11: Values of different parameters used in Sec. 3.9.6

Chapter 4

Wireless Backhaul Node Placement for Small Cell Networks

4.1 Introduction

We perform joint cost optimal aggregator node placement, power control, channel scheduling and routing to minimize operational expenses of the overall network in this part of our work. We develop a mixed integer non-linear programming (MINLP) formulation and then reformulate the MINLP to a mixed integer linear program (MILP) using linear relaxation techniques. We use branch-and-bound algorithm to solve the MILP. We also develop a greedy algorithm with polynomial complexity to solve the MINLP. We apply our solution methodologies to design the wireless backhaul network in an example downtown Manhattan scenario. We use a ray tracing tool, consisting of actual building locations and heights in Manhattan, to investigate the impact of aggregator node placement in wireless backhaul networks.

This chapter is organized in the following way: Section 4.2 discusses interference patterns in different bands. Section 4.3 and 4.4 show the network optimization problems in microwave band based backhaul and sub-6 GHz band based backhaul respectively. Section 4.5 presents how we solve the network optimization problems through linear relaxation techniques and branch-and-bound algorithm. In section 4.6, we show a polynomial time greedy algorithm to place aggregator nodes in an interference limited network. We show the simulation results in section 4.7.

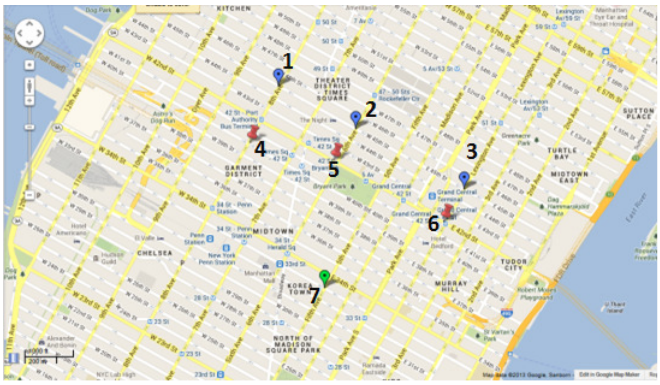

Figure 4.1: An example wireless backhaul network in downtown Manhattan scenario. Figure taken from [6]

4.2 Interference Models

Throughout this work, we denote small cells by edge nodes (EN) and backhaul nodes by aggregator nodes (AN). We assume that aggregator nodes communicate with gateway nodes in millimeter band using LOS path. Edge nodes can connect with aggregator or gateway nodes in microwave band or sub-6 GHz band using NLOS path. We use 5.8 GHz band, 28 GHz band and 60 GHz as representatives of sub-6 GHz, microwave and millimeter wave band respectively.

4.2.1 Interference limited versus interference free setting between edge and aggregator/gateway nodes

Typically, the antennas that operate at 28 GHz have high gain and very narrow beam width. We assume that aggregator nodes perform switched beams and cannot communicate with multiple edge nodes at the same time slot. On the other hand, due to the narrow beam width at both transmitter and receiver antennas, substantial interference suppression is achieved between non-adjacent links, i.e., two links that do not share a common node. We consider time/frequency division multiple access and interference free regime while considering microwave band between edge nodes and aggregator nodes.

The antennas that operate at sub-6 GHz typically come with wide beam width. An aggregator node can communicate with different small cells simultaneously using

space division multiple access (SDMA) techniques. However, edge nodes that intend to communicate with a particular aggregator node generate interference to neighbouring aggregator nodes. We consider the spatial multiplexing capability of aggregator nodes and use a power control based protocol interference model to capture the interference pattern in sub-6 GHz band.

4.2.2 Interference free setting between aggregator and gateway nodes

We assume that aggregator nodes - located at the roof tops of tall buildings - get LOS paths to gateway nodes and can use millimeter band for communications to/from the gateway nodes. Typically, the antennas that operate at millimeter wave band have narrow beam width. We assume that non-adjacent links do not interfere with each other and nodes cannot perform space division multiple access due to the complexity of multi-beam operation. Hence, similar to the microwave band, we assume an interference free setting and time/frequency division multiple access based fractional resource allocation in the links that connect aggregator and gateway nodes.

The next two sections provide the network optimization formulations in the following two scenarios: first, edge nodes communicating to aggregator or gateway nodes using microwave band in NLOS path and second, edge nodes communicating to aggregator or gateway nodes using sub-6 GHz band in NLOS path. In both these scenarios, aggregator nodes connect to gateway nodes using interference free millimeter wave band in LOS path.

4.3 Network optimization with microwave band in NLOS paths and mm wave band in LOS path

We consider a two-hop network with $\mathcal{EN}$ set of edge nodes and $\mathcal{GN}$ set of gateway nodes. Edge nodes act as sources (sinks) and gateway nodes act as sinks (sources) of data traffic in the uplink (downlink). Let $\mathcal{AN}$ denote the set of possible node locations of aggregator nodes. Aggregator nodes just relay data between sources and sinks.

Fig. 4.1 shows an example wireless backhaul network in downtown Manhattan. Blue,

Notation	Description
$\mathcal{N}$	Set of all nodes
$\mathcal{EN}$	Set of edge nodes
$\mathcal{AN}$	Set of candidate locations for aggregator nodes
$\mathcal{GN}$	Set of gateway nodes
E	Number of edge nodes
A	Number of candidate aggregator node locations
G	Number of gateway nodes
y_j	Binary decision variable for aggregator node deployment
c_{y_j}	Operational expense of deployment at node j
$\mathcal{M}_{5.8}$	Set of channels at 5.8 GHz
M	Number of channels
f_{ij}	Flow in link ij
W_{ij}	Allotted bandwidth in link ij
d_i	Demand of edge node i
W	Bandwidth of discrete channels at 5.8 GHz
N_0	Noise spectral density
B	Maximum no. of edge nodes that can be spatially multiplexed
p_{ij}^m	Allotted power between node i and j in channel m
g_{ij}^m	Link gain between node i and j in channel m
x_{ij}^m	If node i and j communicate in channel m
x_j^m	If node j uses channel m
x^m	If channel m is used
T_j	Maximum number of radios at node j
P_I	Interference threshold in protocol interference model
C_{p_i,W_j}	Capacity of link evaluated at power p_i and bandwidth W_j

Table 4.1: List of Notations

$$\min \sum_{j \in \mathcal{AN}} c_{y_j} y_j \tag{4.1a}$$

$$\sum_{j \in \mathcal{AN}} f_{ij} + \sum_{k \in \mathcal{GN}} f_{ij} = d_i \quad \forall i \in \mathcal{EN} \tag{4.1b}$$

$$\sum_{i \in \mathcal{EN}} f_{ij} = \sum_{k \in \mathcal{GN}} f_{jk} \quad \forall j \in \mathcal{AN} \tag{4.1c}$$

$$f_{ij} \leq W_{ij} \log_2\big(1 + \frac{p_{ij} g_{ij,28}}{N_0 W_{ij}}\big) \ \forall i \in \mathcal{EN}\,, \forall j \in \mathcal{AN}, \mathcal{GN} \tag{4.1d}$$

$$f_{ij} \leq W_{ij} \log_2\big(1 + \frac{p_{ij} g_{ij,60}}{N_0 W_{ij}}\big) \ \forall i \in \mathcal{AN}\,, \forall j \in \mathcal{GN} \tag{4.1e}$$

$$\sum_{j \in \mathcal{AN}, \mathcal{GN}} W_{ij} \leq W_{max,28}\,, \sum_{j \in \mathcal{AN}, \mathcal{GN}} p_{ij} \leq p_{max,28} \ \forall i \in \mathcal{EN} \tag{4.1f}$$

$$\sum_{i \in \mathcal{EN}} W_{ij} \leq y_j \cdot T_j W_{max,28} \ \forall j \in \mathcal{AN} \tag{4.1g}$$

$$\sum_{i \in \mathcal{EN}} W_{ij} \leq T_j \cdot W_{max,28} \ \forall j \in \mathcal{GN} \tag{4.1h}$$

$$\sum_{k \in \mathcal{GN}} W_{jk} \leq W_{max,60}\ , \sum_{k \in \mathcal{GN}} p_{jk} \leq p_{max,60} \ \forall j \in \mathcal{AN} \tag{4.1i}$$

$$f_{ij}, W_{ij}, p_{ij} \geq 0 \, \forall\, (i,j) \in \mathcal{E}\ , y_j \in \{0,1\} \ \forall j \in \mathcal{AN} \tag{4.1j}$$

Figure 4.2: Network optimization formulation when edge and aggregator nodes communicate in an interference free setting

green balloons and red markers denote edge, gateway and candidate aggregator node locations respectively. Our objective is to minimize the aggregator node deployment cost while ensuring the network connectivity between edge and gateway nodes.

Let us focus on the uplink of the backhaul network. Assume that d_i denotes the demand of each small cell. Let W_{ij}, p_{ij} and f_{ij} denote the allotted bandwidth, power and flow of link ij respectively. Let y_j denote a binary decision variable at node j, i.e., it represents whether one should place an aggregator node at the candidate location j. Let $W_{max,b}$ and $p_{max,b}$ denote the maximum allowed bandwidth and power *per radio* in band b. Node j can deploy up to T_j number of radios.

Fig. 4.2 shows the network optimization formulation for this scenario. Eq. (4.1a) denotes the objective function where we minimize the aggregator node deployment cost. Eq. (4.1b) and (4.1c) denote the flow conservation constraints. First, each edge node's outgoing data traffic to the aggregator nodes and gateway nodes should equal

$$\min \sum_{j \in \mathcal{AN}} c_{y_j} y_j \tag{4.2a}$$

Equations (4.1b), (4.1c), (4.1i), (4.1e).

$$f_{ij} \leq \sum_{m \in \mathcal{M}_{5.8}} W \log_2\big(1 + \frac{p_{ij}^m g_{ij}^m}{N_0 W}\big) \quad \forall i \in \mathcal{EN}\,, \forall j \in \mathcal{AN}, \mathcal{GN} \tag{4.2b}$$

$$p_{kh}^m + (p_{max} - \frac{P_I}{g_{kj}}) x_{ij}^m \leq p_{max} \;\forall k \in \mathcal{EN},\, h \in \mathcal{AN}, \mathcal{GN},\, k \neq i,\, h \neq j \tag{4.2c}$$

$$\sum_{i \in \mathcal{EN}} x_{ij}^m \leq B y_j\,,\, \forall m \in \mathcal{M}_{5.8}\,,\, \forall j \in \mathcal{AN} \tag{4.2d}$$

$$\sum_{i \in \mathcal{EN}} x_{ij}^m \leq B\,,\, \forall m \in \mathcal{M}_{5.8}\,,\, \forall j \in \mathcal{GN} \tag{4.2e}$$

$$\sum_{j \in \mathcal{AN}, \mathcal{GN}} \sum_{m \in \mathcal{M}_{5.8}} x_{ij}^m \leq T_j \;\forall i \in \mathcal{EN} \tag{4.2f}$$

$$\sum_{m \in \mathcal{M}} x_j^m \leq T_j \;\forall j \in \mathcal{AN}, \mathcal{GN} \tag{4.2g}$$

$$p_{ij}^m \leq p_{max} x_{ij}^m \quad \forall (i,j) \in \mathcal{E},\, \forall m \in \mathcal{M}_{5.8} \tag{4.2h}$$

$$x_{ij}^m \leq x_j^m \,\forall i \in \mathcal{EN},\, j \in \mathcal{AN}, \mathcal{GN},\, m \in \mathcal{M}_{5.8} \tag{4.2i}$$

$$p_{ij}^m,\, f_{ij} \geq 0,\, x_{ij}^m,\, y_j,\, x_j^m \in \{0,1\},\; \forall i \in \mathcal{EN},\, j \in \mathcal{AN}, \mathcal{GN},\, m \in \mathcal{M}_{5.8} \tag{4.2j}$$

$$f_{jk},\, p_{jk,60},\, W_{jk,60} \geq 0,\, \forall j \in \mathcal{AN},\, k \in \mathcal{GN} \tag{4.2k}$$

Figure 4.3: Network optimization formulation when edge and aggregator nodes communicate using a protocol interference model

the edge node's demand. Second, each aggregator node's incoming flow should equal its outgoing flow. Eq. (4.1d) and (4.1e) couple the flow, bandwidth and power variables at each link. It is assumed that edge nodes and aggregator nodes communicate in the 28 GHz and 60 GHz bands, respectively. Equations (4.1f)-(4.1i) denote the maximum available bandwidth and power constraints at each node. Equation (4.1g) couples all other constraints with the the aggregator node deployment variable of the optimization objective. Equation (4.1j) describes the variables of the optimization problem.

The optimization problem of Fig. 4.2 is a mixed integer non-linear program (MINLP). It contains $|\mathcal{AN}|$ number of binary decision variables. Next, we describe the optimization formulation of sub-6 GHz transmission based networks since it is another MINLP. Thereafter, we provide the solution methodology for solving these MINLP's.

4.4 Network optimization with sub-6 GHz in NLOS paths and mm-wave in LOS paths

Due to the wide beam width of antennas at sub-6 GHz, non-adjacent links can interfere with each other. To tackle this interference, we split the overall bandwidth at sub-6 GHz into a set of discrete channels. The edge nodes use these channels to communicate with aggregator or gateway nodes. Our goal is to schedule and allocate power in these channels optimally so that non-adjacent links do not interfere with each other.

Let x_{ij}^m, p_{ij}^m and g_{ij}^m denote the binary scheduling variables, power allocation and gain for link ij in channel m respectively.

$$x_{ij}^m = \begin{cases} 1, & \text{if node } i \text{ transmits to node } j \text{ using channel } m. \\ 0, & \text{otherwise.} \end{cases} \tag{4.3}$$

We use protocol interference model in our work. Our work can be extended to SINR interference model, too. Assume that node i transmits to node j in channel m, i.e., $x_{ij}^m = 1$. Another node k can transmit to node h in channel m if p_{kh}^m causes negligible interference in node j.

$$p_{kh}^m + (p_{max} - \frac{P_I}{g_{kj}^m}) x_{ij}^m \leq p_{max} \, \forall \, k \in \mathcal{N}, \, h \in \mathcal{N}, \, k \neq h \tag{4.4}$$

where P_I is the interference threshold.

Due to the wide beam width of sub-6GHz antennas, an aggregator or gateway node can cover multiple edge nodes using SDMA technology. Hence,

$$\sum_{i \in \mathcal{EN}} x_{ij}^m \leq B \, , \, \forall m \in \mathcal{M}_{5.8} \, , \, \forall j \in \mathcal{AN}, \mathcal{GN} \tag{4.5}$$

where $\mathcal{M}_{5.8}$ is the set of discrete channels at 5.8 GHz and B is the maximum number of edge nodes that one radio of aggregator/gateway node can cover using SDMA technology. For simplicity, we assume that the aggregator or gateway node can employ very large number of antennas at their end and fully suppress the interference among

covered edge nodes by using a minimum-mean-squared-error decoder when the ratio of number of antennas to number of edge nodes becomes very high [96]. The value of B depends on the the number of antennas at the aggregator/gateway node. Our model can accommodate the case of imperfect interference suppression as a gap to capacity. We relate the value of B, the number of aggregator node antennas and desired interference suppression in the numerical simulations section.

Fig. 4.3 shows the network optimization formulation with the protocol interference and spatial multiplexing constraints. The optimization objective of (4.1a), flow conservation constraints of (4.1b), (4.1c) are same as in Fig. 4.2. Also, power and bandwidth allocation equations between aggregator and gateway nodes (equation (4.1i) and (4.1e)) re-appear in Fig. 4.3.

Equation (4.2d) couples the aggregator node deployment decision variables to all other constraints by ensuring that a candidate location must be selected for deployment if it uses any channel. Power control based protocol interference model appears at (4.2c). Spatial multiplexing capability of aggregator and gateway nodes appear at (4.2d) and (4.2e). Eq. (4.2f) shows that the number of channels that an edge node can use is limited by the maximum number of allowed radios in that node. Eq. (4.2g) denotes that an aggregator or gateway node j can place up to T_j number of radios. Eq. (4.2h) couples the power allocation and scheduling variables. Eq. (4.2i) couples the link scheduling and node scheduling variables. Eq. (4.2j) and (4.2k) describe the variables of the optimization program.

The optimization problem of Fig. 4.3 is also a MINLP. It contains $|\mathcal{AN}| + |\mathcal{EN}| * |\mathcal{M}| * \big(|\mathcal{AN}| + |\mathcal{GN}|\big)$ number of binary variables. The number of integer variables (both scheduling variable x_{ij}^m and aggregator node deployment variable y_j) in this scenario is much higher than that of Fig. 4.2 which only contains deployment variable y_j. Section 4.5 shows how we solve these MINLP's.

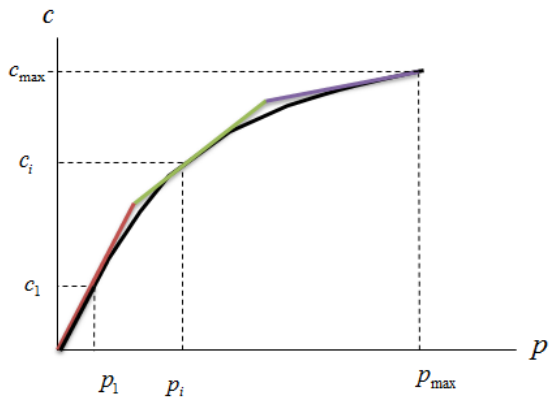

Figure 4.4: Linear relaxation of the capacity function. First order Taylor approximation at points p_1,p_i and p_{max} provide an upper bound of the log function.

4.5 Solution of the Optimization Problem

We reformulate the MINLP's to mixed integer linear programs (MILP) to speed up the optimization convergence and to be able to use free solvers. We relax the log functions of the capacity equations into a set of linear functions, solve the resultant MILP using branch-and-bound algorithm and find a feasible solution of the optimization problem from the relaxed solution. We describe these steps in the next three sub-sections.

4.5.1 Linear relaxation of the capacity function

The capacity functions of (4.1d), (4.1e) and (4.2b) are concave functions with respect to the allotted power p and bandwidth W [86]. Hence, each capacity function can be upper bounded into a set of linear functions by taking slopes at different points [44]. Let us define a set of power variables $\mathcal{P}_I = \{p_1, \cdot, p_i, \cdot, p_{max}\}$ and bandwidth variables $\mathcal{W}_J = \{W_1, \cdot, W_j, \cdot, W_{max}\}$ for a link with gain g. Let $C = W \log_2(1 + \frac{pg}{N_0 W})$ denote the capacity function and $C_{p_i,W_j} = W_j \log_2(1 + \frac{p_i g}{W_j})$ represent the capacity with power p_i and bandwidth W_j. We bound the flow f in the link by taking first order Taylor approximation in each of the power-bandwidth pairs:

$$\begin{aligned} f \quad &\leq \quad C_{p_i,W_j} + m_{p_i} \cdot (p - p_i) + m_{W_j}(W - W_j) \\ &\qquad \forall p_i \in \mathcal{P}_I \, , \forall W_j \in \mathcal{W}_J \end{aligned} \tag{4.6}$$

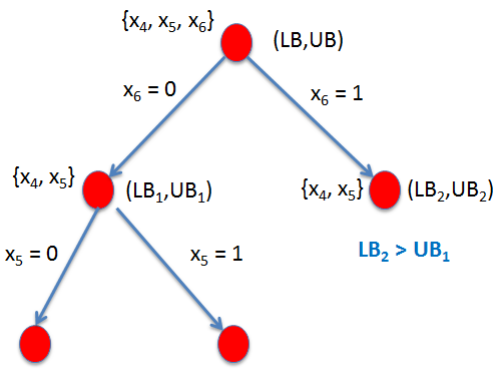

Figure 4.5: Branch and bound algorithm of an optimization problem that contains three binary variables (x_4, x_5 and x_6).

where,

$$m_{p_i} = \frac{\partial C}{\partial p}\bigg|_{p=p_i}, \; m_{W_j} = \frac{\partial C}{\partial W}\bigg|_{W=W_j} \tag{4.7}$$

$$f \leq c\bigg|_{p=p_i, W=W_i} + \Big[\frac{\partial c}{\partial p}\bigg|_{p=p_i}, \frac{\partial c}{\partial W}\bigg|_{W=W_j}\Big]\big[(p-p_i),(c-c_j)\big]^T$$
$$\forall p_i \in \mathcal{P}_I \,, \forall W_j \in \mathcal{W}_J. \tag{4.8}$$

Here, $\frac{\partial c}{\partial p}\Big|_{p=p_i}$ and $\frac{\partial c}{\partial W}\Big|_{W=W_j}$ denote the partial derivatives of the capacity c with respect to the power and bandwidth variables, evaluated at $p = p_i$ and $w = w_j$ respectively. The capacity of the link with p_i power and W_j bandwidth is represented by c_{ij}.

Fig. 4.4 shows our linear relaxation procedure. We relax the non-linear equations of (4.1d), (4.1e) and (4.2b) in this way and the MINLPs of Fig. 4.2 and 4.3 reformulate to MILPs.

4.5.2 Branch-and-bound algorithm

A brute force solution of the MILP requires exponential number of searches. We use YALMIP [97] and GNU Linear Programming Kit (GLPK) [98] to solve the MILPs. GLPK uses branch-and-bound algorithm to solve the MILP, which operates as follows: branch-and-bound algorithm branches in each binary variable, as shown in Fig. 4.5. In each branch, the algorithm calculates a lower bound using continuous relaxation of the binary variables and an upper bound by finding a feasible solution. The algorithm

updates the global lower and upper bound and stops when their difference becomes smaller than the pre-defined optimality gap [99].

Fig. 4.5 shows how branch-and-bound reduces the search complexity by pruning branches that are not useful. At the beginning, the algorithm calculates lower bound (LB) and upper bound (UB)of the overall problem. The algorithm branches on x_6 and calculates the lower and upper bound for $x_6 = 0$ (LB_1,UB_1) and $x_6 = 1$ (LB_2, UB_2) respectively. If $LB_2 \geq UB_1$, the algorithm prunes $x_6 = 1$ branch and continues further on $x_6 = 0$ branch.

In standard branch-and-bound procedure, partitioning is done by choosing the variable with the largest relaxation error [44]. The reason for this partitioning is that such a variable could lead to a large gap between the upper and the lower bound. However, such standard procedures do not exploit the specific properties of the problem.

Our partitioning approach to speed up the convergence of the branch-and-bound algorithm is based on the fact that the aggregator node placement decision variables (y_j) are more important than scheduling variables (x_{ij}^m). Hence, aggregator node placement decision variables are branched before scheduling variables.

4.5.3 Feasible solution

Any feasible solution of MILP may not be a feasible solution of the original MINLP since we relaxed the capacity function into a set of linear functions. This is because some edge nodes' flow may exceed the capacity of their links with the allotted power and bandwidth. Therefore, we find a feasible solution in the following ways.

- *Tightening the relaxation gap:* We increase the granularity of piecewise linear approximation.

- *Checking for spare bandwidth:* We ensure that each aggregator node uses its entire allocated bandwidth before declaring infeasibility. We find this by fixing the scheduling and deployment variables of the MILP output, and running the MINLP for bandwidth, power and flow variables which is a convex optimization problem [86].

- *Iterate the process:* If previous step does not provide a feasible solution, we iterate the whole process by re-formulating the MINLP where the currently infeasible edge nodes form the new set of edge nodes and unselected aggregator nodes form the new set of aggregator nodes.

4.5.4 Algorithm running time

The only integer variables of Fig. 4.2, i.e., network optimization with microwave in NLOS and mm-wave in LOS, are deployment decision variables. Due to the low number of deployment decision variables, the branch-and-bound algorithm converges quickly. Using GLPK [98] and branch-and-bound algorithm, we ran a problem instance of Fig. 4.2 that consisted of 18 edge nodes, 16 candidate aggregator node locations and 3 gateway nodes. The solution converged in 30 seconds with 0% optimality gap. Such time complexity is acceptable, since aggregator node deployment is an offline planning task.

The integer variables of Fig. 4.8, i.e., network optimization with sub-6 GHz in NLOS and mm-wave in LOS, come from both deployment decision variables and binary scheduling variables. The number of binary scheduling variables is proportional to the product of the number of edge nodes, number of candidate aggregator node locations and number of channels at 5.8 GHz. In a scenario containing 18 edge node, 16 candidate aggregator node, 3 gateway node and 6 discrete channels, there are roughly $(18 \cdot 16 \cdot 6 + 18 \cdot 3 \cdot 6) = 2052$ scheduling variables. Using GLPK [98] and branch-and-bound method, we solved this problem instance in 30 minutes with 0.5 optimality gap. This running time is also acceptable since this is an offline planning algorithm. However, due to the exponential worst case complexity, this running time could be much higher for a higher number of edge nodes and candidate aggregator nodes. This prompted us to develop a polynomial time algorithm for the network optimization with sub-6 GHz in NLOS and mm-wave in LOS path.

Line	Operation
1	Assume each edge node (EN) uses its maximum power and one discrete channel.
2	Using the assumption of line 1, calculate the capacity between each edge node to all aggregator nodes (AN) and gateway nodes (GN).
3	A link between between EN and AN/GN exists only if it can sustain the demand of the EN.
4	Each AN and GN is associated with a set whose elements are the edge nodes that it can cover.
5	Select the GN set with the highest set size
6	Assign all adjacent EN's to this GN.
7	Assign channel to the sets in such a way so that the EN's of the newly selected set do not interfere with the previously selected AN's/GN's and the newly selected AN/GN do not get interfered by the previously selected EN's.
8	Remove the selected EN's and GN from available set. Go to line 5. Iterate until all GN are selected or all EN's are covered.
9	If all EN's are covered, stop. Else, proceed.
10	Select the AN with the maximum coverage.
11	Assign all adjacent EN's to this AN.
12	Maintain the channel assignment condition of line 8.
13	Remove the selected EN's and AN from available set. Go to line 9. Iterate until all EN's are covered

Table 4.2: Greedy Set Covering based Network Optimization with sub-6 GHz in NLOS Paths and mm-wave band in LOS paths

4.6 Greedy Set Covering based Network Optimization with sub-6 GHz in NLOS Path and mm-wave band in LOS path

In this section, we develop a greedy polynomial time algorithm for the network optimization problem of Fig. 4.3. We make the following assumption in our algorithm: an edge node can only use one channel and talk to one aggregator or gateway node. Table 4.2 summarizes our greedy algorithm. We describe the complexity of the greedy algorithm below. Throughout the complexity analysis, we use E, G, A and M to denote the number of edge nodes, gateway nodes, candidate locations of aggregator nodes and discrete channels respectively.

Lines $1-3$ of table 4.2 find out if an edge node can sustain its demand to aggregator and gateway nodes. This provides the connectivity between every edge node to all

other aggregator and gateway nodes in the network ($O(AE + GE)$). We end up with a number of sets where each set is associated with an aggregator or gateway node and the elements of the sets are the edge nodes that can be covered by that particular aggregator or gateway node. The union of all sets represent the edge nodes that can be covered by these aggregator or gateway nodes.

Our objective is to cover all edge nodes while minimizing the deployment cost of the selected sets. Gateway nodes have already been deployed. Our optimization variables are aggregator node deployment decision variables. Hence, we first select the gateway node affiliated sets and cover as many edge nodes as possible. If gateway nodes cannot cover all edge nodes, we keep selecting aggregator nodes one after the other until all edge nodes are covered. We employ the greedy set covering algorithm to select the gateway and aggregator nodes [100]. Line $5 - 8$ and $10 - 13$ show gateway and aggregator node selection procedure using the greedy set covering approach.

In each outer loop, greedy set covering algorithm selects a set by performing three steps: first, counting size of each set; second, finding the set with the highest set size; and third, removing the edge nodes of the newly selected from other sets. There can be at most E edge nodes in each set and there can be at most $A + G$ sets, in total. Hence, counting set size at each loop can take at most $(A + G)E$ operations. Finding the set with the highest size takes at most $(A + G)$ operations. Removing elements from other sets involve at most $(A + G)E$ operations. The outer loop can run at most $(A + G)$ times. Hence, the overall complexity of our covering algorithm is: $O((A+G)(A+G)E)$.

We employ greedy coloring algorithm [100] to assign channels to the newly selected sets. Line 7 of Table 4.2 shows how we color, i.e., assign channels to, newly selected sets. The edge nodes of a newly selected set cannot interfere with the aggregator or gateway nodes of the previously selected sets [101]. There can be at most $(A+G)$ newly selected sets and each set can contain at most E edge nodes. Each set can interfere with at most $(A+G)$ previous sets and this interference can happen for at most M channels. Hence, the overall complexity associated with greedy coloring is $O((A + G)(A + G)EM)$.

The above analysis suggests that the total complexity of the overall algorithm is dominated by the greedy coloring algorithm $O((A+G)(A+G)EM)$. Let's assume that

Features	5.8 GHz	28 GHz	60 GHz
Rain Attenuation (dB) [103]	0	2.5	10
Oxygen Absorption (dB) [103]	0	0.5	15
Antenna gain (dB)	17 [53]	38 [53]	38 [104]
Maximum transmit power (dBm)	19 [53]	19 [53]	25
Fading margin (dB)	15	25	25
Channel width (MHz)	40 [53]	56 [53]	160 [104]
Number of channels	6	6	6

Table 4.3: Backhaul features at different bands

the number of edge nodes is roughly equal to the number of candidate aggregator node locations. Also assume that the number of gateway nodes is much smaller than both number of edge nodes and aggregator nodes. That means, $G << E \approx A$. *With this assumption, our proposed greedy algorithm has a complexity of* $O(E^3M)$.

4.6.1 Performance bound

Greedy weighted set covering guarantees an optimality gap of at most $\ln(K)$ *where* K *is the size of the set that contains the highest number of edge nodes [102].*

Our greedy coloring algorithm does not guarantee that the available channels will be sufficient to color all elements of the graph. This happens since graph coloring is an NP-hard problem in general [100].

Simulation results suggest that our algorithm performs similar to the branch-and-bound based algorithm in terms of aggregator node deployment cost and edge node coverage.

4.7 Numerical results

We consider an example wireless backhaul network in downtown Manhattan and obtain channel gains using ray tracing tools. We place edge nodes at street levels, aggregator nodes at the top of nearby tall buildings and gateway nodes at the top of the tallest buildings of downtown Manhattan. Fig. 4.6 shows the example wireless backhaul network. Our ray tracing tool uses actual building locations and building heights of downtown Manhattan and a diffraction based propagation model to generate link

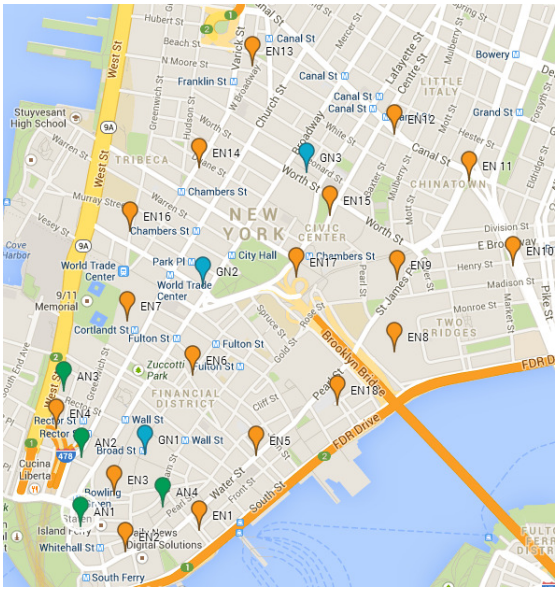

Figure 4.6: A realistic network scenario in downtown Manhattan. Orange and light blue markers denote locations of edge nodes and gateway nodes. Green markers denote candidate locations of aggregator node deployment.

gains. These link gains are incorporated with the backhaul features of Table 4.3. We assume equal deployment cost for all aggregator nodes' locations and 100 Mbps demand from edge nodes.

4.7.1 Network connectivity with microwave band

At first, we use the 28 GHz link gains between the edge and aggregator/gateway nodes and 60 GHz link gains between aggregator and gateway node. We run the network optimization problem of Fig. 4.2. Fig. 4.7 shows the network connectivity in this scenario. Two candidate aggregator locations – highlighted with green rectangle marker around them – get selected for aggregator node deployment. The optimality gap is 0% in this scenario.

Our resultant network is free of primary interference. Adjacent links use different bandwidth in the network scenario of Fig. 4.7. However, non-adjacent nearby links are allowed to share bandwidth. This happens since we assumed an interference free regime in the network optimization formulations of microwave band. We now check the validity of our assumptions. Assuming that antennas have no side lobes, we find that

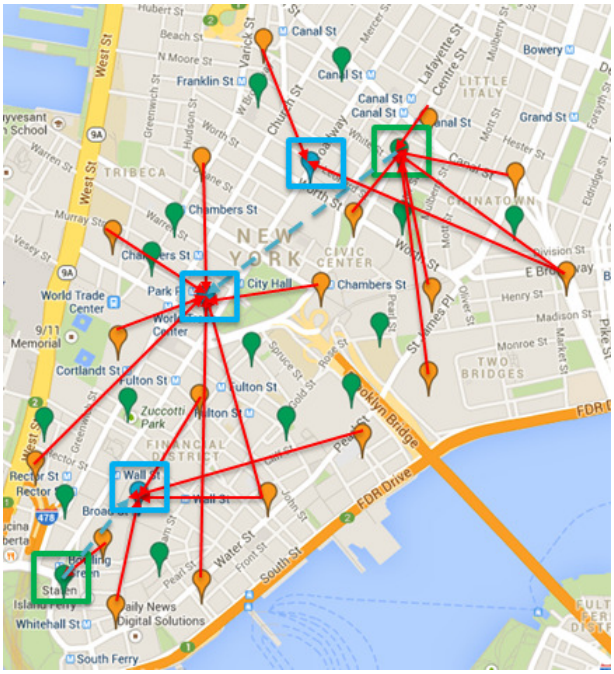

Figure 4.7: Network connectivity when edge nodes (orange markers) transmit in 28 GHz (red lines) to aggregator nodes (green markers) and gateway nodes (highlighted with light blue rectangle around it). Aggregator nodes transmit in 60 GHz (dashed blue lines) to gateway nodes. Figure taken from [6]

the maximum interference among non-adjacent links that use the microwave band falls 19 dB below the noise threshold.

4.7.2 Network connectivity with sub-6 GHz band

In this setup, we use the 5.8 GHz link gains between edge and aggregator/gateway nodes and 60 GHz links gains between aggregator and gateway nodes. Using these link gains, we run the optimization problem of Fig. 4.3. We assume an aggregator/gateway node can cover up to four edge nodes in the same channel using SDMA at 5.8 GHz.

Fig. 4.8 shows the associated network connectivity. Each solid colored line represents a discrete channel from the 5.8 GHz channel set. Some aggregator/gateway nodes communicate with multiple edge nodes in the same discrete channel using the spatial multiplexing capability. Two non-adjacent nearby links perform power allocation and get colored in such a way that no edge interferes with each other. One Edge node (highlighted with orange rectangle marker around it) does not have good enough link gain with any aggregator or gateway node to sustain its demand. Therefore, it becomes

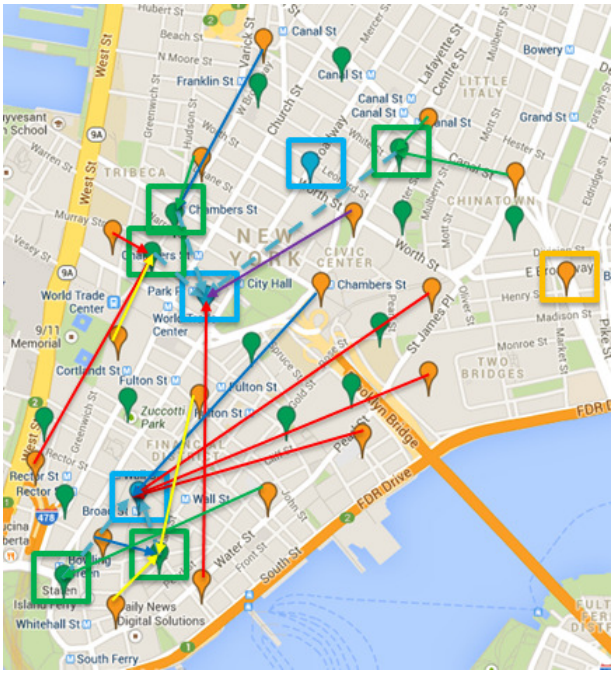

Figure 4.8: Network connectivity when edge nodes transmit in 5.8 GHz and aggregator nodes transmit in 60 GHz. Figure taken from [6]

an infeasible edge node. The rest of the edge nodes require the deployment of five aggregator nodes – highlighted with green rectangle marker around them – to meet their demand. The optimality gap is 40% in this case. We ran MILP of both sub-6 GHz and microwave band for 30 minutes. Optimization problem of Fig. 4.3 contains higher number of binary variables (both scheduling and node placement variables) than that of Fig. 4.2 (only node placement variables). Hence, sub-6 GHz based network optimization converges slowly.

It should be noted that we have not modeled many practical aspects such as antenna alignment, material reflectivity, etc. that affect the link gain at 28 GHz. Our intention was not to compare sub-6 GHz and 28 GHz band. We just contrast their respective optimization problems.

Performance of greedy algorithm with sub-6 GHz in NLOS and mm-wave band in LOS path

Network connectivity results of Fig. 4.8 were obtained with the branch-and-bound solution procedure. Recall that we provided a greedy algorithm with polynomial time

Demand	Branch-and-bound		Greedy	
(Mbps)	Covered EN	Selected AN	Covered EN	Selected AN
50	18	4	18	4
100	17	5	16	5
150	16	5	16	5
200	16	6	16	6
250	15	7	15	7

Table 4.4: Performance comparison between branch-and-bound and greedy algorithm in network optimization with sub-6 GHz in NLOS and mm-wave band in LOS

complexity in Sec. 4.6 to design a wireless backhaul network that uses sub-6 GHz in NLOS and mm-wave band in LOS path. Now, we compare the performance of branch-and-bound based solution and greedy algorithm in this scenario.

Table 4.4 compares the performance of branch-and-bound and greedy algorithm. Each row of Table 4.4 represents a network scenario of Fig. 4.6 where the first column denotes the demand across edge nodes of the network. We observe how branch-and-bound based solution and the greedy algorithm perform in terms of edge node coverage and aggregator node deployment.

Table 4.4 shows that the number of covered edge nodes decrease and the required number of aggregator node deployments increases with increasing demand. This is not surprising since some edge nodes may not have adequate link gain with any aggregator or gateway node to sustain higher demand. Due to per node bandwidth and power constraint, these nodes cannot be covered with higher demand. Also, as demand increases, link gains between edge nodes and gateway nodes do not remain good enough to sustain high data rate. This increases the required number of aggregator node deployment in the network.

Table 4.4 shows that the greedy algorithm performs exactly the same as the branch-and-bound methodology in all these scenarios. The branch-and-bound algorithm was run for roughly 20 minutes in each scenario and the resulting optimality gaps ranged between 0.4 to 0.6. Branch-and-bound algorithm might have performed better if we ran it for much longer period.

Also, our current greedy algorithm only applies to the scenario where each edge node

can use one channel. Our future work will extend this algorithm to a general scenario where each edge node can use multiple discrete channels at 5.8 GHz to communicate with the aggregator and gateway nodes.

Unlike branch-and-bound, greedy algorithm has polynomial time complexity. Our greedy algorithm code only required a few seconds to converge. Due to its equal performance and low complexity, greedy algorithm can be used to design wireless backhaul networks that consist of higher number of nodes.

4.7.3 Relationship between Interference Suppression and the number of spatially multiplexed edge nodes

This section focuses on the scenario where one aggregator node (AN) supports multiple edge nodes (EN) at the same channel. Fig. 4.9 shows how the number of edge nodes influences the SINR that the edge nodes experience.

Channel between the aggregator node and each edge node undergoes a combination of large scale and small scale fading. We assume that each edge node sees 20 dB signal-to-noise-ratio (SNR) due to large scale fading. Instantaneous values of random small scale fading parameters differ between edge nodes, and follow Winner II B5d channels [105]. Winner II B5d channels provide small scale fading coefficients between two non-line-of-sight stationary feeders that are located at rooftop and street level.

The aggregator node contains eight antennas and employs minimum-mean-squred-error algorithm to suppress interference among edge nodes. Fig. 4.9 shows that the cumulative probability of SINR decreases as the number of supported edge nodes increases.

We use an SNR based equation, not SINR based equation, in (4.2b) to describe the capacity of multiple edge nodes that are connected to the same aggregator node. Fig. 4.9 shows how one can use a SNR based equation by properly selecting the maximum number of supported edge nodes and desired outage probability. For example, the aggregator node can support four edge nodes simultaneously with 20 dB SINR and 10% outage probability. If the aggregator node wants to support six edge nodes with 10% outage probability, the supported edge nodes will experience 17 dB SINR which

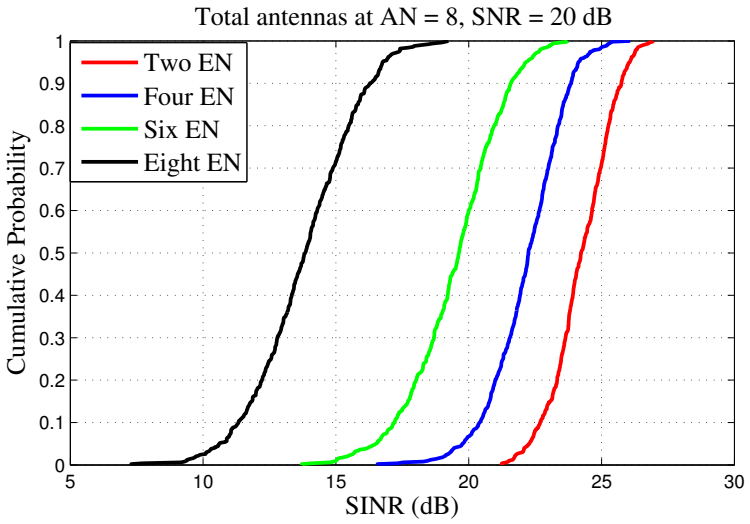

Figure 4.9: CDF of SINR curves

is 3 dB below from the SNR of their individual links.

Network operator can select different number of maximum supported edge nodes and capacity gap (coming from the difference between SINR and SNR of the link) and employ them in the optimization problem of Fig. 4.3.

4.8 Chapter Summary

Small cells can keep up with the increasing demand of wireless networks; but require backhaul to transport data to (from) a gateway node. Wireless backhaul can provide an inexpensive option to small cells. Aggregator nodes, located at roof tops of tall buildings near small cells, can provide high data rate to multiple small cells in NLOS paths, sustain the same data rate to gateway nodes in LOS paths and take advantage of all available bands for wireless backhaul.

This part of our work performed joint cost optimal aggregator node placement, power allocation, channel scheduling and routing to optimize the wireless backhaul network. We investigated wireless backhaul network using both sub-6 GHz and microwave bands. We considered the different interference patterns and multiple access features in these bands and incorporated them in backhaul network optimization. We developed two solution methodologies - branch-and-bound and greedy - to solve these network

optimization problems. Simulation results showed that aggregator nodes can play a significant role in transporting traffic between small cells and gateway nodes.

Chapter 5

A Wireless Channel Sounding System for Small Cell Networks

5.1 Introduction

In this chapter, we describe our effort in designing a rapid wireless channel sounding system for small cell networks. This system uses the Universal Software Radio Peripheral (USRP) and GNU Radio software. Our design measures channel propagation characteristics simultaneously from multiple transmitter locations. The system also accommodates multiple battery-powered transmitters and receivers. Therefore, we can set-up the channel sounder rapidly at a field location and measure expeditiously by analyzing different transmitters' signals during a single walk or drive through the environment. Our design can be used for both indoor and outdoor channel measurements in the frequency range of 1 MHz to 6 GHz. We expect that the proposed approach, with a few further refinements, can transform the task of propagation measurement as a routine part of day-to-day wireless network engineering.

5.2 Measurement System

We use GNU Radio software and USRP daughterboards in the channel sounding experiments. The top and bottom parts of Fig. 5.1 show the transmit and receive block diagrams of the USRP respectively. On the transmitter side, the host processor sends complex baseband samples to the field programmable gate array (FPGA) through an ethernet cable. The FPGA board low pass filters and up-converts the signal to a higher sampling rate. Thereafter, the signal goes through the digital-to-analog converter (DAC) and the passband frequency conversion stage to the transmitter antenna.

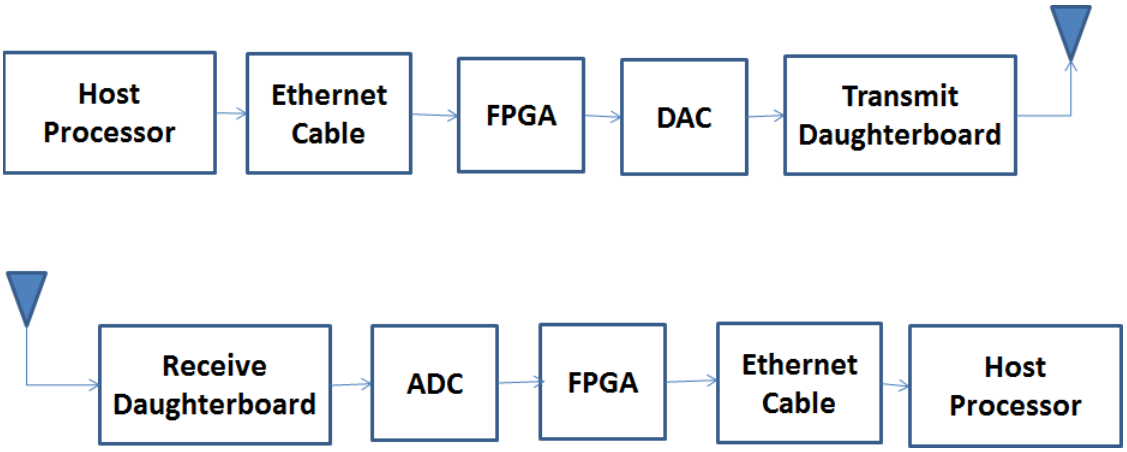

Figure 5.1: USRP block diagram

The receiver side operates exactly in the opposite manner.

The host processor views these complex baseband samples as floating point numbers. GNU Radio is an open source software that allows the use of digital signal processing algorithms on these floating point numbers.

We use USRP networked (N) and embedded (E) series radios in our experiments. The N series and E series softwares allow up to 50 MS/s and 8 MS/s data transfer rate respectively from the host processor. The temporal resolution of the sliding correlator channel sounding experiments depend on the maximum sampling rate of the radio. Therefore, we use the N series radios in sliding correlator channel sounding experiments. Note that, the N series radios require external laptops for each transmitter and receiver. Due to the availability of external power source in office building, we use the N series radio based sliding correlator channel sounding in indoor experiments.

On the other hand, the use of an external laptop in outdoor environment is inconvenient due to its heavy weight and limited battery lifetime. An E series radio contains an embedded processor and can work as a stand-alone pre-programmed transceiver. Hence, we use USRP E series transmitters in outdoor experiments. The embedded processor of E series radios can provide sampling rates up to 8 MS/s (4 Mega Symbols per second with 2 samples per symbol). In a sliding correlator channel sounding system, this sampling rate limits the temporal resolution to 250 ns. This resolution is too low to handle the rich multipath delay spread of an outdoor environment. Therefore, we

perform frequency domain channel sounding in outdoor experiments.

5.3 Sliding Correlator Channel Sounding

5.3.1 Methodology

In the sliding correlator approach, the transmitters send a pseudo-noise (PN) sequence with a 60 nanosecond (ns) pulse duration and the receiver obtains the wideband path loss and multipath delay profile. The upper and lower parts of Fig. 5.2 use a single transmitter and receiver to show the transmit and receive diagrams of the sliding correlator system respectively .

Transmission

The transmitter sends $\mathbf{x}$, a Galois linear feedback shift register (GLFSR) maximal length PN sequence of degree 10. We can write $\mathbf{x}$ as follows:

$$x[n] = \sum_{r} c[n - rN] \tag{5.1}$$

where, $N = 1023$ and $\mathbf{c}$ is a chip sequence of length 1023, $\mathbf{c} = [c_0, \cdots, c_{1022}]$. Here, $c_i \, \forall \, i \in [0, 1022]$ takes the value of either $+1$ or -1. Defining $\mathbf{R}_{cx}$ as the correlation output of $\mathbf{c}$ and $\mathbf{x}$ and using the properties of PN sequence,

$$R_{cx}[n] = \left\{ \begin{array}{ll} 1 & n = 0, N, -N, 2N, -2N, \cdots \\ -\frac{1}{N} & otherwise \end{array} \right\} \tag{5.2}$$

The signal $\mathbf{x}$ is passed through a root raised cosine (RRC) filter and then sent to the real input of the USRP transmitter module. The imaginary input comes from a null source. The USRP transmitter module sends the complex baseband samples to the USRP transmit path and establishes the transmit frequency and sampling rate. The baseband equivalent transmitted signal is given by:

$$x(t) = \sum_{n} x[n] p(t - nT_s) \tag{5.3}$$

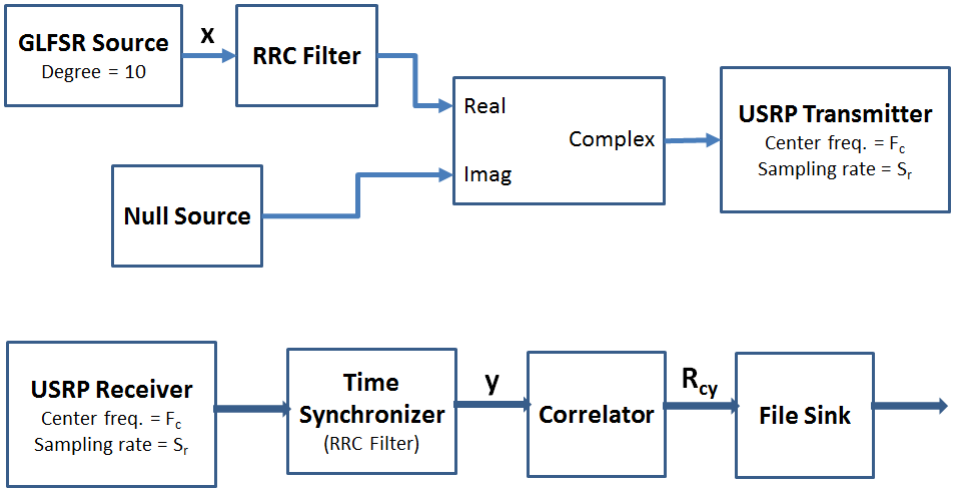

Figure 5.2: Sliding Correlator Channel Sounder System

Parameter	Value
Pathloss dynamic range	45-105 dB
Temporal resolution	60 ns
Maximum multipath delay	61 ms

Table 5.1: (Sliding correlator channel sounder system parameters)

where T_s is the period of the RRC generated pulse.

Multipath Channel

The impulse response of the multipath channel can be written as:

$$h(t) = \sum_{l=0}^{L-1} \alpha_l \delta(t - \tau_l) \tag{5.4}$$

Here, L is the number of multipaths in the channel, α_l is the complex gain of each multipath and τ_l is the associated delay. We assume $\tau_0 = 0$ since we focus on relative delay.

Reception

The baseband equivalent received signal, in time domain, is obtained by:

$$y(t) = (x * h)(t) = \sum_{l=0}^{L-1} \alpha_l x(t - \tau_l) \tag{5.5}$$

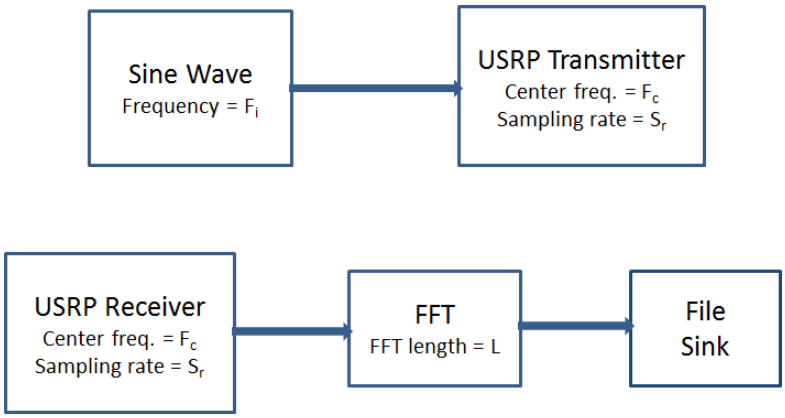

Figure 5.3: Frequency Domain Channel Sounder System

Parameter	Value
Pathloss dynamic range	45-120 dB
Frequency resolution (Δf)	2 MHz
Number of steps (N)	10
Temporal resolution	27.8 ns

Table 5.2: (Frequency domain channel sounder system parameters)

$y(t)$ goes through the USRP receive path, gets sampled and arrives at the USRP receiver module of Fig. 5.2. The time synchronizer block finds the proper phase of the RRC pulses. A detailed theoretical description of the time synchronizer can be found in [106] and the open source code description can be found in [107]. Proper timing synchronization leads to the following discrete received signal $\mathbf{y}$,

$$y[j] = y[jT_s] = \sum_{l=0}^{L-1} \alpha_l \sum_n x[n]p[(j-n)T_s - \tau_l] \tag{5.6}$$

Equation (5.6) follows from (5.3) and (5.5). Assume that the multipath delay τ_l is an integer multiple of the pulse period T_s. With this assumption, $\tau_l = c_l T_s$ where c_l is a non-negative integer. The properties of the RRC filter suggest that $p(nT_s) = 0$ if $n \neq 0$ [108]. Therefore,

$$\begin{aligned} y[j] &= \sum_{l=0}^{L-1} \alpha_l \sum_n x[n]p[(j-n-c_l)T_s] \\ &= \sum_{l=0}^{L-1} \alpha_l x[j-c_l] \end{aligned} \tag{5.7}$$

Now, the correlator block produces,

$$R_{cy}[n] = corr(\mathbf{c}, \mathbf{y}) = \sum_{l=0}^{L-1} \alpha_l R_{cx}[n - c_l] \tag{5.8}$$

where, $\mathbf{R}_{cx} = corr(\mathbf{c}, \mathbf{x})$. Using (5.2) in (5.8), one can easily find the complex multipath gain α_l at delay, $\tau_l = c_l T_s$. For example, $R_{cy}[0], R_{cy}[N], \cdots$ lead to the calculation of α_0 whereas, $R_{cy}[1], R_{cy}[N+1], \cdots$ lead to α_1. The multipath power-delay profile can be obtained from the powers of the individual multipath components $|\alpha_l|^2$. The path loss can be found from the difference of the known transmit power and the total power in the multipath components ($\sum_{l=0}^{L-1} |\alpha_l|^2$).

Note that, path loss calculation does not require time synchronization. On the other hand, the correct estimate of multipath power delay profile requires time synchronization. The time synchronization algorithm [107] only operates at moderate and high signal-to-noise-ratio. Therefore, although we had a path loss dynamic range of 45 to 105 dB, we could measure multipath delay profile only from 45 to 80 dB path loss range.

5.3.2 Multiple transmitter sliding correlator channel sounding algorithm

Different transmitters repeatedly access their allotted time slots and transmit the GLFSR PN sequence. The receiver captures the PN sequences from each transmitter and finds the path loss and delay profile for each of them. The overall algorithm is summarized below:

1. Assume there are N transmitters. Transmitter i transmits in the desired frequency band during the time slot $[t_{i-1} + r * T_p\,,\, t_i + r * T_p] \,\forall\, r \;\in\; [0, 1, \cdots, M]$. Here, $t_i - t_{i-1} = \Delta t$ is the allotted time slot length of each transmitter during each time period T_p and $T_p = \Delta t \times N$. Also, $M \times T_p$ is the total experiment duration.

2. The user opens the floor map image in the receiver laptop and clicks a point that corresponds to the present location. The receiver flow graph is initiated at time $p \times T_p$ where p is the nearest integer.

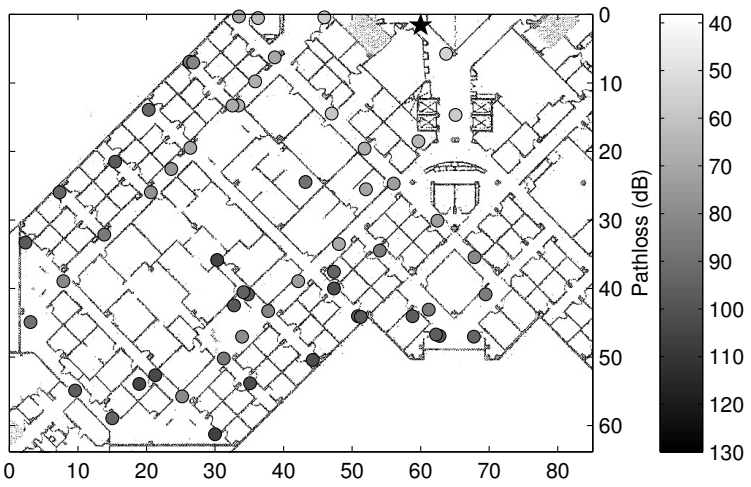

Figure 5.4: Path loss data for indoor transmitter 1

3. The receiver captures the samples during the time slot $[pT_p, (p+1)T_p]$, splits the floating point numbers into N segments and uses the i^{th} segment to calculate the path loss and delay profile of the i^{th} transmitter.

4. The wideband path loss, delay profile and X & Y coordinates of the location are stored in the laptop.

5.3.3 Challenges of multiple transmitter channel sounding in the sliding correlator method

Time synchronization

We use the USRP N series radios, controlled by external laptops, in the sliding correlator channel sounding method. The clock timing of these laptops is synchronized in advance through network time protocol (NTP) servers [109]. The synchronized laptops control the TDMA operation of the multiple transmitters.

Near-far effect

In an ideal N transmitter TDMA system, $N-1$ transmitters remain silent when one transmits. In order to implement this method in our setup, the $N-1$ USRP radios have to either turn off or transmit null source during the active transmission period

of the other radio. The frequent turn on-and-off leads to the freezing up of USRP radios. On the other hand, USRP radios leak a small amount of power while transmitting a null source. This leakage power leads to the classical near-far problem in a multiple transmitter scenario, i.e., the channel measurements of the far transmitter get overwhelmed by the leakage from the near transmitter, due to the large difference of path loss among the transmitters. In order to avoid these two problems, we take the following approach: when transmitter i transmits, transmitter $j \forall \in [1, N]$, $j \neq i$ transmits in the industrial, scientific and medical radio band at the lowest power possible. The receiver receives samples in the desired frequency band and therefore, the channel measurements of different transmitters remain independent of each other.

The design parameters of the sliding correlator channel sounder are given in Table 5.1.

5.4 Frequency Domain Channel Sounding

5.4.1 Methodology

In the frequency domain channel sounding method, the transmitters and the receiver synchronously sweep a given frequency band in Q discrete steps of Δf. By sweeping a large frequency band, one can obtain a very fine temporal resolution [68]. The top and bottom parts of Fig. 5.3 show the transmitter and receiver block diagrams of a frequency domain channel sounder using a single transmitter and receiver.

5.4.2 Multiple transmitter frequency domain channel sounding algorithm

Assume that there are Q carrier frequency steps and K transmitters. There is a predefined list of carrier frequencies, $\mathbf{F}_c = [F_{c_1}, \cdots, F_{c_Q}]$ and sinusoidal frequencies, $\mathbf{f} = [f_1, \cdots, f_K]$. The algorithm can be described as follows:

1. The USRP clocks of the transmitters and the receiver are time synchronized on-the-fly through global positioning system (GPS) [110].

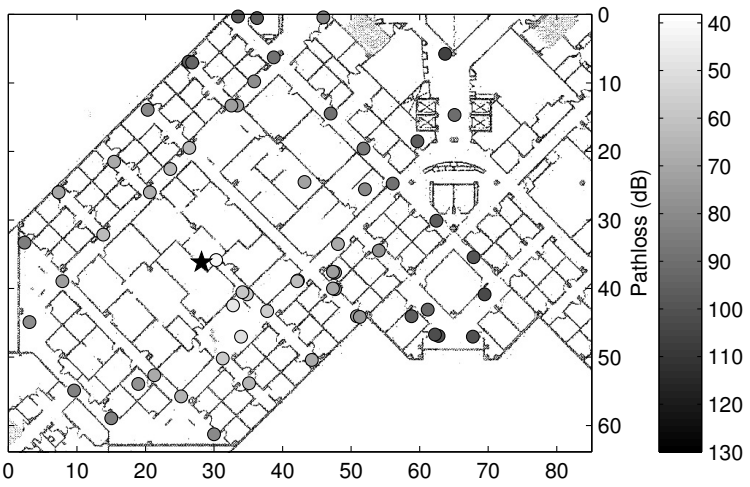

Figure 5.5: Path loss data for indoor transmitter 2

2. Transmitter k steps through the carrier frequency list and transmits a sinusoidal tone at $[F_{c_1} + f_k, \cdots, F_{c_Q} + f_k]$ frequencies in Q steps.

3. The receiver synchronously steps through the carrier frequency list with sampling rate S_r and performs an FFT of length L on the received samples.

4. Transmitter k's signal falls in the $\frac{L \times f_k}{S_r}$ bin of the FFT. The narrowband path loss of the k^{th} transmitter at frequencies $[F_{c_1} + f_k, \cdots, F_{c_Q} + f_k]$ is found based on the power in the corresponding bin.

5.4.3 Challenges of multiple transmitter channel sounding in the frequency domain method

Theoretically, a large number of complex sine waves can be accommodated in the Nyquist transmission band $[-\frac{S_r}{2}, +\frac{S_r}{2}]$. However, some of the power in a tone from a given transmitter can leak into adjacent frequency regions due to phase noise and other imperfections. Hence, the transmitters' sinusoidal tones need to be separated by a guard band so that the path loss calculations of different transmitters remain independent of each other. We used 400 kHz guard band to separate the sinusoids. This guard band, along with the maximum sampling rate of the receiver, limit the maximum number of transmitters to $5 - 6$ in our experiments. However, separation of the transmitters in both time and frequency domain, can accommodate a large number of

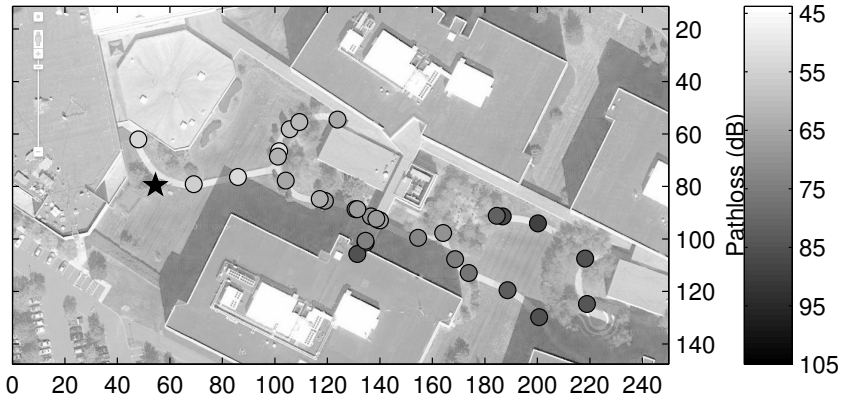

Figure 5.6: Path loss data for outdoor transmitter 1

transmitters in the frequency domain channel sounding method.

5.4.4 Mean wideband path loss

The frequency domain approach provides narrowband path losses in the frequency range $[F_{c_1} + f_k, \cdots, F_{c_Q} + f_k]$. The wideband path loss in this frequency band can be obtained by taking the average of the individual path losses. The time domain power delay profile can be obtained by taking the inverse discrete Fourier transform of the frequency domain coefficients.

The design parameters of the frequency domain channel sounder are given in Table 5.2.

5.5 Experimental Results

5.5.1 Sliding correlator channel sounding results

The indoor channel measurements using the sliding correlator system, were performed in the frequency band near 800 MHz. The experiment was set up in the 5th floor of Building A of AT&T's Middletown facility. Three transmitters were set up in different parts of a wing and the receiver moved through the wing. A total of 200 *simultaneous channel sounding measurements for the three transmitters were made.* The wideband path loss and the multipath delay profile of each transmitter were stored for each location. The X & Y coordinates of the floor map image, corresponding to the measurement

location, were saved, as well.

Fig. 5.4 and Fig. 5.5 plot the wideband path loss of two transmitters as a heat map on the floor plan layout of the wing. *The X & Y ticks in Fig. 5.4-5.7 denote distances in meters.* In all these figures, the star and the circles show the transmitter and measurement locations respectively. The height of the indoor transmitter 1, 2 and the receiver were 45, 94 and 47 inches from the 5^{th} floor level.

Fig. 5.4 and 5.5 show that the path loss increases as the receiver moves away from the transmitter. Fig. 5.4 suggests that the path loss in the two parallel hallways is significantly lower than that inside the rooms. Transmitter's signal in 5.4 does not see a line-of-sight path to the measurement points inside the hallway. *The low values of path loss - i.e., high signal strength - at these measurement points suggest that the strongest multipath component is not coming through the shortest path where it has to penetrate multiple walls. Instead, the strongest multipath component at these points is coming through the corridor where it does not face any wall.*

Since transmitter 2 of Fig. 5.5 is placed in the central location of the wing, the mean path loss from transmitter 2 is lower than that from transmitter 1 of Fig. 5.4. Therefore, transmitter 2 will require less power than transmitter 1 to cover the whole wing.

The RMS delay spreads, averaged across all the measurement points in the wing, were found to be 69 ns and 72 ns for transmitter 1 and 2 respectively.

5.5.2 Frequency domain channel sounding results

The outdoor channel measurements were performed in ten discrete steps of 2 MHz and in the frequency band near 700 MHz. The experiment was set up in the courtyard of Building A of AT&T's Middletown facility. Two transmitters were set up in two different corners of the courtyard. In total, 50 channel sounding measurements were taken *simultaneously for each transmitter* in different locations of this courtyard. The heights of the outdoor transmitter 1, 2 and the receiver were 6, 12 & 3 feet respectively from the ground level. The ten narrowband path loss measurements of each transmitter were stored for each location. The GPS location [110] and the X & Y coordinates in

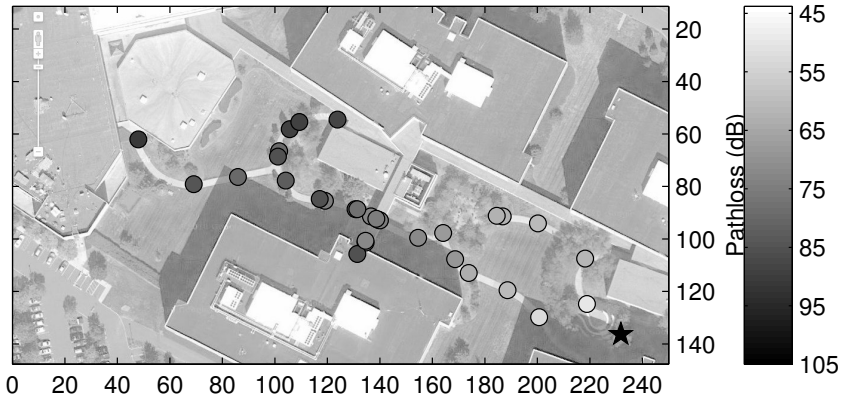

Figure 5.7: Path loss for outdoor transmitter 2

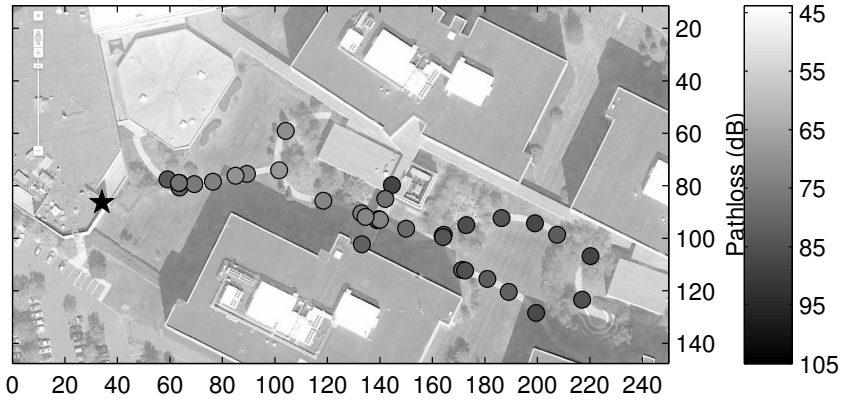

Figure 5.8: Path loss data of outdoor transmitter 3

the satellite image view were saved, as well.

Fig. 5.6 and 5.7 plot the mean wideband path loss of outdoor transmitters 1 and 2 as a heat map on the satellite image view of the courtyard. Similar to the indoor result plots, the star and the circle represent the transmitter and the receiver locations. The mean wideband path loss was calculated by taking the average of 10 narrowband path loss data in the corresponding locations. A comparison between Fig. 5.4 and 5.5, and Fig. 5.6 and 5.7 reveals that the outdoor path losses decrease less rapidly than the indoor ones. This happens because the outdoor signal does not get attenuated through walls.

In a separate run of experiment, we placed one transmitter by a courtyard-facing window of the 5th floor of building A. We took measurements at different points along the courtyard. The height of the transmitter and the receiver were 53 feet and 3 feet

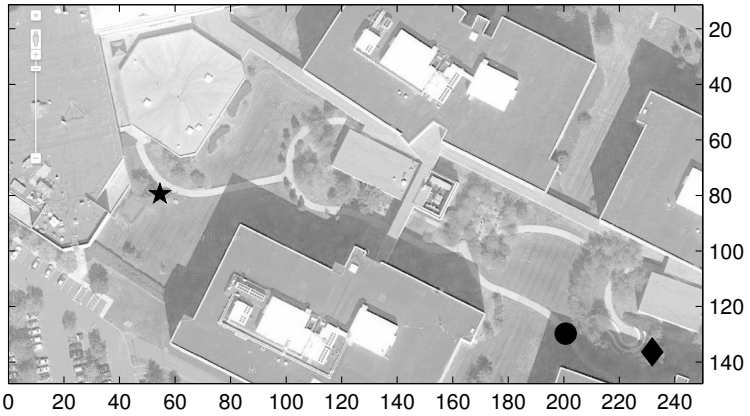

Figure 5.9: Location of the transmitters and the measurement point

respectively from the ground level. Fig. 5.8 plots the mean wideband path loss of this transmitter as a heat map in the court yard image. Compared to the figures in 5.6 and 5.7, Fig. 5.8 shows two noticable differences. In Fig. 5.8, the $4-5$ measurement locations that are nearest to the transmitter show higher path loss than the ones that are slightly further. This happens since these measurement locations are too close to the building to have a line of sight with the transmitter that is located behind the window of the 5^{th} floor. The signal has to penetrate the building walls to reach the receiver at these locations, and therefore faces higher path loss.

We now focus on variation in the narrowband path losses across the frequency band. The star and the diamond shapes in Fig. 5.9 show the locations of outdoor transmitter 1 and 2 respectively. The circle shape denotes the receiver location for a particular measurement. Fig. 5.10 shows the path loss spectrum of transmitter 1 and 2 at the receiver location. The path loss from transmitter 2 varies only by 5 dB in the 18 MHz band. This happens since the receiver is located very close to transmitter 2 and therefore, it does not experience much multipath from transmitter 2. On the other hand, the receiver is located in a far and non-line-of-sight location from transmitter 1. Therefore, it experiences rich multipath from transmitter 1 due to the nearby buildings and foliage. Fig. 5.10 shows that the path loss from transmitter 1 varies by 20 dB across the frequency band.

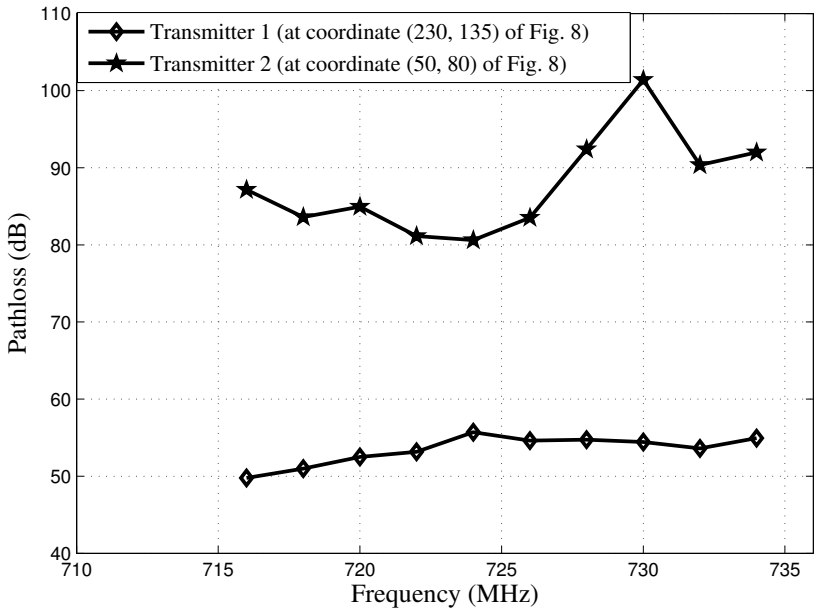

Figure 5.10: Narrowband path loss (at co-ordinate (200, 130) of Fig. 8) of transmitter 1 and 2

5.5.3 Chapter Summary

We designed and implemented rapid wireless channel sounding systems for small cell networks, using both sliding correlator and frequency domain approaches. Our design measured the channel propagation characteristics simultaneously from multiple transmitter locations. Thus, the proposed design allows researchers to quickly verify channel models with real data. It also assists engineers to compare the coverage of multiple small cell base stations with a single run of measurements.

We implemented both time domain (spread spectrum) and frequency domain channel sounding in the vicinity of 700 MHz frequency region. Our time domain channel sounding system provided 45-105 dB path loss range and 60 ns temporal resolution in multi-path delay profile. Our frequency domain channel sounding system provided 45-120 dB path loss range and 2 MHz frequency resolution. We measured channel propagation characteristics both in indoor and outdoor environments.

We designed our channel sounder on USRP platform [67] and used GNUradio [72] to program these radios. Due to the flexibility and programmability of GNUradio codes, our designed channel sounder can measure channel propagation characteristics anywhere in the region of 100 MHz to 6 GHz.

Chapter 6

Conclusion & Future Work

6.1 Thesis Summary

Demand of wireless traffic is increasing rapidly. CISCO, a telecommunication equipment manufacturer, predicts 61% annual traffic growth rate till 2018 [111]. Improvement in physical layer alone cannot meet this increasing traffic growth. Martin Coopers, one of the fathers of cellular telephony, investigated the increase in wireless throughout since 1957 [12]. Breaking down the gains, he found that the major constituents are 25-fold increase through wider spectrum, 1600-fold increase through reduced cell size and 5-fold increase through physical layer improvements [12]. Hence, additional spectrum usage and small cell network design may allow network designers to meet increasing wireless traffic demand in the upcoming years. However, unlike the improvements in physical layer, wider spectrum and reduced cell size increase the deployment and operational expenses of the network. Network designers must focus on minimizing cost while accessing wider spectrum and reducing cell sizes. This realization forms the basis of this PhD thesis.

This PhD thesis focused on different methodologies to increase bandwidth utilization in wireless links and design small cell networks. Among our work on bandwidth utilization, we focused on both cooperative forwarding and non-cooperative transmission scenarios. We investigated how one can access additional bandwidth that is already available in other links of the network or in other non-contiguous chunks of the frequency band. Among our work on small cell networks, we designed wireless backhaul solutions between small cells and gateway nodes for a given set of link gains. Thereafter, we designed a channel measurement system that allowed the network designers

to verify the validity of these link gains in both indoor and outdoor networks.

Chapter 2 considered a resource delegation based cooperative forwarding scenario where nodes exchanged bandwidth among each other as incentives for relaying. In this context, we onsidered joint optimal relay selection and resource allocation in the α-fair network utility maximization and outage probability reduction of a bandwidth exchange network. Our proposed resource allocation formulation maximized the global utility of the cooperative pair while preserving the initial utilities of each individual node. We showed that the relay selection part of the α-fair NUM problem reduced to the nonbipartite matching algorithm. Numerical simulations suggested that the proposed BE enabled relaying provided 20-25% spectrum efficiency gain and 90-98% outage probability reduction in a 20 node network.

We also designed and implemented resource (time slot) delegation based cooperative forwarding among four USRP nodes of ORBIT indoor wireless testbed. We solved the joint time slot allocation and sender-forwarder pair selection problem in this setup. Our proposed algorithm maximized the global goodput of the network while ensuring that no node's goodput drops below its initial value. The ORBIT grid was used as a global control plane to exchange the control information between USRP nodes. Experimental results suggested that resource delegation based cooperative forwarding could significantly improve the sum goodput and proportional fair goodput performance of the network.

If two nodes exchange their originally allotted bandwidth slots to implement cooperative forwarding, they have to utilize non-contiguous spectrum chunks to transmit or receive data. Hence, the investigation of bandwidth exchange led us to the following question: *how do nodes access non-contiguous spectrum chunks? What are the advantages and pitfalls of the popular mechanisms that are commonly used in non-contiguous spectrum access?* While finding answers to the two questions mentioned above, we found that non-contiguous spectrum access is useful not only in a cooperative forwarding setup, but also in most dynamic spectrum access scenarios. We realized that there is a lot of additional bandwidth available in many non-contiguous parts of the spectrum. Wireless links can increase their efficiency by accessing these non-contiguous spectrum

chunks.

MC-MR and NC-OFDMA are the two commercially viable choices to access these non-contiguous spectrum chunks. Fixed MC-MR's do not scale with increasing number of non-contiguous spectrum chunks due to their fixed set of supporting ends. MC-MR also increases circuit power by activating multiple front ends. NC-OFDMA, on the other hand, accesses non-contiguous spectrum chunks with a single front end by nulling the channels where incumbent users are present. NC-OFDMA reduces transmit power consumption by selecting channels with higher link gain but increases circuit power consumption by spanning wider spectrum.

Chapter 3 characterized this trade-off from two perspectives. First, chapter 3 focused on a multi-hop network where each node is equipped with single front end radio and can employ NC-OFDMA to access non-contiguous spectrum chunks. We performed joint power control, channel scheduling, spectrum span selection and routing to minimize system power consumption of this multi-hop network. Our algorithm showed *how the slopes of ADC and DAC's power consumption versus sampling rate curve influenced the scheduling decisions of a multi-hop network.* We developed a mixed integer non-linear program to attain our objective and provided a low complexity greedy algorithm. Numerical results suggested that our algorithm could save 40% system power over classical transmission power based cross-layer algorithms.

Secondly, chapter 3 focused on a point-to-point link where both nodes are equipped with multiple front ends and can employ NC-OFDMA to access non-contiguous spectrum chunks. We performed optimal power control and channel scheduling across both front ends to minimize the system power of this point-to-point link. We designed a mixed integer non-linear program and provided a low complexity greedy algorithm ($O(M^2I)$) where M and I denote the number of channels and radio front ends respectively. Our algorithm showed that, in a practical setting, *each front end of a radio should capture "near-by" non-contiguous spectrum chunks.*

Chapter 2 and 3 focused on the efficient use of additional bandwidth to improve

performance – both in terms of bandwidth exchange in cooperative networks and non-contiguous spectrum access in non-cooperative networks. Apart from looking for additional spectrum, future network designers will have to focus their efforts on reducing cell sizes to improve the signal-to-noise-ratio between base station and users, and to allow more frequency reuse in the system design [12]. This led us to investigate two different aspects of small cell network design in chapter 4 and 5 of the PhD thesis.

Chapter 4 focused on designing wireless backhaul solutions for small cell networks. Small cells can keep up with the increasing demand of wireless networks; but require backhaul to transport data to (from) a gateway node. Wireless backhaul can provide an inexpensive option to small cells. Aggregator nodes, located at roof tops of tall buildings near small cells, can provide high data rate to multiple small cells in NLOS paths, sustain the same data rate to gateway nodes in LOS paths and take advantage of all available bands for wireless backhaul.

This part of our work performed joint cost optimal aggregator node placement, power allocation, channel scheduling and routing to optimize the wireless backhaul network. We investigated wireless backhaul network using both sub-6 GHz and microwave bands. We considered the different interference patterns and multiple access features in these bands and incorporated them in backhaul network optimization. We developed two solution methodologies - branch-and-bound and greedy - to solve these network optimization problems.

The wireless backhaul network design module relied heavily on the reliability of the estimated link gains between different nodes of the backhaul network. This led us to design and implement a wireless channel measurement system that could be used to verify existing channel models for small cell networks.

Chapter 5 of the PhD thesis described our efforts in designing and implementing a rapid wireless channel sounding system. We used both sliding correlator and frequency domain approaches in our work. Our design measured the channel propagation characteristics simultaneously from multiple transmitter locations. Thus, the proposed design would allow researchers to quickly verify channel models for small cell networks with real data. It would also assist engineers to compare the coverage of multiple small cell

base stations with a single run of measurements.

6.2 Future Works

Our work can be extended in many possible directions to improve non-contiguous spectrum access and small cell network design algorithms.

Chapter 2 of this thesis focused on bandwidth exchange based cooperative forwarding and considered one forwarder for one sender and vice versa. The generalization of this algorithm to the multiple sender-forwarder scenario is an area of future research. Chapter 2 also described the implementation of time slot exchange based cooperative forwarding in an indoor wireless testbed. Future works should implement bandwidth exchange based cooperative forwarding in wireless testbeds.

The optimal non-contiguous spectrum algorithms presented in chapter 3 only accounted for the radio front end power and transmitters' emitted power. Recently, there has been significant interest in modeling baseband power consumption, specially, decoders' power consumption [47]. Future research can extend our work to minimize the summation of baseband power, radio front end power and transmitters' emitted power.

Chapter 3's algorithms to minimize system power in multi-front end radio focused only on a point-to-point link. Future work can extend it to multi-front end radio and NC-OFDMA enabled multi-hop networks.

The number of available TV white space channels and corresponding non-contiguous spectrum chunks vary across different regions within USA [2]. Hence, our work in non-contiguous spectrum access can be extended to investigate how a radio with limited number of front ends performs in non-contiguous spectrum access across different regions within USA.

Our algorithms in non-contiguous spectrum access focused on two different methodologies: multi-channel multi-radio platforms and NC-OFDMA. Recently, Fettweis et. al. has proposed a new technique, namely Generalized Frequency Division Multiplexing [112], that implements classic multi-bank filter techniques in a digital manner. This allows GFDM to access non-contiguous spectrum chunks with a single radio front end

without using NC-OFDM. Our work can be extended to investigate the system power consumption of GFDM based networks.

Chapter 4 of this thesis deployed aggregator nodes while assuming fixed traffic demand pattern from each small cell. However, traffic pattern of small cells vary significantly throughout the day. Peak traffic at 'quiet periods' can be up to seven times higher than mean traffic at 'busy periods' [113]. Future work could extend our algorithm to deploy aggregator nodes while considering these different types of variable traffic patterns from small cells.

We focused on wireless backhaul network design in chapter 4 of this thesis. In a metropolitan setting, some edge nodes may not have any nearby tall buildings whose roof tops can be leased. These edge nodes need to be connected through fiber from the gateway node. Network optimization with mixed wired-wireless backhaul remains an area of future research.

We implement the algorithms of our channel measurement system, shown in chapter 5 of the PhD thesis, in software. Hence, the temporal resolution (60 ns) of the channel sounder is limited by the data transfer rate of the ethernet interface that connects the laptop and the USRP radio. By implementing channel measurement algorithms directly on the USRP FPGA, one could avoid this bottleneck and obtain a temporal resolution of 10 ns. This extension remains an area of future research.

Our channel measurement design did not include explicit coordination between transmitters and receivers. Future work could focus on such coordination through explicit communication to dynamically change power, timing, frequency, and other aspects of the system.

Appendix A

Power Consumption of Different Blocks in the Transmitter and Receiver

A.1 Power Consumption of Different Blocks in the Transmitter and the Receiver

Based on Fig. 3.1, the power consumptions of transmitter and receiver can be divided into the following parameters:

$$p_{tc} = p_{dac} + p_{tfilt} + p_{mix} + p_{pa} \quad \text{(A.1)}$$

$$p_{rc} = p_{adc} + p_{rfilt} + p_{mix} + p_{ifa} + p_{lna}. \quad \text{(A.2)}$$

In the above, p_{dac}, p_{mix}, p_{pa}, p_{adc}, p_{ifa} and p_{lna} denote the circuit power consumption in the DAC, mixer, PA, ADC, IFA and LNA respectively. The parameters p_{tfilt} and p_{rfilt} represent the summation of circuit powers in the filters of transmitter and receiver respectively.

The power consumption in the mixer, LNA and IFA are constants with respect to the sampling rate [91]. Baseband filter power depends on sampling rate but we assume it to be constant due to its low power consumption [5]. Let us assume,

$$p_{tfilt} + p_{mix} = k_t \quad \text{(A.3)}$$

$$p_{rfilt} + p_{mix} + p_{ifa} + p_{lna} = k_r \quad \text{(A.4)}$$

The DAC and ADC power consumptions are affine functions of the sampling rate [5,91].

Hence,

$$p_{dac} = k_1 + k_2 fs \tag{A.5}$$

$$p_{adc} = k_3 + k_4 fs \tag{A.6}$$

Now, using (A.5),(A.6),(A.3) and (A.4) in (A.7) and (A.8).

$$p_{tc} = k_1 + k_2 fs + k_t = \alpha_1 + \alpha_2 fs \tag{A.7}$$

$$p_{rc} = k_3 + k_4 fs + k_r = \beta_1 + \beta_2 f \tag{A.8}$$

In the above, $\alpha_1 = k_1 + k_t$, $\beta_1 = k_3 + k_r$, $\alpha_2 = k_2$ and $\beta_2 = k_4$.

Due to its dependence on transmit power, we do not include programmable amplifier's circuit power consumption term p_{pa} in the overall circuit power consumption equations of (A.7) and (A.8). Instead, we couple it with the transmit power consumption p and include it in the total power equations of (3.3) and (3.4).

We now describe the specific power consumption values that we used in numerical simulations.

A.1.1 Power consumption of analog blocks

We assume low power consumption at these blocks and use the following values [5]: $p_{tfilt} = 5$ mW, $p_{mix} = 30.3$ mW, $p_{rfilt} = 7.5$ mW, $p_{ifa} = 3$ mW, $p_{lna} = 20$ mW.

A.1.2 Power consumption of programmable amplifier

Power consumption of the programmable amplifier depends on the drain efficiency, peak-to-average-power ratio and transmit power of the system. Specifically, $p_{pa} = \frac{PAPR}{\eta} p = k_{pa} p$ where $k_{pa} = \frac{PAPR}{\eta}$ and p is the emitted power at RF. We assume a class-B or a higher class (C, D or E) amplifier with $\eta = 0.75$ [5].

We consider OFDM to be our inherent modulation scheme. There have been many works in the literature that analytically relate PAPR with the number of subcarriers of an OFDM system. Readers are suggested to go through [114, 115] for a detailed

survey on this topic. In the presence of large number of subcarriers, [116] provides the following analytical expression of PAPR:

$$Prob\{PAPR > \gamma\} \approx 1 - exp\{-Ne^{-\gamma}\sqrt{\frac{\pi}{3}\gamma}\} \tag{A.9}$$

where N is the number of subcarriers in the system and γ is the probability that PAPR will be greater than this value.

Our algorithm optimizes the scheduling variables, i.e., the number of subcarriers used by the transceiver. In [116], the authors suggest that the statistical distribution of the PAPR of the OFDM signals is not very sensitive to the increase in the number of subcarriers. Hence, we consider the worst case PAPR (corresponding to the highest number of subcarriers) and assume it to be constant throughout the simulations.

Our system power minimization based multi-hop NC-OFDMA algorithm is mostly applicable in the opportunistic use of TV channels for fixed devices. The available TV channels for fixed devices range from 54 MHz to 698 MHz [1]. IEEE 802.22 employs 2048 subcarriers per 6 MHz TV channel [117]. The number of subcarriers used in our algorithm is upper bounded by $2000 \times \frac{698-54}{6}$. Plugging this in (A.9) and assuming $\gamma = 0.005$, we find PAPR to be around $12.5dB$. Intelligent use of coding schemes can reduce PAPR by $3-4$ dB [115]. Hence, we assume $PAPR$ to be 9 dB in our numerical simulations.

A.1.3 Power consumption of ADC and DAC

The specific values of k_1, k_2, k_3 and k_4 vary from one DAC/ADC to the other. Fig. A.1 plots the power consumption vs. sampling rate curve of AD 9777 [7] (DAC of USRP radio) and DAC 3162 [8] (termed as "low power DAC" by texas instruments). Fig. A.2 plots the power consumption vs. sampling rate curve of ADS62P4 [9] (ADC of USRP radio) and ADS4249 [10] (termed as "low power ADC" by texas instruments).

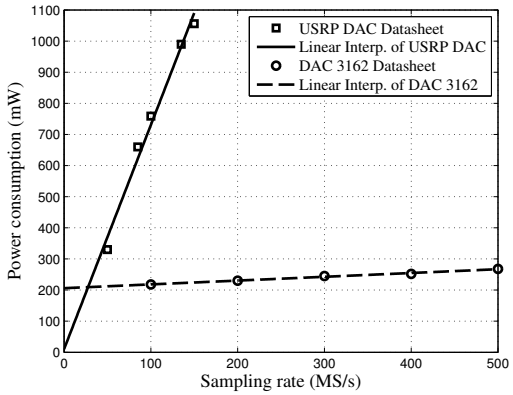

Figure A.1: Power consumption of AD 9777 (digital-to-analog-converter of USRP radio) and DAC 3162 (low power DAC for software defined radios). The rectangular [7] and the circular [8] dots are taken from the data sheets; the straight lines are the linear interpolations of the dots.

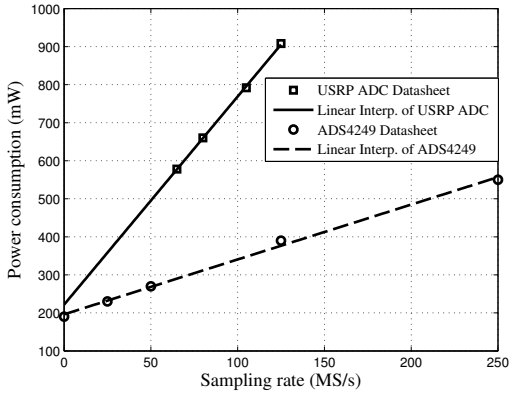

Figure A.2: Power consumption of ADS 62P4 (ADC of USRP radio) and ADS 4249 (low power ADC of TI). The rectangular [9] and the circular [10] dots are taken from the data sheets; the straight lines are the linear interpolations of the dots.

Appendix B

Codebook Design and Matching Algorithms in Bandwidth Exchange

B.1 Codebook Design in Proposed DF Relaying

Let's consider two codebooks $\mathcal{W}$ and $\mathcal{C}$ that consist of $2^{R_{sf}}$ and 2^{R_c} codewords respectively. Assume, $\mathcal{W} = \{w_1, w_2, \cdots, w_{2^{R_{sf}}}\}$ and $\mathcal{C} = \{c_1, c_2, \cdots, c_{2^{R_c}}\}$. Here $R_{sf} \geq R_c$. Consider a partition $\mathcal{S} = \{S_1, S_2, \cdots, S_{2^{R_c}}\}$ of $\mathcal{W}$, i.e., $\mathcal{W}$ has been partitioned into 2^{R_c} cells. Each cell S_i contains $2^{R_{sf}-R_c}$ codewords of $\mathcal{W}$. Assume a one-to-one correspondence between $\mathcal{C}$ and $\mathcal{S}$, i.e., each codeword of $\mathcal{C}$ represents one particular cell of $\mathcal{S}$.

The BS (node 0), sender s and forwarder f get the codebooks off-line. At the beginning of the transmission, sender s sends a codeword w_i from $\mathcal{W}$ using R_{sf} bits. The forwarder node decodes the codeword correctly. However, since $R_{sf} \geq R_{s0}$, the BS cannot decode it correctly. The BS has a list of possible codewords of size $2^{R_{sf}-R_{s0}}$. Now, the forwarder f finds the cell S_i where w_i lies and sends c_i using R_c bits. The BS receives c_i and intersects S_i with the list of possible codewords. If $R_c \geq R_{sf} - R_{s0}$ and $R_c \leq R_{f0}$, this half duplex DF cooperation completely removes the BS's uncertainty about w_i [83, 84].

Thus, the achievable rates of node s and f are governed by this information theoretic generalization of the max-flow-min-cut theorem:

$$\begin{aligned} R_s^{be} &\leq \min(R_{sf}, R_{s0} + R_c) \\ R_c + R_f^{be} &\leq R_{f0} \end{aligned}$$

B.2 Matching and nonbipartite MWM algorithm

Consider an undirected graph $\mathcal{G} = (\mathcal{V}, \mathcal{E})$ where $\mathcal{V}$ denotes the set of vertices and $\mathcal{E}$ denotes the set of edges. A matching $\mathcal{M}$ is a subset of $\mathcal{E}$ such that $e_1 \cap e_2 = \emptyset$ for $e_1, e_2 \in \mathcal{M}$ if $e_1 \neq e_2$ [87].

Let x_e denote whether an edge $e \in E$ will be selected in the matching, i.e., x_e can be 0 or 1. Let r_e represent the edge weights. The maximum weighted matching in a non-bipartite graph takes the following form [87]:

$$\textbf{max} \sum_{e \in E} r_e x_e \tag{B.1a}$$

$$\textbf{s.t.} \sum_{e \in \delta(v)} x_e \leq 1 \, \forall \, v \, \in \, \mathcal{V} \tag{B.1b}$$

$$\sum_{e \in E(\mathcal{U})} x_e \leq \lfloor \frac{|\mathcal{U}|}{2} \rfloor \, \forall \; odd \, sets \; \mathcal{U} \subset \mathcal{V} \tag{B.1c}$$

$$x_e \in \mathcal{B}^n \tag{B.1d}$$

In (B.1b), $\delta(v)$ denotes the edges connected with node v. In (B.1c), $E(\mathcal{U})$ represents the edges contained in the set $\mathbf{U}$. Equation (B.1d) shows that x_e takes Boolean values. However, Edmonds [81] showed that the we can replace $x_e \in \mathcal{B}^n$ by $x_e \in \mathcal{R}_+^n$ and still obtain integral optimal solutions. Thus the combinatorial optimization problem can be converted to a linear program.

B.3 Distributed Local Greedy MWM

- Each node i knows its adjacent link weights. Node i picks the "candidate" node j, based on the heaviest link weight and sends an "add" request.
- Wait for the response from node j.
- If node i receives an "add" request from node j, i and j pick each other as the cooperative pair. i sends "drop" request to its other neighbouring nodes.
- If node i receives a "drop" request from node j, node i removes the (i, j) link from

its adjacent edge set. Node i goes to the state of step 1.

The distributed local greedy MWM provides at least 50% performance of centralized optimal matching. Distributed local greedy MWM requires $O(N^2)$ amount of message passing.

References

[1] C. Gerami, N. B. Mandayam, and L. J. Greenstein, "Backhauling in TV white spaces," in *Proc. IEEE GLOBECOM'2010*, Dec. 2010, pp. 1–6.

[2] "Show my white space," accessed May 2012, http://whitespaces.spectrumbridge.com/whitespaces.

[3] "Fastest growing cities in usa," accessed September 2013, http://www.forbes.com/pictures/edgl45fgfj/no-1-new-orleans-la/.

[4] N. Alliance, "Small cell backhaul requirements," White Paper, Jun. 2012.

[5] S. Cui, A. Goldsmith, and A. Bahai, "Energy-constrained modulation optimization," *IEEE Transactions on Wireless Communications*, vol. 4, pp. 2349 – 2360, Sep 2005.

[6] "Downtown Manhattan: Google map," accessed February 2014, https://www.google.com/maps/.

[7] "AD9777: 16-bit interpolating dual dac converter," accessed April 2012, http://www.analog.com/static/imported-files/data_sheets/AD9777.pdf.

[8] "Dual-Channel, 10/12 Bit, 500 MSPS Digital-to-Analog converters," accessed April 2012, http://www.ti.com/lit/ds/symlink/dac3162.pdf.

[9] "Dual channel, 14-bits, 125/105/80/65 MSPS ADC with DDR LVDS/CMOS outputs," accessed April 2012, http://www.ti.com/lit/ds/symlink/ads62p42.pdf.

[10] "Dual-Channel, 14-Bit, 250-MSPS Ultralow-Power ADC," accessed April 2012, http://www.ti.com/lit/ds/symlink/ads4249.pdf.

[11] "Qualcomm data challenge," accessed March 2013, http://www.qualcomm.com/media/documents/wireless-networks-rising-meet-1000x-mobile-data-challenge.

[12] M. Dohler, R. W. Heath, A. Lozano, C. B. Papadias, and R. Valenzuela, "Is the PHY layer dead?" *IEEE Communications Magazine*, vol. 4, pp. 159–165, Apr 2011.

[13] J. Andrews. (1998) How can cellular networks handle 1000x data? Technical talk at University of Notre Dame. [Online]. Available: http://users.ece.utexas.edu/~jandrews/pubs/Andrews_NotreDame_May2011.pdf

[14] C. Cordeiro, K. Challapali, D. Birru, and S. Shankar, "IEEE 802.22: the first worldwide wireless standard based on cognitive radios," in *Proc. IEEE DySPAN'2005*, Nov. 2005, p. 328337.

[15] "Enabling innovative small cell use in 3.5 GHZ band NPRM & order," accessed March 2013, http://www.fcc.gov/document/enabling-innovative-small-cell-use-35-ghz-band-nprm-order.

[16] S. Rangan, T. S. Rappaport, and E. Erkip, "Millimeter-wave cellular wireless networks: Potentials and challenges," *Proceedings of the IEEE*, vol. 102, pp. 366–385, Mar 2014.

[17] J. N. Laneman, D. N. C. Tse, and G. Wornell, "Cooperative diversity in wireless networks : efficient protocols and outage behavior," *IEEE Trans. Info. Theory*, vol. 50(12), pp. 3062–3080, Dec. 2004.

[18] L. Lai, K. Liu, and H. E. Gamal, "The three node wireless network: Achievable rates and cooperation strategies," *IEEE Trans. Info. Theory*, vol. 52(3), pp. 805–828, Mar. 2006.

[19] O. Ileri, S.-C. Mau, and N. Mandayam, "Pricing for enabling forwarding in self-configuring ad hoc networks," *IEEE JSAC*, vol. 23, pp. 151–162, Jan. 2005.

[20] S. Buchegger and J.-Y. L. Boudec, "Self-policing mobile ad hoc networks by reputation systems," *IEEE Communication Magazine*, vol. 43, pp. 101–107, Jul. 2007.

[21] M. Felegyhazi, J. P. Hubaux, and L. Buttyan, "Nash equilibria of packet forwarding strategies in wireless ad hoc networks," *IEEE Trans. on Mobile Computing*, vol. 5, pp. 463–475, May 2006.

[22] D. Zhang, R. Shinkuma, and N. B. Mandayam, "Bandwidth exchange: An energy conserving incentive mechanism for cooperation," *IEEE Trans. Wireless Comm*, vol. 9(6), pp. 2055–2065, Jun. 2010.

[23] "ORBIT: Open access research testbed for next-generation wireless networks," accessed April 2012, http://www.orbit-lab.org.

[24] J. Zhang and Q. Zhang, "Stackelberg game for utility-based cooperative cognitive radio networks," in *Proc. ACM MOBIHOC'2009*, May 2009, pp. 23–31.

[25] H. Xu and B. Li, "Efficient resource allocation with flexible channel cooperation in ofdma cognitive radio networks," in *Proc. IEEE INFOCOM'2010*, Mar. 2010, pp. 1–9.

[26] C. T. K. Ng and G. J. Foschini, "Transmit signal and bandwidth optimization in multiple-antenna relay channels," *IEEE Trans. Wireless Comm.*, vol. 59, pp. 2987–2992, Nov. 2011.

[27] L. Tassiulas and A. Ephremides, "Stability properties of constrained queing systems and scheduling for maximum throughput in multihop radio networks," *IEEE Trans. Automatic Control*, vol. 37(12), pp. 1936–1949, Dec. 1992.

[28] M. J. Neely, E. Modiano, and C. E. Rohrs, "Dynamic power allocation and routing for time-varying wireless networks," *IEEE Journal on Selected Areas in Communications*, vol. 23(1), pp. 89–104, Jan. 2005.

[29] S. Sarkar and L. Tassiulas, "End-to-end bandwidth gurantees through fair local spectrum share in wireless ad-hoc networks," in *Proc. IEEE Conference on Decision and Control*, Dec. 2011, pp. 564–569.

[30] Y. Yi and M. Chiang, "Stochastic network utility mazmimization and wireless scheduling," in *Next Generation Internet Architectures and Protocols*, B. Ramamurthy, G. Rouskas, and K. Sivalingam, Eds. New York: Cambridge University Press, 2011, pp. 1–35.

[31] X. Lin and N. B. Shroff, "The impact of imperfect scheduling on cross-layer rate control in wireless networks," in *Proc. IEEE INFOCOM 2005*, Mar. 2005, pp. 1804–1814.

[32] V. Mahinthan, J. M. L. Cai, and X. Shen, "Maximizing cooperative diversity energy gain for wireless networks," *IEEE Trans. Wireless Comm*, vol. 7(6), pp. 2540–2549, 2007.

[33] M. Kodialam and T. Nandagopal, "Characterizing the capacity region in multi-radio multi-channel wireless mesh networks," in *Proc. ACM MOBICOM '05*, Aug. 2005, pp. 73–87.

[34] P. Kyasanur and N. H. Vaidya, "Capacity of multi-channel wireless networks: impact of number of channels and interfaces," in *Proc. ACM MOBICOM '05*, Aug. 2005, pp. 43–57.

[35] L. Yang, Z. Zhang, W. Hou, B. Y. Zhao, and H. Zheng, "Papyrus: A software platform for distributed dynamic spectrum sharing using sdrs," *ACM SIGCOMM Computer Communications Review*, vol. 41, pp. 31–37, 2011.

[36] L. Yang, B. Y. Zhao, and H. Zheng, "The spaces between us: Setting and maintaining boundaries in wireless spectrum access," in *Proc. ACM MOBICOM '10*, Sep. 2010, pp. 37–48.

[37] L. Yang, W. Hou, L. Cao, B. Y. Zhao, and H. Zheng, "Supporting demanding wireless applications with frequency-agile radios," in *Proc. 7th USENIX conference on Networked Systems Design and Implementation*, Apr. 2010, pp. 1–5.

[38] R. Rajbanshi, A. M. Wyglinski, and G. J. Minden, "An efficient implementation of nc-ofdm transceivers for cognitive radios," in *Proc. IEEE CROWNCOM '06*, Jun. 2006, pp. 1–5.

[39] G. Zhang and S. Feng, "Subcarrier allocation algorithms based on graph-coloring in cognitive radio nc-ofdm system," in *Proc. 3rd IEEE International Conference on Computer Science and Information Technology*, Jul. 2010, pp. 535–540.

[40] E. Manasseh, S. Ohno, and M. Nakamoto, "Pilot design for non-contiguous spectrum usage in ofdm-based cognitive radio networks," in *Proc. 20th European Signal Processing Conference (EUSIPCO)*, Aug. 2012, pp. 465–469.

[41] "ADC performance evolution: Walden figure-of-merit (fom)," accessed August 2012, http://converterpassion.wordpress.com/2012/08/21/.

[42] "AD9467: 16-bit, 200 MSPS/250 MSPS Analog-to-Digital converter," accessed April 2012, http://www.analog.com/static/imported-files/data_sheets/AD9467.pdf.

[43] Y. Shi and Y. T. Hou, "Optimal power control for multi-hop software dened radio networks," in *Proc. IEEE INFOCOM '07*, May 2007, pp. 1694–1702.

[44] Y. Shi, T. Hou, S. Kompella, and H. Sherali, "Maximizing capacity in multihop cognitive radio networks under the SINR model," *IEEE Transactions on Mobile Computing*, vol. 10, pp. 954–967, 2011.

[45] Y. Shi and T. Hou, "A distributed optimization algorithm for multi-hop cognitive radio networks," in *Proc. IEEE INFOCOM '08*, Apr. 2008, pp. 1292–1300.

[46] G. Li, Z. Xu, C. Xiong, C. Yang, S. Zhang, Y. Chen, and S. Xu, "Energy-efficient wireless communications: tutorial, survey, and open issues," *IEEE Transactions on Wireless Communications*, vol. 18, pp. 28–35, 2011.

[47] P. Grover, K. A. Woyach, and A. Sahai, "Towards a communication-theoretic understanding of system-level power consumption," *IEEE Journals on Selected Areas in Communications*, vol. 29, pp. 1744 – 1755, sep 2011.

[48] C. Isheden and G. P. Fettweis, "Energy-efficient multi-carrier link adaptation with sum rate-dependent circuit power," in *Proc. IEEE GLOBECOMM '10*, Dec. 2010, pp. 1–6.

[49] J. Jia and W. Zhuang, "Capacity of multi-hop wireless network with frequency agile software defined radio," in *Proc. IEEE INFOCOM Workshop on Cognitive & Cooperative Networks*, Apr. 2011, pp. 41–46.

[50] L. Cao, L. Yang, and H. Zheng, "The impact of frequency-agility on dynamic spectrum sharing," in *Proc. IEEE DySPAN '10*, Apr. 2010, pp. 1–12.

[51] W. Hou, L. Yang, L. Zhang, X. Shan, and H. Zheng, "Understanding the impact of cross-band interference," in *Proc. ACM Workshop on Cognitive Radio Networks*, Sep. 2009, pp. 19–24.

[52] Ceragon, "Mobile backhaul: Fiber vs. microwave case study analyzing various backhaul technology strategies," White Paper, Oct. 2009.

[53] J. Hansryd, J. Edstam, B. Olsson, and C. Larsson, "Non-line-of-sight microwave backhaul for small cells," *Ericsson Review*, vol. 3, pp. 2–8, Feb 2013.

[54] P. Maulin, R. Chandrasekaran, and S. Venkatesan, "Energy efficient sensor, relay and base station placements, for coverage, connectivity and routing," in *Proc. IEEE IPCCC' 2005*, Apr. 2005, pp. 581–586.

[55] D. Yang, S. Misra, X. Fang, G. Xue, and J. Zhang, "Two-tiered constrained relay node placement in wireless sensor networks: Computational complexity and efficient approximations," *IEEE Trans. Mobile Computing*, vol. 11, pp. 1399–1411, Aug 2012.

[56] A. So and B. Liang, "Enhancing WLAN capacity by strategic placement of tetherless relay points," *IEEE Trans. Mobile Computing*, vol. 6, pp. 522–535, May 2007.

[57] B. Lin, P. Ho, L. Xie, and X. Shen, "Optimal relay station placement in IEEE 802.16j networks," in *Proc. ACM IWCMC' 2007*, Aug. 2007, pp. 25–30.

[58] H. Lu, W. Liao, and F. Y. Lin, "Relay station placement strategy in IEEE 802.16j WiMAX networks," *IEEE Transactions on Communications*, vol. 59, pp. 151–158, Jan 2011.

[59] M. Hata, "Empirical formula for propagation loss in land mobile radio services," *IEEE Transactions on Vehicular Technology*, vol. 29(3), pp. 317–325, Aug. 1980.

[60] K. Herring, J. Holloway, D. Staelin, and D. Bliss, "Path-loss characteristics of urban wireless channels," *IEEE Transactions on Antennas and Propagation*, vol. 58(1), pp. 171–177, Jan. 2010.

[61] "The ITS irregular terrain model," accessed September 2012, http://flattop.its.bldrdoc.gov/itm.html.

[62] D. J. Cichon and T. Kurner, "Digital mobile radio towards future generation systems: cost 231 final report," European Cooperation in the Field of Scientific and Technical Research, Action 231, 1993.

[63] G. Durgin, T. Rappaport, and H. Xu, "Measurements and models for radio path loss and penetration loss in and around homes and trees at 5.85ghz," *IEEE Transactions on Communications*, vol. 46(11), pp. 1484–1495, Aug. 1998.

[64] V. Sridhara and S. Bohacek, "Realistic propagation simulation of urban mesh networks," *Computer Networks*, vol. 51(12), p. 33923412, Aug. 2007.

[65] D. S. C. Phillips and D. Grunwald, "Bounding the error of path loss models," in *Proc. IEEE Symposium on New Frontiers in Dynamic Spectrum Access Networks (DySPAN) '11*, May 2011, pp. 71–82.

[66] D. Cox, "Delay doppler characteristics of multipath propagation at 910 mhz in a suburban mobile radio environment," *IEEE Transactions on Antennas and Propagation*, vol. 20(5), pp. 625–635, Sep. 1972.

[67] "ETTUS research," accessed April 2012, http://www.ettus.com.

[68] S. S. Ghassemzadeh, R. Jana, C. W. Rice, W. Turin, and V. Tarokh, "Measurement and modeling of an ultra-wide bandwidth indoor channel," *IEEE Transactions on Communications*, vol. 52(10), p. 17861796, Oct. 2004.

[69] S. J. Howard, K. Pahlavan, R. Co, and M. A.Marlboro, "Measurement and analysis of the indoor radio channel in the frequency domain," *IEEE Transactions on Instrumentation and Measurement*, vol. 39(5), pp. 751–755, Oct. 1990.

[70] D. Porrat, "UHF propagation in indoor hallways," *IEEE Transactions on Wireless Communications*, vol. 3(4), pp. 1188–1198, Jul. 2004.

[71] M. H. Firooz, J. Zhang, N. Patwari, and S. K. Kasera, "Channel sounding for the masses: Low complexity gnu 802.11b channel impulse response estimation," *IEEE Transactions on Wireless Communications*, vol. 11(1), pp. 1–8, Jan. 2012.

[72] "GNU Radio Website," accessed September 2012, http://www.gnuradio.org.

[73] M. N. Islam, A. Sampath, A. Maharshi, O. Koymen, and N. B. Mandayam, "Wireless backhaul node placement for small cell networks," in *Proc. IEEE CISS '14*, Mar. 2014, pp. 1–6.

[74] M. N. Islam, B. J. Kim, P. Henry, and E. Rozner, "A wireless channel sounding system for rapid propagation measurements," in *Proc. IEEE ICC '13*, Jun. 2013, pp. 5720–5725.

[75] M. N. Islam, S. Balasubramanian, N. B. Mandayam, I. Seskar, and S. Komplella, "Implementation of distributed time exchange based cooperative forwarding," in *Proc. IEEE MILCOM '12*, Oct. 2012, pp. 1–6.

[76] M. N. Islam, N. B. Mandayam, and S. Komplella, "Optimal resource allocation and relay selection in bandwidth exchange based cooperative forwarding," in *Proc. IEEE WiOPT '12*, May 2012, pp. 192–199.

[77] ——, "Optimal resource allocation in a bandwidth exchanged enabled relay network," in *Proc. IEEE MILCOM '11*, Nov. 2011, pp. 242–247.

[78] R. Kumbhkar, M. N. Islam, N. B. Mandayam, and I. Seskar, "Rate optimal design of a wireless backhaul network using tv white space," submitted to 7th International Conference on Communication Systems & Networks (COMSNETS 2015). Available online at http://arxiv.org/abs/1409.1661.

[79] M. N. Islam, N. B. Mandayam, S. Kompella, and I. Seskar, "Power optimal non-contigous spectrum access," submitted to IEEE Transactions on Wireless Communications. Available at http://arxiv.org/abs/1309.0861.

[80] ——, "Power optimal non-contigous spectrum access in multi-front end radio based point-to-point link," to be Submitted to IEEE Communication Letters. Available online at http://arxiv.org/abs/1409.1606.

[81] J. Edmonds, "Paths, trees and flowers," *Canadian Journal of Mathematics*, vol. 17, pp. 449–467, 1965.

[82] J. Hoepman, "Simple distributed weighted matchings," eprint, October 2004, http://arxiv.org/abs/cs/0410047.

[83] T. Cover and H. E. Gamal, "Capacity theorems for the relay channel," *IEEE Trans. Info. Theory*, vol. 25(5), pp. 572–584, Sep. 1979.

[84] T. M. Cover and J. A. Thomas, *Elements of Information Theory*. Hoboken, NJ: John Wiley and Sons, 2005.

[85] J. Mo and J. Warland, "Fair end-to-end window based congestion control," *IEEE/ACM Transactions on Networking*, vol. 8(5), pp. 556–567, Oct. 2000.

[86] S. Boyd and L. Vandenberghe, *Convex Optimization*. Cambridge,MA: Cambridge University Press, 1999.

[87] G. Nemhauser and L. Wolsey, *Integer and Combinatorial Optimization*. Hoboken, NJ: John Wiley and Sons, 1988.

[88] J. van Rantwijk. (accessed February 2012) Maximum weighted matching. http://jorisvr.nl/maximummatching.html/.

[89] "Ethernet frame," accessed April 2012, http://www.infocellar.com/networks/ethernet/frame.htmg.

[90] H. C. Liu, J. S. Min, and H. Samueli, "A low-power baseband receiver IC for frequency-hopped spread spectrum communications," *IEEE J. Solid-State Circuits*, vol. 31, pp. 384–394, mar 1996.

[91] Y. Li, B. Bakkaloglu, and C. Chakrabarti, "A system level energy model and energy-quality evaluation for integrated transceiver front-ends," *IEEE Transactions on VLSI Systems*, vol. 15, pp. 90–103, 2007.

[92] H. D. Sherali and W. P. Adams, *A Reformulation-Linearization Technique for Solving Discrete and Continuous Nonconvex Problems*. Dordrecht/Boston/London: Kluwer Academic Publishers, 1999.

[93] "CVX: Matlab software for disciplined convex programming," accessed July 2013, http://cvxr.com/cvx/.

[94] "Mosek optimization," accessed April 2012, http://www.mosek.com/.

[95] T. H. Cormen, C. E. Leiserson, R. L. Rivest, and C. Stein, *Introduction to Algorithms*. Cambridge,MA: The MIT Press, 2009.

[96] J. Hoydis, S. T. Brink, and M. Debbah, "Massive MIMO in the UL/DL of cellular networks: How many antennas do we need?" *IEEE JSAC*, vol. 31, pp. 160–171, Feb 2013.

[97] J. Lofberg, "YALMIP : A toolbox for modeling and optimization in MATLAB," in *Proc. CACSD Conference*, Taipei, Taiwan, 2004. [Online]. Available: http://users.isy.liu.se/johanl/yalmip

[98] "GLPK GNU linear programming kit," accessed February 2014, http://www.gnu.org/software/glpk/.

[99] D. Bertsimas and J. N. Tsitsiklis, *Introduction to Linear Optimization*. Belmont,MA: Athena Scientific and Dynamic Ideas, LLC, 1997.

[100] T. H. Cormen, C. E. Leiserson, R. L. Rivest, and C. Stein, *Introduction to Algorithms*. Cambridge,MA: MIT press, 2009.

[101] X. W. et. al., "Flashlinq: A synchronous distributed scheduler for peer-to-peer ad hoc networks," in *Proc. IEEE Allerton 2010*, Sep. 2010, pp. 514–521.

[102] V. Chvatal, "A greedy heuristic for the set-covering problem," *INFORMS Mathematics of Operations Research*, vol. 4, pp. 233–235, Aug 1979.

[103] E. Communications, "Overview of the 71-76 & 81-86 GHz frequency bands," White Paper, 2010.

[104] "The future of wireless backhaul, liberator V-320," accessed February 2014, http://www.sub10systems.com/wp-content/uploads/2013/02/Liberator_V320_DataSheet_Jan13.pdf.

[105] P. K. et. al., "WINNER II channel models," 2007, deliverable D1.1.2 V1.2 Available from http://www.ist-winner.org/WINNER2-Deliverables/D1.1.2v1.2.pdf.

[106] F. J. Harris, *Multirate Signal Processing for Communication Systems*. Upper Saddle River, NJ: Prentice Hall, 2008.

[107] "GNUradio polyphase time synchronizer," accessed September 2012, http://gnuradio.org/doc/doxygen/.

[108] J. G. Proakis, *Digital Communications*. New York, NY: Mcgraw Hills, 2001.

[109] "Network Time Protocol Server List," accessed September 2012, http://tf.nist.gov/tf-cgi/servers.cgi.

[110] "GPS synchronization," accessed September 2012, http://www.gpsinformation.org/dale/nmea.htm.

[111] Cisco, "Cisco visual networking index: Forecast and methodology, 20132018," White Paper, Jun. 2014.

[112] G. Fettweis, M. Krondorf, and S. Bittner, "GFDM - generalized frequency division multiplexing," in *Proc. IEEE VTC '09*, Jun. 2009.

[113] S. C. Forum, "Backhaul technologies for small cells," White Paper, Feb. 2014.

[114] Y. Rahmatallah and S. Mohan, "Peak-to-average power ratio reduction in OFDM systems: A survey and taxonomy," *IEEE Communications Survey & Tutorials*, vol. 15, pp. 1567–1592, 2013.

[115] T. Jiang and Y. Wu, "An overview: Peak-to-average power ratio reduction techniques for OFDM signals," *IEEE Transactions on Broadcasting*, vol. 54, pp. 257–268, 2008.

[116] H. Ochiai and H. Imai, "On the distribution of peak-to-average power ratio in OFDM signals," *IEEE Transactions on Communications*, vol. 49, pp. 282–289, 2001.

[117] "IEEE 802.22 PHY overview," accessed April 2014, http://www.ieee802.org/22/Technology/22-10-0106-00-0000-ieee-802-22-phy-overview.pdf.